AD_____

Award Number: W81XWH-04-1-0892

TITLE: Low Vision Research at the Schepens Eye Research Institute

PRINCIPAL INVESTIGATOR: Darlene A. Dartt, Ph.D.
Russell Woods, Ph.D.
Joan Stein-Streilein, Ph.D.
Bruce Ksander, Ph.D.
Andrew Taylor, Ph.D.
Dong Feng Chen, M.D., Ph.D.
Michael Young, Ph.D.

CONTRACTING ORGANIZATION: Schepens Eye Research Institute
Boston, MA 02114-2508

REPORT DATE: October 2005

TYPE OF REPORT: Annual

PREPARED FOR: U.S. Army Medical Research and Materiel Command
Fort Detrick, Maryland 21702-5012

# REPORT DOCUMENTATION PAGE

*Form Approved*
*OMB No. 0704-0188*



| 1. REPORT DATE *(DD-MM-YYYY)* | 2. REPORT TYPE | 3. DATES COVERED *(From - To)* |
|---|---|---|
| 01-10-2005 | Annual | 15 Sep 04 – 14 Sep 05 |

**4. TITLE AND SUBTITLE**
Low Vision Research at the Schepens Eye Research Institute

**5a. CONTRACT NUMBER**

**5b. GRANT NUMBER**
W81XWH-04-1-0892

**5c. PROGRAM ELEMENT NUMBER**

**6. AUTHOR(S)**
Darlene A. Dartt, Ph.D., Russell Woods, Ph.D., Joan Stein-Streilein, Ph.D., Bruce Ksander, Ph.D., Andrew Taylor, Ph.D., Dong Feng Chen, M.D., Ph.D., Michael Young, Ph.D.

E-Mail: dartt@vision.eri.harvard.edu

**5d. PROJECT NUMBER**

**5e. TASK NUMBER**

**5f. WORK UNIT NUMBER**

**7. PERFORMING ORGANIZATION NAME(S) AND ADDRESS(ES)**

Schepens Eye Research Institute
Boston, MA 02114-2508

**8. PERFORMING ORGANIZATION REPORT NUMBER**

**9. SPONSORING / MONITORING AGENCY NAME(S) AND ADDRESS(ES)**
U.S. Army Medical Research and Materiel Command
Fort Detrick, Maryland 21702-5012

**10. SPONSOR/MONITOR'S ACRONYM(S)**

**11. SPONSOR/MONITOR'S REPORT NUMBER(S)**

**12. DISTRIBUTION / AVAILABILITY STATEMENT**
Approved for Public Release; Distribution Unlimited

**13. SUPPLEMENTARY NOTES**
Original contains color plates: All DTIC reproductions will be in black and white.

**14. ABSTRACT**

Abstract is attached at following page.

**15. SUBJECT TERMS**
Inattentional blindness, vision multiplexing, visual displays, retina, laser burn, inflammation, immune privilege, macrophages, retinal progenitor cells, apoptosis

| 16. SECURITY CLASSIFICATION OF: | | | 17. LIMITATION OF ABSTRACT | 18. NUMBER OF PAGES | 19a. NAME OF RESPONSIBLE PERSON |
|---|---|---|---|---|---|
| a. REPORT | b. ABSTRACT | c. THIS PAGE | | | USAMRMC |
| U | U | U | UU | 105 | 19b. TELEPHONE NUMBER *(include area code)* |

# ABSTRACT

The purpose of the grant is to prevent low vision that can occur on the battlefield in two contexts. The first area is inattentional blindness that can occur when using complex visual displays on military equipment, especially head mounted displays. The second are the collateral damage that can occur in the retina after laser burns. The scope of the work is: 1. To determine the optimal augmented vision system by understanding the ability of an individual to access supplemental visual information presented by vision multiplexing and 2. To develop novel treatments that control the inflammatory response and repair neuroretinal damage induced by retinal laser burns. Our major findings are: 1. Applying cartoon-like edge filtering did not overcome inattentional blindness; 2. Laser burns to the retina inhibited immune privilege in the anterior chamber; released immunosuppressive factors, especially PEDF, from the retina and retinal pigmented epithelium, but not from the vitreous, that suppress the inflammatory activity of activated macrophages; induced neuronal cell apoptosis that could potentially be repaired by biodegradable polymer/progenitor cell composites.

# Table of Contents

# DOD FY04 Annual Report
# OCTOBER 31, 2005

## INTRODUCTION

For functional vision to occur the retina must be healthy and intact and the brain able to process the images that it receives. In the military during, operation of complex machinery with optical devices and electronic displays in conditions of stress (battlefield warfare) and degraded vision (darkness, fog), optimally functioning vision is critical for the successful completion of the task. In turn the use of lasers as range finders, in missile guidance, and as weapons increase the possibility of laser damage to the retina. Both these scenarios result in low vision and will be addressed in the present proposal. For the first project we will investigate the processing of visual images to the brain. We will determine the best mode in which to supplement visual displays for maximum perception and performance that is dependent upon the way the brain processes these images. For the second project we will investigate the effect of laser burns on the retina. We will use a multifactorial approach to determine the effect of the laser burn on the immune response that occurs in the retina to the laser burn. Thus, this proposal will address two critical related functions of the retina crucial for vision and visual tasking. Successful completion of this project will advance the military's knowledge in optimizing visual displays for complex equipment and preventing retinal damage that can occur with the misuse for the lasers used in the equipment both for its operation and as disabling weapons.

## BODY

### I. Task 1

To investigate the effect of scale changes, appearance modification and non-scene information on detection rates with uni-ocular and dichoptic displays that simulate augmented vision displays.

### A. Subtasks

1. **Subtask (1):** To investigate the impact of scale change and appearance modifications on detection rates in same-scene augmented vision displays

2. **Subtask (2):** To investigate whether presentation format, uni-ocular or dichoptic, affects detection rates in same-scene augmented vision displays

### B. Hypothesis

We expect that the use of augmented vision systems will be improved by better understanding of the ability to access supplemental visual information that is presented in various modes of vision multiplexing. In particular, we hypothesize that the modes used to present the supplemental information may interact. For example, when the supplemental visual information is presented as an outline-augmented view, it may be better to use a uni-ocular than a dichoptic display. We hypothesize that making an augmented view of the same scene more dissimilar to the natural view, when both views

are available, will improve detection of objects of interest, because separating the two scenes will require less cognitive resources.

## C. Research Accomplishments for Subtask (1)

We investigated the effect of appearance changes via an inattentional blindness experiment, superimposing ballgame and hand-slapping game scenes (same scenes in that both are natural views). With the subject's attention focused on a task involving one scene, an unexpected event would occasionally occur in the other scene. Cartoon-like edge-filtering of one, both or neither of the two scenes was tested to see if it had an effect on the detectability of the unexpected events. This experiment first reproduced aspects of, and then extended, the classic Neisser and Becklen, 1975 (Ref. #1) study that first identified inattentional blindness

We videotaped two different games; a ballgame, in which three players ran around in a circle and passed a basketball back and forth, either directly or with a bounce, and a hand-slapping game, in which just the outstretched forearms and hands of two players were visible, as one player tried to slap the other's hands. When a player missed, the other player became the slapper. Four takes of each game were taped for use as the attended task in the inattentional blindness trials. In the case of the ballgame, the subject would be told to click a mouse button each time there was a pass (but not a feint). For the handgame, the task was to click the mouse at each slap attempt, whether successful or not, while ignoring feints. Each take had a 15 second lead-in for synchronization, followed by one minute of game play that included 30 passes or slap attempts. We also taped 3 scenes for each game that included unexpected events, such as a juggler walking through the ballgame or the handgame players stopping to toss a small ball back and forth.

DigiVision, Inc., produced for us a customized version of their ValueVision video filter based on an edge detection technique we had developed. The filter is unique in that it produces both white and black edges at each edge transition, so that edges are visible against both light and dark backgrounds. Test clips were evaluated to establish suitable contrast and threshold settings for the filter.

We produced an edge-filtered version of each take, and then used Adobe Premiere video post-processing software to overlay the attended and unattended scenes. We composed versions with all four possible combinations of one, both, or neither scene edge-filtered. In all, over 165 overlaid clips were developed.

We developed an experiment control application that ran the videos in a scripted order, provided the questions the experimenter would ask the subject to determine in an event was detected (while carefully avoiding alerting the subject to the existence of unexpected events), recorded the results of each trial, and then was used to analyze the results. The application randomized and balanced the presentation of the unexpected events, the attended takes they were combined with, and the filtering treatment. It also blinded the experimenter to the actual trials underway, so that no cues would be given by the experimenter to the subject.

36 subjects each viewed trials with 6 different unexpected events, with cartooning treatment and event order balanced between subjects. We recorded whether or not each unexpected event was detected, as well as the accuracy and response times in performing the attended (distracter) tasks.

We found no significant effect of edge filtering on event detection, nor did it affect the accuracy of performing the attended task. It did have a small but statistically significant effect on the response times of the attended task.

That edge filtering had no positive or negative effect on event detection was surprising. We know anecdotally (i.e. from user reports) that edge filtering of one of the two scenes helps with the identification of salient features and helps distinguish the scenes, so the fact that it did not impede event detection is encouraging.

Results of this study were presented as a poster at the Vision Sciences Society 2005 conference with an abstract published in the proceedings. They were also presented in a talk at the Society for Information Display 2005 conference, and a 4-page summary was published in the conference proceedings. That summary, providing more detail than has been given in this section, is attached to this report (Appendix 1, #1; Ref. #2). We are preparing a manuscript for submission.

**D. Research Accomplishments for Subtask (2)**

We have conducted preliminary tests in preparation for the next inattentional blindness experiments that will compare uni-ocular to dichoptic viewing. A novel DLP-based display system was developed to provide dichoptic (or uni-ocular) viewing with minimal crosstalk between eyes. The first experiment (described above) used scenes that, while both natural scenes, were different (ballgame and hand-slapping game). The next experiment will use two views of the same scene, the two views differing by scale (i.e. magnification/minification), and thus will share content. One of the views will show a wider-angle view than the other, and thus contain information not in the other view. This is the format of our low-vision device, and similar to some military augmented-vision systems. We have constructed the necessary dual camera set up to record the scene simultaneously in two scales. Preliminary investigations of the impact of this shared context suggest that it may be easier to follow the events in the two views than with the classic inattentional blindness experimental format that we adopted in the first experiment. We are preparing to create the necessary videos.

A recent study showed that, even when subjects are warned that unexpected events may occur, the unexpected events are missed, when the attended task is sufficiently difficult (Ref. #3). We are preparing an experiment to investigate whether the second scene is necessary for inattentional blindness. In other words, to test whether inattentional blindness is a consequence of augmented vision displays, or an inherent limitation of the visual system.

## II. Task 2

To develop novel treatments to control inflammatory responses and repair neuroretinal damage induced by retinal laser burns.

### A. Subtasks

1. **Subtask (1):** To standardize the mouse model of retinal laser injury.

   **a. Research Accomplishments for Subtask (1)**

   In an effort to produce a model of retinal laser burns, we carried out a series of experiments that examined the effects of a series of different laser exposures in the mouse model. We varied (i) pulse duration (10 – 100 milliseconds), (ii) total energy (50 – 200 milliwatts), (iii) spot size (50 – 300 mm), and (iv) spot location (peripheral to central). Laser burns were examined via indirect ophthamoscope specifically designed for use in mice and fluorescein angiogram (0.2 ml of fluorescein sodium at a 1% solution).

   Mice were anesthetized with a 1:1 mixture of 100 mg/ml ketamine and 20 mg/ml xylazine. Pupils were dilated with a topical application of 5.0% phenylephrine and 0.8% tropicamide. Laser burn was produced with OcuLight SLx Diode laser (IRIS Medical OcuLight, Mountain View, CA) at a wave-length of 810 nm. Eyes were enucleated at 1-14 days after treatment for Cresyl Violet or Hematoxylin and Eosin staining to reveal retinal morphology and subject to histolopathogical evaluation.

   Within 24 hr after laser burn, we observed obvious damage to the layer of retinal pigment epithelium (RPE) and disruption and pyknosis in the outer nuclear layer (ONL, photoreceptor cells). Consistent with that has been reported in human and other animals, a greater damage to these structures was seen with increasing pulse duration and energy levels, but was inversely correlated with the size of laser spots. This work has demonstrated that mouse can be used as a feasible, effective, and reproducible model for the studies of retinal laser burn.

2. **Subtask (2)**: To study the effect of retinal laser burns on local and peripheral immunity.

   **a. Research Accomplishments for Subtask (2)**

   Local immunity-We have developed the Laser burn model in C 57 BL/6 mice. We have shown that at all time points within 6 h to 3 weeks the burned mice are unable to develop anterior chamber associated immune deviation (ACAID) when antigen is inoculated into the anterior chamber of the eye. Significant loss of retinal neurons, induced by the laser and its sequelae, is the primary cause of visual function deficiency after retinal laser burns. The inflammatory response induced by the primary tissue damage triggers a secondary spreading of the retinal injury and contributes critically to the subsequent and long-lasting destruction of surrounding retinal tissue. Here, we hypothesize that application of neuroproctective agents and suppression of inflammatory response are crucial

steps in diminishing or limiting the extent of the laser-induced primary and secondary retinal damage and, therefore, may be therapeutic strategies for the treatment of retinal laser injuries. We established a of mouse model of retinal laser injury. A diode laser burn of 50 mW energy and 50 ms pulse duration was delivered to the retina through a slit lamp microscope. Four spots (200 nm diameter) were burned at the 9 o'clock position of the retina in the right eye of B6 mice (Appendix 2, Fig. 1).

Laser burn destroyed the outer nuclear layer (ONL), photoreceptor segment, Bruch's membrane and retinal pigment epithelium (RPE) (Appendix 2, Figs. 2&3). The infiltrating inflammatory cells can be seen in the ONL (blue arrow). Also, the choroids vessels are dilated (green arrow) indicating that an inflammatory response occurs after a retinal burn by the laser.

We tested the postulate that a laser burn to the retina would have far reaching effects the ability of the anterior chamber in the front of the eye to maintain immune privilege and its ability to induce tolerance to anterior chamber inoculated antigens. We observed that indeed as early as 6 hours post laser burn, the ability of ACAID induction was lost. The ACAID procedure was followed at 2, 4,11, 14 and 21 days and at no time were we able to induce tolerance to anterior chamber inoculated antigen (Appendix 2, Fig. 4)

We interpret this to mean that a change in the immunosuppressive environment in the back of the eye is influencing on the anterior segment of the eye

The retinal laser burns interferes with immune privilege since presentation of antigen to the anterior chamber induces an immune response instead of suppression or tolerance when the eye is burned with a laser (Appendix 2, Fig. 5). This is in contrast to non-burned eyes in which presentation of antigen suppresses the immune response.

Peripheral immunity-We predict that laser-induced retinal inflammation will be significantly reduced by treatment with a soluble protein (soluble Fas Ligand) that blocks the activation of neutrophils, which are one of the earliest cells to infiltrate the site of inflammation and are responsible for expanding and amplifying the inflammatory response.

After performing a series of preliminary experiments where we varied the: (i) power level, (ii) wave length, (iii) spot size, and (iv) exposure time, we successfully established a laser burn murine animal model. Using an infrared diode laser, anesthetized 8 week old C57BL/6J mice were given 4 laser burns at approximately 1 disc diameter from the optic disc. A -15 diopter contact lens was used to focus the laser on the retina. The power level was 50 mW; wave length 810 nm; spot size 125 mm; and the exposure time set at 75 ms. The following is a summary of our histological examination of these burns.

The first effects of the laser burn are observed in the RPE, where we observed thinning and increased pigmentation (Fig 1, Appendix 2). This coincided with an enlargement of the choroid (Fig 2, Appendix 2) and a disruption of Bruch's membrane (Fig 3, Appendix 2). At 24 hours we also observed a loss of cells in the outer and inner nuclear layer, as well as, destruction within the photoreceptor cell layer (Fig 4, Appendix 1). At 72 hours we observed proliferation of the RPE layer and migration of RPE into the sensory retina (Fig 5, Appendix 2).

We are currently in the process of examining the activation of glial cells within t he laser burn in an effort to identify when glial scarring occurs. We will then determine whether the formation of the glial scar coincides with the infiltration of inflammatory cells into the burn site. We will also determine if the formation of the glial scar is reduced in the absence of inflammation.

Since we are interested in the role of inflammation in the development of the glial scars caused by laser burns, we are also interested in the expression of proteins in the retina that may trigger inflammation at the burn site. Stressed cells found at the site of laser burns express high levels of "heat shock proteins" that are an important trigger of inflammation. For this reason, we examined the expression of a small heat shock protein called alpha-B crystallin. We observed that alpha-B crystallin is expressed in the RPE and retina via Western blot analysis (Fig 6, Appendix 2) and via immunohistochemical staining (Fig 7, Appendix 2). Future studies will determine whether this heat shock protein is (i) expressed at higher levels within the laser burn site, and (ii) if it triggers infiltration and activation of inflammatory cells at the burn site.

**Appendix #2 data:**

**Figure 1-** Histology of laser burn site- thinning of the RPE
**Figure 2-** Histology of laser burn site- enlarged choroid.
**Figure 3-** Histology of laser burn site- disruption of Bruch's membrane.
**Figure 4-** Histology of laser burn site- destruction within the INL; ONL; and photoreceptors.
**Figure 5-** Histology of laser burn site- proliferation and migration of RPE.
**Figure 6-** Western blot of alpha-B crystallin in the RPE and retina.
**Figure 7-** Immunohistochemical staining of alpha-B crystallin within the retina.

3. **Subtask (3)**: To evaluate the inflammatory and wound repairing activity of macrophages in retinal wound healing after retinal laser burns.

**a. Research Accomplishments for Subtask (3)**

There are three specific technical objectives to this Task: a. Determine the capacity of the tissues of the posterior eye (vitreous, neural retina, retinal pigment epithelial cell monolayer) to suppress the inflammatory activity of macrophages; b. Determine the capacity of the very same tissues to suppress inflammatory activity of macrophages following retinal laser wounding; and c. to identify potential anti-inflammatory factors produced/released by these ocular tissues The

ultimate objective will be to treat the laser burned retina with the natural ocular anti-inflammatory factors that promote the expected anti inflammatory, wound repairing activity of macrophages found in a healthy retina. We have accomplished the first technical objective and half of the remaining objectives. What remains is for us examine posterior eye of laser burned eyes and to use these findings to identify the anti-inflammatory factors that we can use to protect the neural retina from the destructive effects of inflammatory macrophages.

For technical objective (a) the experiments were conducted as described in the approved Statement of Work. To investigate the normal immunoregulatory activity of the vitreous, neural retina, retinal pigment epithelial cell monolayer (RPE), posterior eye cups were created from healthy eyes of C57BL/6J mice (Ref. #4). A circumferential cut was made just below the ciliary body, and the anterior segment, lens, and vitreous were removed. The neural retina remaining in the posterior segment eye cup was extracted from the eye cup and placed into its own culture with serum-free media. The remaining eye cup with a monolayer of RPE was placed into a culture well containing media to below the eye cup's rim and into the eye cup was added serum-free media. The vitreous was extracted from the back of the lens and placed into a serum free media culture. The tissues were incubated for 24 hours, and the conditioned media were collected and were added to cultures of monocytic leukemic cells (macrophages) that were stimulated with or without LPS (lipopolysaccharide) to induce inflammatory cytokine production. The cytokines produced by the macrophages were detected by assaying the 24 and 48 hours culture supernatants for cytokines in a multiplex ELISA to detect simultaneously in the supernatants IL-1beta, IL 6, IL-10, IL-12p70, TNF-alpha, G-CSF, GM-CSF, Chemokines: MIP-1α, RANTES, and KC.

We found that the neural retina and the RPE released factors that differentially suppressed the inflammatory activity of LPS-stimulated macrophages (Fig 1, Appendix 3). The neural retinal and RPE conditioned media suppressed endotoxin induced IL-1beta and TNF-alpha production by the macrophages. In addition, the retinal conditioned media significantly enhanced production of the anti-inflammatory cytokine IL-10 by the LPS-stimulated macrophages. However, pro-inflammatory nitric oxide generated by the LPS stimulated macrophages was suppressed by the neural retinal conditioned media, but enhanced by the RPE conditioned media (Fig 2A, Appendix 3). With the exception of RPE enhanced nitric oxide generation, the neural retina and the RPE promoted a pattern of anti-inflammatory activity by the LPS-stimulated macrophages, which were the opposite of the expected pattern of cytokines induced by LPS stimulation. Also, note that the factors from the neural retina and RPE do not induce any activity in the unstimulated macrophages.

We did another assay and immunoblotted for the intracellular enzyme Arginase I in the LPS-stimulated macrophages following treatment with the conditioned media. We found that only the RPE conditioned media induced in Arginase I LPS-stimulated macrophages (Fig 2B, Appendix 3). Normally, the expression of

nitric oxide synthase and are counter regulated in macrophages, because both enzymes compete for the same substrate, L-arginine. However, in recent publications it has been found that macrophages expressing both nitric oxide synthase and Arginase I are highly immunosuppressive macrophages in that they are efficient inducers of T cell apoptosis (Ref. #5) Such macrophages are useful in blocking the activation of T cells that mediate inflammation and autoimmune disease. The induction of Arginase I in the macrophages is in line with the alternative pattern of cytokines and macrophage activation we are observing when we treated the LPS-stimulated macrophages with secreted factors of the neural retina and RPE. Therefore, the factors produced by the tissues of the posterior of the eye promote the production of anti-inflammatory factors and anti-inflammatory functions of activated macrophages.

For technical objective (b) e have recently obtained tissues from mouse eyes with laser burned retinas and are now analyzing them as in objective (a) to complete this objective. In a related experiment not associated with this grant, we have assayed the effects of the factors released by the RPE and neural retina of mouse eyes suffering from autoimmune disease. We found that there was a loss in neural retinal suppression of nitric oxide production by LPS stimulated macrophages. This suggests that trauma to the retinal tissues, here autoimmune disease, alters the immunoregulatory activity of the posterior segment of the eye. However, as in objective a, the factors produced by the neural retina and the RPE of the diseased retina did not induce activity in the resting macrophages.

For technical objective (c) based on a previous project, to be reported (Zamiri P, Masli S, Streilein JW, and AW Taylor. Pigment epithelial growth factor suppresses inflammation by modulating macrophage activation. Invest. Ophthalmol. Vis. Sci. 2005. Submitted), there was a hint that the cytokine Pigment Epithelium Derived Factor (PEDF) may have immunosuppressive activity (Ref. #6) on LPS-stimulated macrophages. The factor is known to be produced in the eye by the RPE (Ref. #7). Ironically, but not unexpectedly (Ref. #8), we found that when we neutralized with antibody to PEDF the neural retina was also neutralized in its ability to suppress TNF-alpha production by the LPS-stimulated macrophages (Fig 3, Appendix 3). No other activity was affected in the neural retinal or RPE condition media suppression of inflammatory activity by LPS-stimulated macrophages. These findings tell us that the PEDF is not actively released by the RPE in the eye cup (Ref. #7), and that it may be held in the neural retina (Ref. #8). Moreover, these findings suggest that there are several factors produced and released by the neural retina and RPE to regulate immunity As soon as we can understand which factors are important in the healthy retina and what is lost in the wounded retina we will be able to test candidate factors to promote macrophage anti-inflammatory activity.

**4. Subtask (4)**: To control laser-induced neuroretina damage with neuroprotective agents and neural replacement/transplantation therapy:

**a. Research Accomplishments for Subtask (4)**

Significant loss of retinal neurons, induced by laser burns and their subsequent inflammation, is the primary cause of visual function deficiency after retinal laser burn. We hypothesize that application of neuroprotective agents and suppression of inflammatory response are crucial steps in diminishing or limiting the extent of the laser induced primary and secondary retinal damage, therefore, may be therapeutic strategies for retinal laser injury. The use of retinal progenitor cells to repair the damage caused by laser burns can also result in improved outcome

With the increasing use of lasers in military, industry, and laboratory research, there has been a significant increase in laser-induced retinal injury. In clinical ophthalmology, use of laser normally results in retinal damage that is larger than expected from the size of coagulated area. Currently, little is known about the pathogenesis of retinal laser burns, and no proven method is available to prevent or treat the injury.

In the past year, we proposed to develop an experimental model of retinal laser burn in mice and study retinal pathology and neuronal death resulted from the retinal laser burn. Moreover, we proposed to use this model to evaluate the effect of neuroprotective agent lithium or retinal transplantation therapy to the survival and function of retinal neurons after retinal laser injury.

We have made substantial progress in the generation of tissue engineering constructs for repair of the injured retina. We have demonstrated these constructs result in a 16 fold increase in cell survival following grafting to the retina of mice with retinal degeneration (rd), and found that differentiation into photoreceptors is increased compared to controls without polymer substrates. We have also evaluated protein expression by retinal progenitor cells.

A defining feature of laser-induced retinal injury is the death of neurons. However, little was known about the pathology and mechanisms of neuronal loss in laser injured eye. Thus, we began by asking whether laser induces neuronal apoptosis in the retina, as identified by terminal deoxynucleotidyl transferase dUTP nick-end labeling (TUNEL). We assessed quantitatively the extent and time course of laser-induced retinal neuron apoptosis. Following retinal laser burn, mice were sacrificed on days 1, 3, 5, 7, 14, and 28 after the injury. The retinal sections (15 $\mu$m) were prepared and double labeled with TUNEL and primary antibodies against markers of retinal neurons. These include antibodies against brn-3b (for retinal ganglion cells) and rod/rhodopsin or cone opsins for photoreceptor cells.

We noted that with 24 hr, massive cell apoptosis was observed in the ONL and RPE layer, primarily associated with photoreceptors and RPE cells. Cell apoptosis decreased drastically in 3 days, and was undetectable after 7 days. The result demonstrates that induction of apoptotic signaling events is a mechanism that laser irradiation induces retinal cell loss.

We continue to make significant progress in our efforts to use biodegradable polymers as part of a larger effort aimed at retinal tissue engineering. We have further developed techniques for constructing biodegradable polymer/ progenitor cell composites (Appendix 4, #1), and successfully grafted them in a number of models. We have found that biodegradable polymers can have a massive effect on the survival of grafted progenitor cells, increasing yield up to 16 fold. The mechanism of this increase in survival is related to both the supportive substrate and the presence of survival factors on the substrate (Appendix 4, #2). Another significant benefit of the polymer substrate is an increase in differentiation of photoreceptors in the rho knock out mouse recipient (Appendix 4, #2). Our next step will be to combine composite grafts with laser injury as a means to reconstruct the injured retina

## KEY RESEARCH ACCOMPLISHMENTS

### I. Task 1

- A complex inattentional blindness experiment was prepared and conducted.
- We applied cartoon-like edge filtering to determine if it would improve a subject's ability to notice unexpected events. There was no substantial impact of the edge filtering on event detection.
- We have begun planning and preparation of the study to compare uni-ocular to dichoptic viewing.
- We have begun planning and preparation of a study to investigate the impact of attention on event detection.
-

### II. Task 2

**Subtask 1**

- The optimal laser burns to mouse retina can be obtained with 20 spots using a duration of 50 ms, spot size of 125 m, central spot location, and 50 mV of power.

**Subtask 2**

- Retinal laser burn induces heat that in turn damages retinal neurons, RPE and choroid.
- Retinal laser burn breaks the blood-ocular barrier and induces inflammation.
- Within the time period of 6 hours to 21days after retinal laser burn, ACAID was inhibited.
- After retinal laser burn, anterior chamber injection induces delayed hypersensitivity rather than tolerance. An anterior chamber inoculation has never been shown to be immunizing before. It appears that the retinal laser burn breaks immune privilege mechanisms of the eye.
- Identified the expression of the small heat shock protein, alpha-B crystallin, with the RPE and sensory retina.

**Subtask 3**

- Factors released by the neural retina and the RPE suppress inflammatory activity of activated macrophages.
- Factors released by the vitreous have no effect on the inflammatory activity of activated macrophages.

- Tissue damaging disease in the eye alters the anti-inflammatory properties of the neural retina and the RPE.
- PEDF is one of the possible anti-inflammatory factors produced and released by the neural retina and RPE.
- A mechanism of the immune privileged ocular microenvironment is to promote the alterative activation of macrophages when stimulated with endotoxin.

**Subtask 4**

- Developed biodegradable polymer/ progenitor cell composites.
- Demonstrated these constructs result in a 16 fold increase in cell survival following grafting to the rd retina.
- Found that differentiation into photoreceptors is increased compared to controls without polymer substrates.
- Uncovered the mechanisms underlying these results.
- Evaluated protein expression by mouse retinal progenitor cells in an experimental model of retinal laser injury in mice.
- Demonstration of neuronal apoptosis in laser-induced retinal cell loss.
- Laser-induced neuronal apoptosis occurs primarily in the outer nuclear layer (or photoreceptor cells) and peaks day 1 after the laser burn and disappears after day 7.

**REPORTABLE OUTCOMES**

**I. Task 1**

1. Poster presented at Vision Sciences Society Meeting, May 2005, and abstract published in Journal of Vision. "The effect of edge filtering on inattentional blindness." (Apfelbaum et al, 2005a) (Appendix 1, #2)

2. Talk presented at Society for Information Display 2005 Conference, May 2005 and 4-page abstract published in the Conference Proceedings. "The effect of edge filtering on vision multiplexing." (Apfelbaum et al, 2005b, attached as Appendix 1, #1 SIDAbstract).

**II. Task 2**

**Subtask 1**

None

**Subtask 2**

1. We are submitting an abstract to the 2006 ARVO meeting that describes our initial experimental results.

2. Presentation of these results at "Strategies and Solutions- the changing landscape of military ophthalmology. September 28 and 29th, 2005.

**Subtask 3**

Manuscripts:

1. P Zamiri, S Masli, N Kitaichi, AW Taylor, and JW Streilein(deceased). Thrombospondin plays a vital role in the immune privileged eye. Invest. Ophthalmol. Vis. Sci. 2005; 46:908-919. (PMID: 15728547). (Appendix 3, Manuscripts, #1)

2. Zamiri P, Masli S, Streilein JW, and AW Taylor. Pigment epithelial growth factor suppresses inflammation by modulating macrophage activation. Invest. Ophthalmol. Vis. Sci. 2005. Submitted.

Abstracts:

1. Mechanisms of retinal immune privilege, Federation of Clinical Immunology Societies, 2005, Boston, MA. (Appendix 3, Abstracts, #1)
2. Contribution of neuroretinal and pigmented epithelial cell factors to subretinal immunity, The Association for Research in Vision and Ophthalmology (ARVO), 2005, Ft. Lauderdale. (Appendix 3, Abstracts, #2)

**Subtask 4**

Manuscripts:

1. E. B. Lavik, H. Klassen, K. Warfvinge, R. Langer, and M. J. Young, 2005. Fabrication of degradable polymer scaffolds to direct the integration and differentiation of retinal progenitors. Biomaterials, 26 (16):3187-96. (Appendix 4, Manuscripts #1)
2. Tomita, M., Lavik, E., Zahir, T., Klassen, Langer, R., and Young, M. Retinal progenitor cell transplantation using biodegradable polymers. Stem Cells, in press. (Appendix 4, Manuscripts #2)

Abstracts:

1. Proteomic Comparison Between Retinal Progenitor Cells and Brain Progenitor Cells Derived From Early Neonatal Mice. *H.Greenlee1A, T.E. Dunn1B, D.S. Sakaguchi1C, M.J. Young2.* ABiomedical Sciences, Bioinformatics and Computational Biology, and Interdepartmental Neuroscience, BBiomedical Sciences and Bioinformatics and Computational Biology, CDepartment of Genetics, Development & Cell Biology and Interdepartmental Neuroscience, 1Iowa State University, Ames, IA; 2Schepens Eye Research Institute, Department of Ophthalmology, Harvard Medical School, Boston, MA, ARVO abstract 2005. (Appendix 4, Abstracts #1)
2. Enhanced Survival and Differentiation Into Photoreceptor in Retinal Progenitor Cells Transplantation Using Polymer Composite Graft. *M.Tomita1, E.Lavik2, H.Klassen3, T.Zahir1, R.Langer4, M.J. Young1.* 1Department of Ophthalmology, The Schepens Eye Research Institute, Harvard Medical School, Boston, MA; 2Yale University, New Haven, CT; 3Children's Hospital of Orange County and U.C. Irvine, Orange, CA; 4Massachusetts Institute of Technology, Cambridge, MA, ARVO abstract 2005. (Appendix 4, Abstracts #2)

## CONCLUSIONS

### I. Task 1

Surprisingly, edge filtering had no positive or negative effect on event detection. Anecdotally, we know that edge filtering of one of the two scenes helps with the identification of salient features and helps distinguish the scenes, so the fact that it did not impede event detection is encouraging. On the positive side, the event detection rates of about half in our first experiment, does suggest that users with restricted peripheral vision (whether by visual impairment or due to the situation) may detect about half of the events that occur outside of the natural field of view,

and therefore would not have been detected otherwise (i.e. without the augmented vision system). We have yet to test whether the display format (uni-ocular or dichoptic) and context (presentation of two views of the same scene) alters this result

II. **Task 2**

**Subtask 1**

We can induce inflammation by laser burns to the retina.

**Subtask 2**

Retinal laser burns may compromise the patient's ability to protect the visual axis of that eye because of its ability to abolish immune privilege. The laser burned eye may be more susceptible to infection and would make the patient a high-risk candidate for corneal graft transplantation. The fact that the back of the eye was burned but the suppression is lost in the front of the eye shows how interactive the various parts of the eye are. Moreover the cells in the retina called retinal pigment epithelial cells may be the main source of immunosuppressive molecules for the entire eye. We can no longer think of the eye as individual compartments but rather but are compelled to think of the eye as one functioning and interacting organ.

We have developed a murine laser burn model. That will be used to determine if inflammation exacerbates glial scarring at the burn site.

**Subtask 3**

We found that the neural retina and the RPE contribute to the ocular microenvironment factors that regulate the activation and function of macrophages. These factors prevent the induction of inflammation. The observed suppression of inflammatory activity while promoting anti-inflammatory activity in the LPS-stimulated macrophages suggests that within the posterior segment of the eye there is an alternative activation of macrophages (Appendix 3, #4; Ref. #9). Therefore, it would be of interest to continue as planned to investigate the effects of the neural retina and RPE from laser-wounded eyes, and to pursue the possibility that healthy eyes promote alternative activation of macrophages. If macrophages in the retina are alternatively activated, it would mean that the eye actively promotes macrophage anti-inflammatory and wound repair functions countering the signals of inflammation. It will also suggest that any therapy that promotes this alternative activation pathway in macrophages will be beneficial in preventing the collateral damage to the neural retina within the laser wounded retina.

**Subtask 4**

Our recent results have demonstrated that we can successfully induce laser injury in the mouse retina. This has greatly expanded our ability to our future work at repairing the diseased retina. This complex task requires a broad approach, and we submit that the application of tissue engineering strategies offer great promise for someday restoring vision to the blinded eye. We will now extend our work and build upon our accomplishments, combining slow release biomaterials with biodegradable polymer/ progenitor cell composites with laser injured retinas, such that a new outer retina can be constructed.

**REFERENCES**


1. Neisser, U. and Becklen, R. (1975). Selective looking: Attending to visually specified events. *Cognitive Psychol.* 7, 480 494.
2. Apfelbaum HL, Apfelbaum DH, Woods RL, Peli E (2005b) The effect of edge filtering on vision multiplexing. *SID Int Symposium, Dig Tech Papers*, Society for Information Display, 36: 1398-1401. (SID 2005 Meeting, Boston, MA, 25-27 May, 2005)
3. Rensink RA. (2005) Robust inattentional blindness (abstract). *J. Vision* 5(8):
4. Zamiri P, Zhang Q, Streilein JW. Vulnerability of allogeneic retinal pigment epithelium to immune T cell mediated damage in vivo and in vitro. Invest Ophthalmol Vis Sci 2004;45(1):177-84.
5. Bronte V, Zanovello P. Regulation of immune responses by L-arginine metabolism. Nat Rev Immunol 2005;5(8):641-54.
6. Wu GS, Rao NA. A novel retinal pigment epithelial protein suppresses neutrophil superoxide generation. I. Characterization of the suppressive factor. Exp Eye Res 1996;63(6):713-25.
7. Tombran-Tink J, Shivaram SM, Chader GJ, Johnson LV, Bok D. Expression, secretion, and age related downregulation of pigment epithelium-derived factor, a serpin with neurotrophic activity. J Neurosci 1995;15(7 Pt 1):4992-5003.
8. Wu YQ, Notario V, Chader GJ, Becerra SP. Identification of pigment epithelium-derived factor in the interphotoreceptor matrix of bovine eyes. Protein Expr Purif 1995;6(4):447-56.
9. Gordon S. Alternative activation of macrophages. Nat Rev Immunol 2003;3(1):23-35.

## APPENDICES

Appendix 1

1. Talk presented at Society for Information Display 2005 Conference, May 2005 and 4-page abstract published in the Conference Proceedings. "The effect of edge filtering on vision multiplexing." (Apfelbaum et al, 2005)
2. Poster presented at Vision Sciences Society Meeting, May 2005, and abstract published in Journal of Vision. "The effect of edge filtering on inattentional blindness." (Apfelbaum et al, 2005a) (Appendix 1, #2)

Appendix 2

Figure 1. Photomicrograph of a human eye fundus to show position of the laser burn in the mouse eye.

Figure 2. Right panel: Damage caused by the retinal laser burn. Left panel: photomicrograph of a mouse eye stained with H& E.

Figure 3. Time course of retinal laser burn. Left panel shows the burn 4 days post retinal laser burn, the injury is seen in the ONL.

Figure 4. Effect of retinal laser burn on ACAID suppression of Delayed Hypersensitivity response in the ear.

Figure 5. Figure 5. Effect of retinal laser burn on ability to immunize via the eye.

Figure 6. Histology of laser burn site- thinning of the RPE

Figure 7. Histology of laser burn site- enlarged choroid.

Figure 8. Histology of laser burn site- disruption of Bruch's membrane.

Figure 9. Histology of laser burn site- destruction within the INL; ONL; and photoreceptors.

Figure 10. Histology of laser burn site- proliferation and migration of RPE.

Figure 11. Western blot of alpha-B crystallin in the RPE and retina.

Figure 12. Immunohistochemical staining of alpha-B crystallin within the retina.

Appendix 3

Figures:

Figure 1. The effects of healthy neural retinal (NR) and retinal pigmented epithelial cell eye cup (RPE) conditioned media (CM) on macrophages (MØ) activated with or without endotoxin (LPS).

Figure 2. The effects of the conditioned media on LPS-stimulated Nitric Oxide (NO) generation and Arginase I expression

Figure 3. The effects of neutralizing PEDF in the condition media on the condition media suppression of TNF-alpha production by LPS-stimulated macrophages.

Figure 4. Summary of results.

Manuscripts:

1. P Zamiri, S Masli, N Kitaichi, AW Taylor, and JW Streilein(deceased). Thrombospondin plays a vital role in the immune privileged eye. Invest. Ophthalmol. Vis. Sci. 2005; 46:908-919. (PMID: 15728547)

Abstracts:

1. Mechanisms of retinal immune privilege, Federation of Clinical Immunology Societies, 2005, Boston, MA.

2. Contribution of neuroretinal and pigmented epithelial cell factors to subretinal immunity, The Association for Research in Vision and Ophthalmology (ARVO), 2005, Ft. Lauderdale.

Appendix 4

Manuscripts:

1. E. B. Lavik, H. Klassen, K Warfvinge, R Langer, and M. J. Young, 2005. Fabrication of Degradable Polymer Scaffolds to Direct the Integration and Differentiation of Retinal Progenitors. Biomaterials, 26 (16):3187-96.

2. Manuscript- Tomita, M., Lavik, E., Zahir, T., Klassen, Langer, R., and Young, M. Retinal progenitor cell transplantation using biodegradable polymers. Stem Cells, in press.

Abstracts:

1. Proteomic Comparison Between Retinal Progenitor Cells and Brain Progenitor Cells Derived From Early Neonatal Mice. *H.Greenlee1A, T.E. Dunn1B, D.S. Sakaguchi1C, M.J. Young2.* ABiomedical Sciences, Bioinformatics and Computational Biology, and Interdepartmental Neuroscience, BBiomedical Sciences and Bioinformatics and Computational Biology, CDepartment of Genetics, Development & Cell Biology and Interdepartmental Neuroscience, 1Iowa State University, Ames, IA; 2Schepens Eye Research Institute, Department of Ophthalmology, Harvard Medical School, Boston, MA, ARVO abstract 2005.

2. Enhanced Survival and Differentiation Into Photoreceptor in Retinal Progenitor Cells Transplantation Using Polymer Composite Graft. *M.Tomita1, E.Lavik2, H.Klassen3, T.Zahir1, R.Langer4, M.J. Young1.* 1Department of Ophthalmology, The Schepens Eye Research Institute, Harvard Medical School, Boston, MA; 2Yale University, New Haven, CT; 3Children's Hospital of Orange County and U.C. Irvine, Orange, CA; 4Massachusetts Institute of Technology, Cambridge, MA, ARVO abstract 2005.

**BIBLIOGRAPHY**


1. Poster presented at Vision Sciences Society Meeting, May 2005, and abstract published in Journal of Vision. "The effect of edge filtering on inattentional blindness." (Apfelbaum et al, 2005a)
2. Talk presented at Society for Information Display 2005 Conference, May 2005 and 4-page abstract published in the Conference Proceedings. "The effect of edge filtering on vision multiplexing." (Apfelbaum et al, 2005b, attached as Appendix 1, #1 SIDAbstract).
3. We are submitting an abstract to the 2006 ARVO meeting that describes our initial experimental results.
4. Presentation of these results at "Strategies and Solutions- the changing landscape of military ophthalmology. September 28 and 29th, 2005b.
5. Mechanisms of retinal immune privilege, Federation of Clinical Immunology Societies, 2005, Boston, MA.
6. Contribution of neuroretinal and pigmented epithelial cell factors to subretinal immunity, The Association for Research in Vision and Ophthalmology (ARVO), 2005, Ft. Lauderdale. Abstract #2
7. P Zamiri, S Masli, N Kitaichi, AW Taylor, and JW Streilein(deceased). Thrombospondin plays a vital role in the immune privileged eye. Invest. Ophthalmol. Vis. Sci. 2005; 46:908-919. (PMID: 15728547)
8. Zamiri P, Masli S, Streilein JW, and AW Taylor. Pigment epithelial growth factor suppresses inflammation by modulating macrophage activation. Invest. Ophthalmol. Vis. Sci. 2005. Submitted.
9. E. B. Lavik, H. Klassen, K. Warfvinge, R. Langer, and M. J Young, 2005. Fabrication of Degradable Polymer Scaffolds to Direct the Integration and Differentiation of Retinal Progenitors. Biomaterials, 26 (16):3187-96.
10. Tomita, M., Lavik, E., Zahir, T., Klassen, Langer, R., and Young, M. Retinal progenitor cell transplantation using biodegradable polymers. Stem Cells, in press.
11. Proteomic Comparison Between Retinal Progenitor Cells and Brain Progenitor Cells Derived From Early Neonatal Mice. *H.Greenlee1A, T.E. Dunn1B, D.S. Sakaguchi1C, M.J. Young2.* ABiomedical Sciences, Bioinformatics and Computational Biology, and Interdepartmental Neuroscience, BBiomedical Sciences and Bioinformatics and Computational Biology, CDepartment of Genetics, Development & Cell Biology and Interdepartmental Neuroscience, 1Iowa State University, Ames, IA; 2Schepens Eye Research Institute, Department of Ophthalmology, Harvard Medical School, Boston, MA, ARVO abstract 2005.
12. Enhanced Survival and Differentiation Into Photoreceptor in Retinal Progenitor Cells Transplantation Using Polymer Composite Graft. *M.Tomita1, E.Lavik2, H.Klassen3, T.Zahir1, R.Langer4, M.J. Young1.* 1Department of Ophthalmology, The Schepens Eye Research Institute, Harvard Medical School, Boston, MA; 2Yale University, New Haven, CT; 3Children's Hospital of Orange County and U.C. Irvine, Orange, CA; Massachusetts 4Institute of Technology, Cambridge, MA, ARVO abstract 2005.

## LIST OF PERSONNEL RECEIVING PAY FROM THE RESEARCH EFFORT

Eliezer Peli,
Robert Goldstein
Henry Apfelbaum
Doris Apfelbaum
Russell Woods
Daniel Brios
Chun Ho Lau
Minoru Tomita
Raymond Chapman
Hong Qiao
Christine Watte

Appendix 1, #1



# 41.2: The Effect Of Edge Filtering On Vision Multiplexing

*H. Apfelbaum[1], D. Apfelbaum, R. Woods, E. Peli*
**The Schepens Eye Research Institute, Harvard Medical School, Boston, MA**

## Abstract

**We developed a video filter that produces cartoon-like images consisting of bipolar white and black transitions at luminance edges of the input video, for use in augmented-vision devices. When tested in an inattentional blindness experiment it had no effect on the detectability of unexpected events, but did affect speed of responses to the attended task. Response time improved when the unattended scene was filtered and degraded when the attended scene was filtered.**

## 1. *Introduction*

Many devices developed in our lab for visually-impaired people employ vision multiplexing – the simultaneous presentation of more than one view to one or both eyes [10]. For example, images on a TV screen are magnified around the current center of interest in the scene, to aid people with poor visual acuity [4]. Since much of the magnified scene is off screen, superimposing an edges-only view of the full scene, allowing attention to be divided between the magnified and full-scene edge views, might provide context. In another example, a head-mounted device (HMD), consisting of spectacles with a small video camera and a see through display in the center of one spectacle lens, presents a wide-angle minified view combined with the normal see-through vision. The minified view helps a person with severe peripheral vision loss notice potential hazards, as well as aiding orientation [2, 13]. The minified view can be processed to produce a cartoon like edges-only display ([6, 13, 14])

A person's ability to make use of multiplexed visual information and avoid confusion is central to the utility of such devices. In a classic experiment, Neisser & Becklen identified the phenomenon they termed *inattentional blindness* [9]. Inattentional blindness is the *inability* to maintain awareness of events in more than one of two superimposed scenes. Subsequent experiments have confirmed the robustness of this effect, with an entire book devoted to it [7]. An example of its operational significance was given by Haines [5], where pilots watching augmented flight path information in the head up display of a landing simulator missed seeing another airplane intruding on the runway. Further studies have probed how similar the two scenes can be and yet still be distinguished (very similar; [8, 12]), or how expectations and cognitive load affect detectability (they do, [1, 3]). In our lab, we are seeking ways to mitigate inattentional blindness so that, for example, a pedestrian user of the HMD we are developing for people with restricted visual fields would notice a car visible first in the minified view.

In this study we investigated the effect of edge filtering on inattentional blindness and on the ability to follow superimposed/multiplexed scenes. First we closely reproduced parts of the original Neisser & Becklen [9], and then treated one or both scenes with edge filtering. We found no evidence that edge filtering affected the detection of unexpected events. However, filtering the *un*attended scene did improve performance of the attended task, as measured by response time, whether the attended task was filtered or not, while filtering the attended scene reduced performance of the attended task, whether the unattended task was filtered or not.

## 2. *Methods*

### 2.1 *Games*

36 normally sighted subjects (visual acuity 20/30 or better) between the ages of 19 and 35 years were shown video segments of two different games superimposed on one another, a ballgame in which three players ran around in a circle and tossed a basketball among themselves, and a hand-slapping game in which the hands and forearms of two players were seen as one player tried to slap the outstretched hands of the other. A subject was instructed to follow one of the games carefully. Attention to the game was ensured by asking the subject to click once each time the ball was passed (either directly or with a bounce) or once each time a slap was attempted (whether successful or not). Odd, unexpected, events were introduced in the unattended scene, and, post trial, carefully worded questions were asked to determine if the events were noticed (without prematurely alerting the subject to the existence of unexpected events).

Trials were scored for hit accuracy, average response time, and whether or not the subject detected and properly identified an unexpected event. Response time was measured as the time between an actual slap attempt or pass and the time the subject responded by clicking the mouse. A response was considered an accurate hit if the response occurred within a half-second window around the time of the actual slap or pass plus the subject's average response time for accurate hits in that trial (determined iteratively).

Four different takes (separate video tapings) of each game, without unexpected events, were used to minimize familiarity with the action of the attended task. Each take had a 15-second lead-in for synchronization (with two bounces or finger snaps), followed by 60 seconds of play. In all cases, the attended game included 30 true passes or slap attempts, although that detail was not shared with the subject.

Three different unattended scenes with unexpected events ("UEs") were taped for each game. Only one take of each UE scene was needed. In one ballgame UE scene, about halfway through the play period, a man juggling three balls entered the scene at the right, strolled to the center of the ballgame, juggled in place for a few seconds, and strolled off to the left. Meanwhile, the ballplayers continued as usual, passing the ball 30 times during the minute of play (Figure 1).

In a second ballgame UE scene, about halfway through the minute of play, a woman strolled through, carrying an open umbrella. She was in the scene for about 8 seconds as the ballgame continued around her.

[1] Corresponding author: H. Apfelbaum, Schepens Eye Research Institute, 20 Stamford Street, Boston, MA 02114, (617) 912-2688, hla@eri.harvard.edu.

 ISSN/0005-0966X/05/3602-1398-$1.00+.00 

In a third ballgame UE scene, at about 20 seconds into play one of the players threw the ball out of the scene. The players continued to fake play for the next 20 seconds, as if they still had a ball. About 20 seconds before the end of play the ball was tossed back in and they then used it as usual.

The 3 handgame UE scenes all had the play interrupted briefly at about 20 seconds and again at 40 seconds. In one, the players shook hands. In another, they tossed a small ball back and forth, and in a third they played an odd/even finger choose-up game.

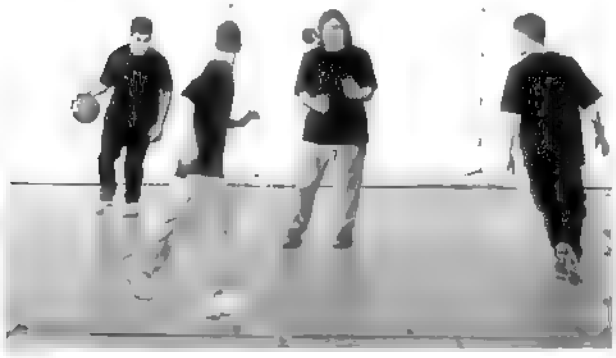

**Figure 1: An example of an unexpected event. A juggler strolls through the unattended ball game, pausing mid screen.**

## 2.2 Edge filter

A modified ValueVision filter (DigiVision, Inc, San Diego, CA) was used to produce cartoon-like edges-only video. The luminance component of the camcorder S-video signal was processed through the filter, using its bipolar binary mode [11]. The bipolar mode is unique to this modified filter. The nominal off-edge output of the filter is gray. Each detected edge is represented by both a positive-going and negative-going transition from the nominal value. Bipolar mode is especially effective in the superposition situation, as it ensures that edges will show against both light and dark backgrounds.

Figure 2a shows white and black edges on a field of gray produced by the edge filter. Figure 2b shows the effect of the bipolar edge scheme we employed, while Figure 2c shows that white-only edges are less visible.

## 2.3 Presentations

The play period of each presentation had a superimposition of a handgame scene and a ballgame scene. Either, neither, or both scenes might be edge filtered. The superimposition was performed with video editing software. If both scenes of a presentation were to be in full color (neither edge-filtered), they were simply mixed equally. If both were to be shown as edges only, track threshold settings selected just the white edges (i.e., those with video luminance higher than the nominal gray output of the filter) from the black-gray/white edge-filtered video of each scene and merged them, yielding the white edges from each scene over a black background.

If just one of the scenes was to be shown in edge-filtered mode, masks were used to let the color video through wherever the filtered video was gray, and otherwise showed the white or black edges. Contrast was set high in this process to preserve crisp edges.

In all, the experiment design called for the creation of 16 single-scene presentations and 124 overlaid presentations.

## 2.4 Experiment design

The experiment was balanced along several dimensions, requiring the testing of 36 subjects. Each subject was presented with a different combination and ordering of presentations. The subject watched the presentations on a 15"-diagonal TV monitor from about 1 m and responded via a mouse button. Together with the pseudo-randomized order of presentations, the design ensured that the experimenter did not know which trials included unexpected events and could not give subconscious cues to the subject.

The subjects viewed up to 26 trials, although only eight of those trials provided the data used in the analyses. In each trial, the subject was given instructions about the task, shown a presentation, and then asked follow-up questions. The subject was asked to click the mouse once for each of the synchronization bounces or snaps, and then once for each event (toss or slap attempt) in the subsequent game. The subject was told that the first several trials are just practice trials. The first four trials of a session familiarized the subject with the games, edge filtering, and overlaying, and provided practice at the attended tasks. No unexpected events were shown. The key trials were 5 through 12, all of which were overlaid presentations. Six of those trials included unexpected events, with each different UE scene shown only once. The randomized inclusion of two trials without unexpected events helped to reinforce the unexpectedness of the other trials and further blind the experimenter. The order of the

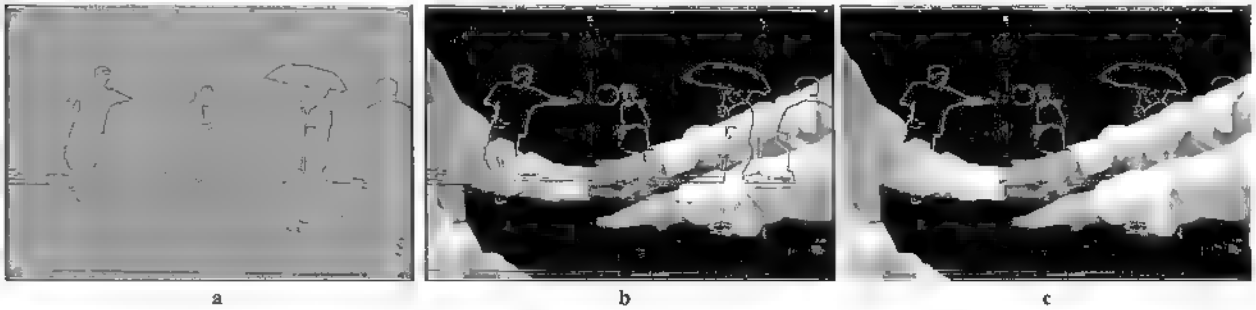

a b c

**Figure 2: (a) Raw edge filter output for the umbrella woman unexpected event, showing light and dark edge transitions. (b) Bipolar edges superimposed on a full-color scene. Note how the bipolar edges permit visibility of the edges over both very bright and very dark portions of the background image. (c) White edges alone are insufficient; visibility is minimized over bright areas.**

unexpected events appeared random, but was carefully balanced through the use of six different digram-balanced 6x6 Latin squares. Each row of a square identified the UE order for one session. All that the experimenter knew and told the subject was which game was to be attended.

Four possible edge-filtering combinations were used in the critical presentations: Full color attended and unattended scenes, full color attended scene and edge-filtered unattended scene; edge-filtered attended scene and full color unattended scene; and both attended and unattended scenes edge-filtered. Each of the first three combinations was used with each game's unexpected event trials in a session. Since the Edge/Edge combination is not of interest in the devices we are considering, it was used for the two trials that did not include unexpected events. The edge-filtering order was also balanced across sessions and pseudo-random within a session. Finally, the use of the four non-UE takes for each game was balanced and randomized, with each take used once as an attended scene in trials 5 - 12, and one take for each game used as the unattended scene in the two non-UE trials.

The introduction and first two questions asked after each trial presentation led the subject to believe that the purpose of the experiment was to determine how filtering affects the difficulty of the attended task, not that we were interested in how often unexpected events were noticed. The key question after each presentation was "Was there anything worth noting in the background video that was distracting or interfered with following the game?" Based on the response to that question, the experimenter scored the trial as an event detected correctly, detected partially, vaguely sensed, or unseen.

To ensure that detections were scored properly, questions asked after trial 12 mentioned each of the unexpected events and asked if the subject had noticed any of them but didn't think them worth mentioning. Descriptions of three plausible events that had not been shown were included to detect cheating. Then, each of the presentations with unexpected events the subject had not identified was shown again (optional trials 13 – 18), and the subject was instructed to watch, but not bother clicking the mouse. In most cases, all of those events were then noticed, and the subject was asked if the unexpected event had been seen on an earlier trial. Finally, for those events that the subject still hadn't identified, just the brief event portion of the scene was shown, in full color and without overlay, and the subject was asked if that had been seen on the first round of trials. Two scenes of the ballgame with unexpected events that had been mentioned after trial 12 but never seen were included to catch cheating (yielding optional trials 19 – 26). Since the experimenter was masked as to the unexpected events being shown, it was possible that the subjects' identifications of unexpected events were misinterpreted. After each session the experimenter had an opportunity to adjust the scoring of any trials that later questioning proved incorrectly marked.

## 2.5 Results

For all statistical analyses $p \leq 0.05$ was noted as indicating statistical significance.

Unexpected events were detected 123 (57%) of the 216 times they were shown in trials 5 - 12, as determined by immediate or later questioning. Figure 3 shows the number of subjects who detected a given number of unexpected events.

We found no significant effect of edge filtering on detection, $\chi^2(2, 216) = 0.79$, $p = 0.67$. Power analysis showed that we had a 24% chance of revealing a 10% difference in detection rates, 70% chance for 20% difference and 97% chance for 30% difference. Analyzed separately by game, we found no effect of edge filtering on the number of ballgame UEs detected, Cochran's $Q = 2.15$, $p = 0.34$, or on the number of handgame UEs detected, $Q = 0.09$, $p = 0.96$.

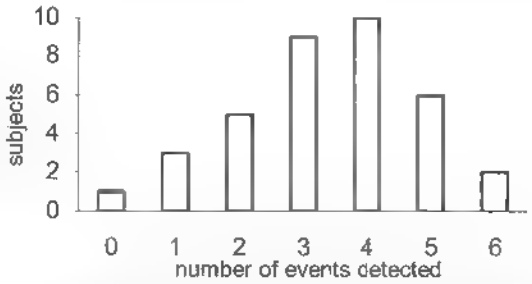


**Figure 3: Frequency of detection of unexpected events by subjects. Only 2 out of 36 subjects detected all 6 unexpected events.**

Edge filtering did affect response time, RMANOVA $F(3, 105) = 5.52$, $p < 0.001$, as shown in Table 1. $F_r$, Friedman analysis of variance by ranks, showed that hit accuracy, which averaged 96.7%, was not affected by filtering, $F_r = 1.2$, $p = 0.76$.

Attended handgame take showed no significant effect on hit accuracy, $F_r = 2.3$, $p = 0.52$, but attended ballgame take did, $F_r = 10.1$, $p = 0.018$. This was likely due to the difficulty of seeing a pass when a player in the foreground obscured it; it took longer for subjects to realize that a pass occurred.

**Table 1: Effect of filtering on attended task response time in msec. (±std dev). Response time to the attended task improved if the unattended task was filtered and degraded if the attended task was filtered.**

| | | Unattended Scene: Full color | Unattended Scene: Edge filtered |
|---|---|---|---|
| Attended Scene | Edge filtered | 532 (±84) | 522 (±96) |
| Attended Scene | Full color | 500 (±97) | 496 (±100) |

Handgame and ballgame take both affected response time, RMANOVA $F(3, 105) = 22.7$, and 82.2, respectively, $p < 0.001$.

Unexpected event scene had a strong affect on detectability $\chi^2(5, 216) = 54.8$, $p < 0.001$. Table 2 shows the detection rate by scene. Response time was not affected by handgame UE scene RMANOVA $F(2, 70) = 0.43$, $p = 0.65$, nor ballgame UE scene, $F(2, 70) = 0.35$, $p = 0.71$. Similarly, hit rate was not affected by

ballgame UE scene, Fr = 2 05, p = 0.36, and perhaps marginally by handgame UE scene, Fr = 3 84, p = 0 15 Some subjects commented that some of the handgame motions were particularly distracting.

**Table 2: Frequency of detection by treatment and event type, out of 12 trials each.**

| Att'd/Unatt'd | Full/Full | Full/Edge | Edge/Full |
|---|---|---|---|
| Juggler | 10 | 7 | 10 |
| Lost ball | 3 | 2 | 2 |
| Umbrella | 8 | 8 | 3 |
| Choose-up | 9 | 10 | 9 |
| Handshake | 4 | 3 | 4 |
| Ball toss | 10 | 10 | 11 |

## 3. *Discussion*

Finding no effect of edge filtering on unexpected event detection was somewhat disappointing, as we hoped that using edge filtering would help a low-vision user of an augmented vision system notice hazards. We are encouraged, however, by the degree that edge filtering of one of two overlaid scenes does help distinguish them, as evidenced by the shorter reaction times of the Full/Edge condition, as this should make it easier to switch attention between them at will. The differences in detectability of the various unexpected events we used may help identify effective scanning and training techniques that could be used with the low vision aids we are developing, but that will require considerably more study.

While we did not test subjects with white-only edges in addition to bipolar edges, it is immediately apparent that the bipolar edges are easier to see, especially against the white sleeves of the handgame players. The fact that the edges appear white in some places and black at others apparently did not disturb the subjects. Indeed, no one even mentioned noticing the shift.

Augmented displays of the type described in [2, 6, 13, 14] can not benefit from bipolar edges, as the video image is strictly additive; where the see-through view is bright, the augmented view can not superimpose black. That is not the case in a purely video configuration, as in [4] and this study, so there may be reason to pursue a video "see-through" HMD configuration instead of using an optical see-through technique.

## 4. *Acknowledgments*

Supported in part by NIH grant EY12890 and by DOD grant W81XWH-04-1-0892. We thank Prof. U. Neisser for providing videotaped examples from his experiments, E. M. Fine for design and analysis advice, J. Barabas for videography, the Levinthal-Sidman JCC for use of the basketball court, the ballplayers recruited from the JCC staff, the handgame players from our group at Schepens, and C. Simmons for juggling.

## 5. *References*

[1] R. Becklen and D. Cervone, "Selective looking and the noticing of unexpected events," Memory & Cognition, 11/6, 601-608 (1983).

[2] A.R. Bowers, G. Luo, N.M. Rensing and E. Peli, "Evaluation of a prototype minified augmented-view device for patients with impaired night vision," Ophthalmic and Physiological Optics, 24/4, 296-312 (2004).

[3] J. Braun, "It's great but not necessarily about attention," Psyche, an Interdisciplinary Journal of Research on Consciousness, 7(6) Mar 2001, Australia (2001).

[4] R. Goldstein, H. Apfelbaum, G. Luo and E. Peli, "Dynamic magnification of video for people with visual impairment," SID 2003, Society for Information Display, 1152-1155 (2003).

[5] R.F. Haines, A Breakdown in Simultaneous Information Processing, in Presbyopia Research: From Molecular Biology to Visual Adaptation, 171-175 (Plenum, New York, 1991).

[6] G. Luo and E. Peli, "Kinematics of visual search by tunnel vision patients with augmented vision see-through HMD," SID 2004: Society for Information Display, 1578-1581 (2004).

[7] A. Mack and I. Rock, Inattentional Blindness: MIT Press/Bradford Books series in Cognitive Psychology (Cambridge, MA, US: The MIT Press, (1998). xiv, 273pp., 1998).

[8] S.B. Most, D.J. Simons, B.J. Scholl, R. Jimenez, E. Clifford and C.F. Chabris, "How not to be seen: The contribution of similarity and selective ignoring to sustained inattentional blindness," Psychological Science, 12/1, 9-17 (2001).

[9] U. Neisser and R. Becklen, "Selective looking: Attending to visually specified events," Cognitive Psychology, 7, 480-494 (1975).

[10] E. Peli, "Vision multiplexing: an engineering approach to vision rehabilitation device development," Optometry and Vision Science, 78/5, 304-315 (200.).

[11] E. Peli, "Feature detection algorithm based on a visual system model," Proceedings of the IEEE, 90.1, 78-93 (2002).

[12] D.J. Simons and C.F. Chabris, "Gorillas in our midst: Sustained inattentional blindness for dynamic events," Perception, 28/9, 1059-1074 (1999).

[13] F. Vargas-Martin and E. Peli, "Augmented view for tunnel vision: Device testing by patients in real environments," SID Symposium Digest of Technical Papers, 32/1, 602-605 (2001).

[14] F. Vargas-Martin and E. Peli, "Augmented view for restricted visual field: multiple device implementations," Optometry and Vision Science, 79/11, 715-723 (2002).

Appendix 1, #2

ABSTRACT

Neisser & Becklen[1] identified inattentional blindness, the *inability* of observers to maintain awareness of events in more than one of two superimposed scenes. The ability of the brain to make use of such multiplexed visual information and avoid confusion is central to the utility of many augmented vision devices, such as see-through head-mounted displays and head up displays. We are developing a number of such devices as aids for people with vision impairments. The constraints imposed by visual or perceptual phenomena such as binocular or perceptual rivalry and inattentional blindness may limit the utility of these devices. It is possible that specific aspects of the display format might affect these phenomena. Specifically, if the two scenes are easier to separate they may not rival to the same degree.

In this study we investigated the effect of edge filtering on inattentional blindness and the ability to follow superimposed/multiplexed scenes. We closely reproduced parts of the original Neisser & Becklen experiment, and then treated one or both of the video scenes with edge filtering to create a cartoon-like image. The special bipolar edge filtering produced white and black contours at each luminance edge, facilitating clear uninterrupted visibility
of the edge-filtered scene over bright and dark sections of the other scene.

36 normally-sighted young adults viewed superimposed videos that included 6 trials with

unexpected events, while attending scenes that did not have the events. Edge filtering was applied to the attended scene in two of the trials and to the unattended scene in two trials. We found no evidence that edge filtering affected the detection of unexpected events. Filtering the attended scene reduced performance of the attended task slightly, while filtering the *un*attended scene did not significantly affect performance of the attended task, as measured by response time to actions in the attended scene. We were able to see a small priming effect, with later unexpected events detected more easily after the first had been detected.

# Appendix 2

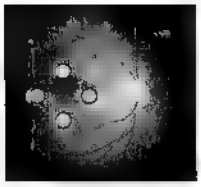

**Figure 1. Photomicrograph of a human eye fundus to show position of the laser burn in the mouse eye.**

# Appendix 2

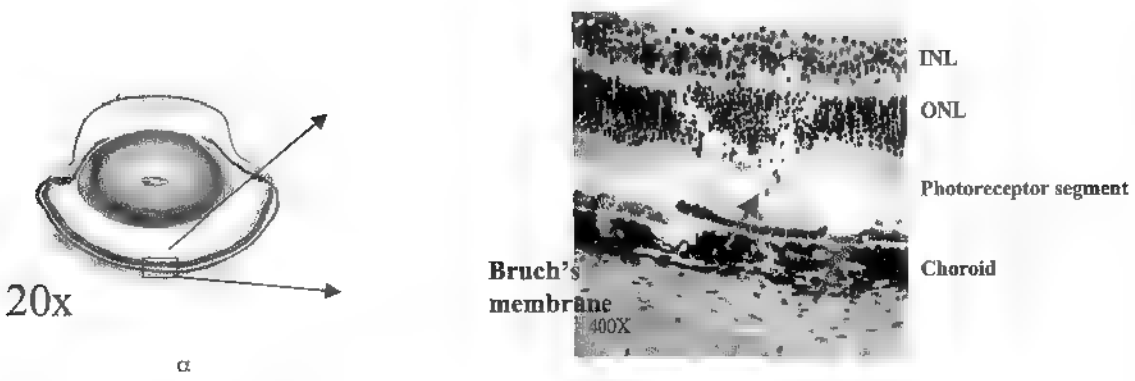


**Figure 2. Right panel: Damage caused by the retinal laser burn. Left panel: photomicrograph of a mouse eye stained with H& E. Inset square is position where the photomicrograph was taken on the right. The right panel shows a high magnification of the area where the burn occurred.**

# Appendix 2

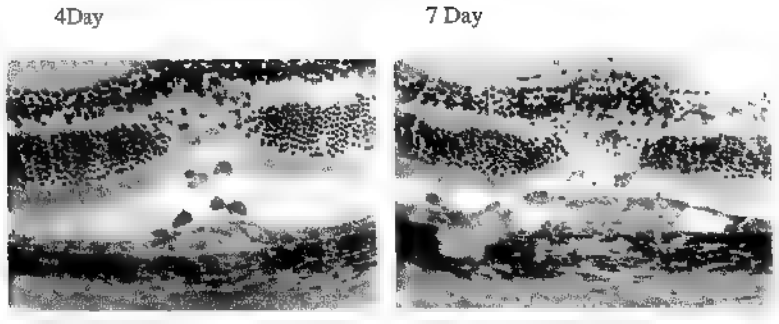


**Figure 3. Time course of retinal laser burn. Left panel shows the burn 4 days post retinal laser burn, the injury is seen in the ONL. Note that some RPE cells appear to move toward the ONL to repair the injury (blue arrow) while other RPE seem to have lost their pigment (yellow arrow). The right panel shows the condition of the retinal laser burn after 7 days. The RPE moved further into the ONL (blue arrow). Now there is also lost of pigment in both the RPE and choroid (yellow arrow). Many of the choroids vessels are dilated (green arrow) demonstrating the persistence of the laser-induced inflammation.**

# Appendix 2

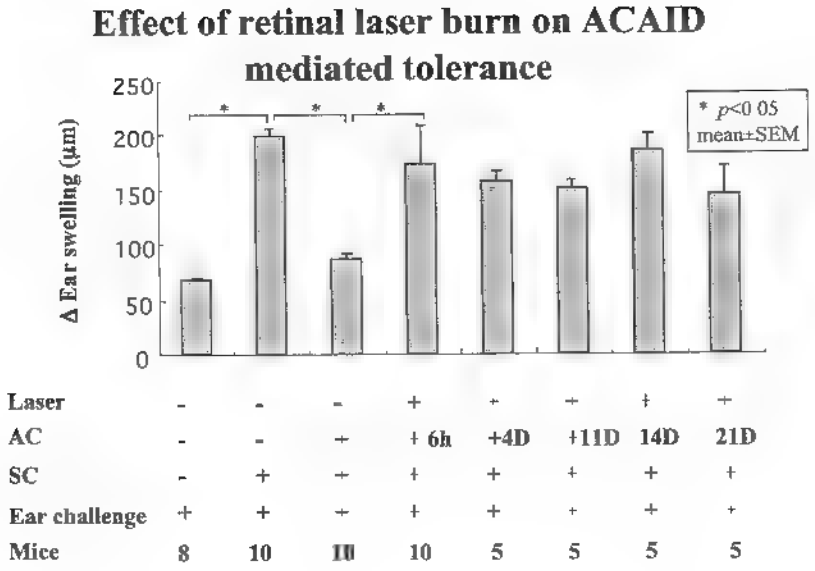


**Figure 4. Effect of retinal laser burn on ACAID suppression of Delayed Hypersensitivity response in the ear. The ordinate represents the increase in ear swelling as measured by an engineer's micrometer. The treatment that each of the animal groups received is listed under the abscissa. AC, represents anterior chamber inoculation; SC, subcutaneous; Ear challenge was with 10$\mu$ of Ovalbumin in PBS at a concentration of 20mg / ml. Twenty-four hours later the ears were measured and change in thickness compared to the size of the ear pinnate before challenge.**

# Appendix 2

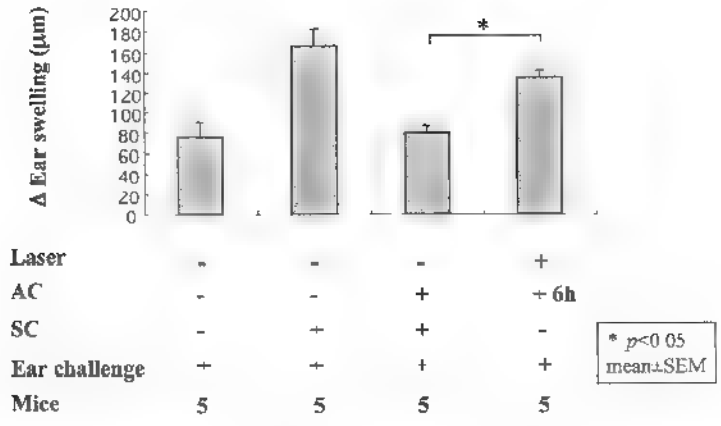


**Figure 5. Effect of retinal laser burn on ability to immunize via the eye.**
**The ordinate shows the change in ear swelling induced by challenge with antigen.**
**The treatment of the experimental animal groups is listed below the abscissa.**

Appendix 2

**Figure 6- 24 hrs after laser burn**

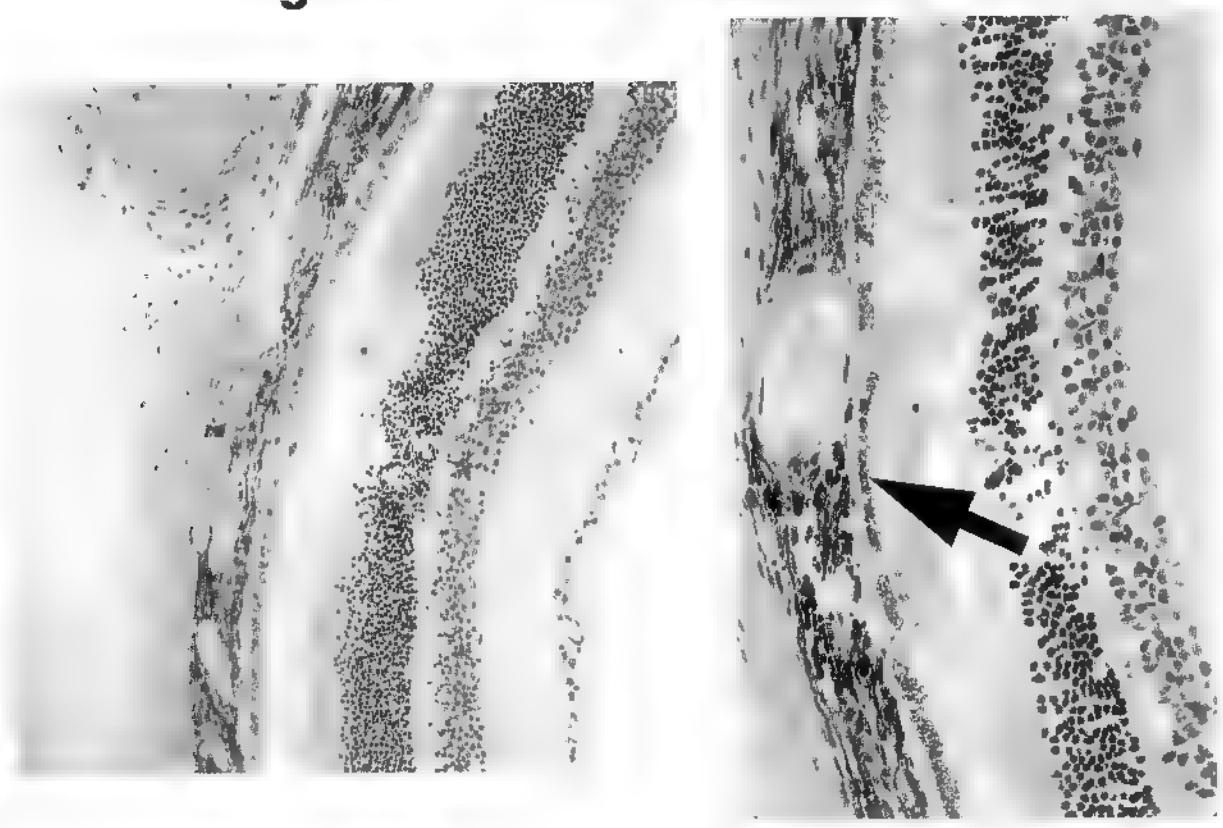

Appendix 2

**Figure 7- 24 hrs after laser burn**

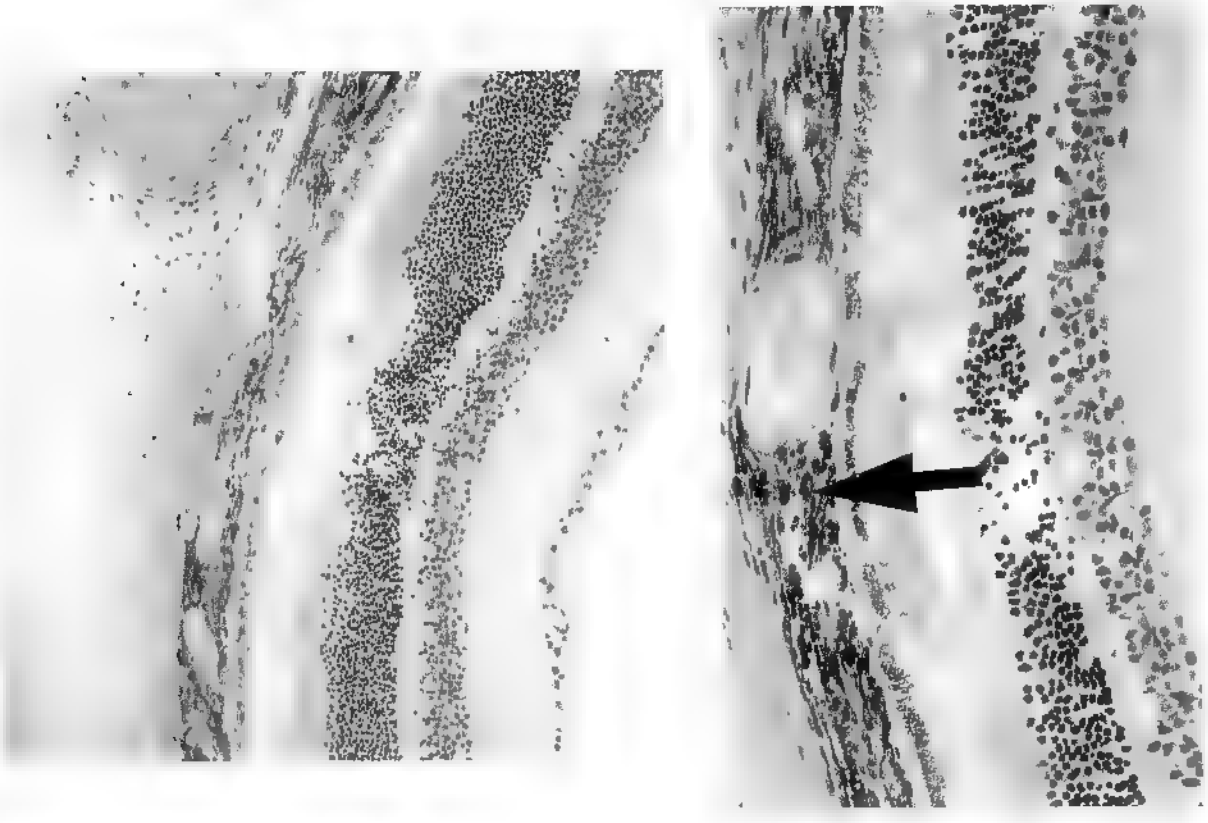

Appendix 2

**Figure 8- 24 hrs after laser burn**

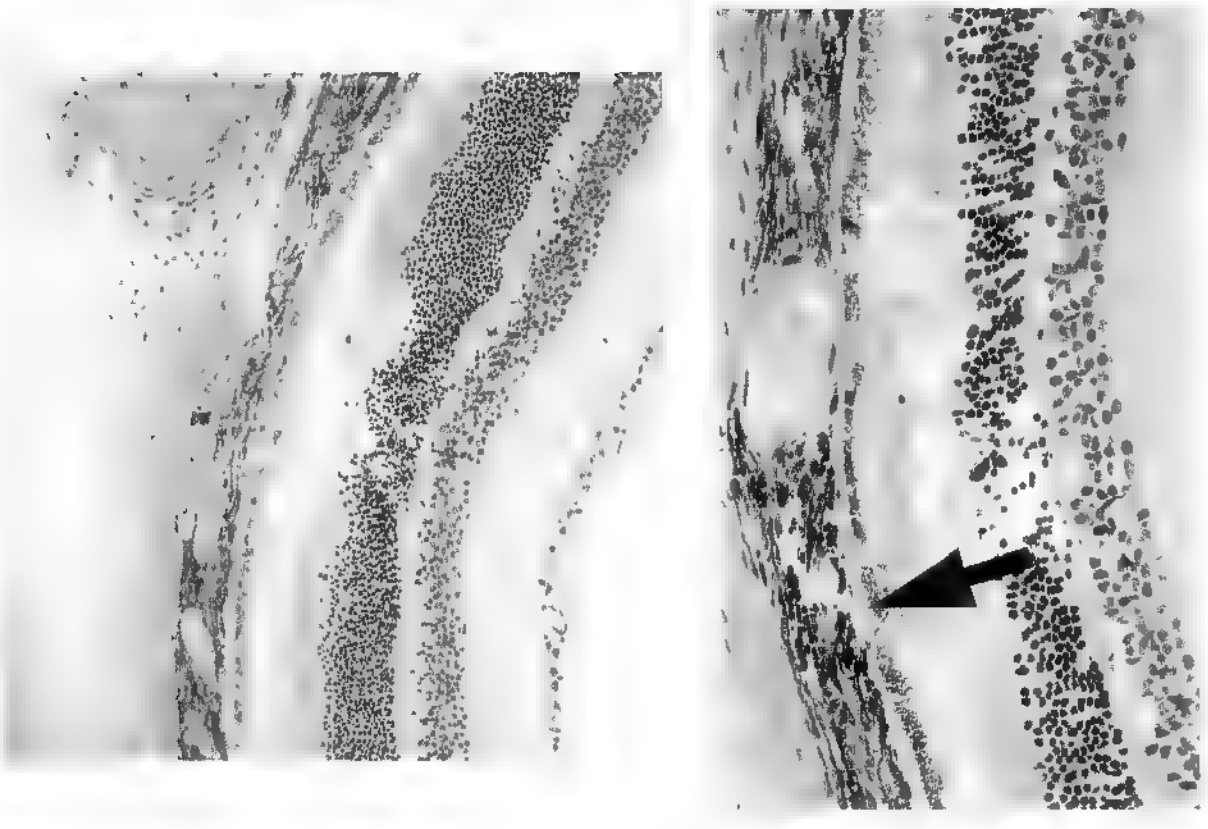

Appendix 2

**Figure 9- 24 hrs after laser burn**

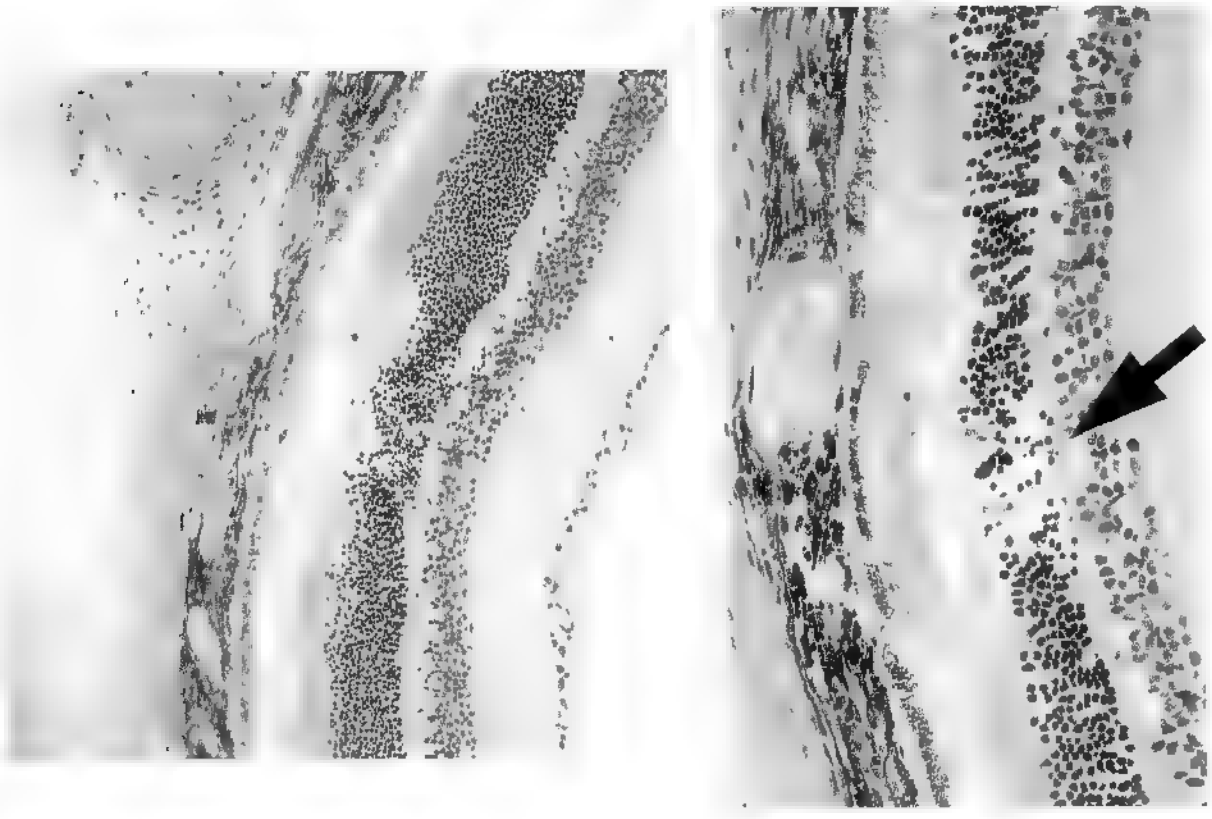

Appendix 2

## Figure 10 - 72 hrs after laser burn

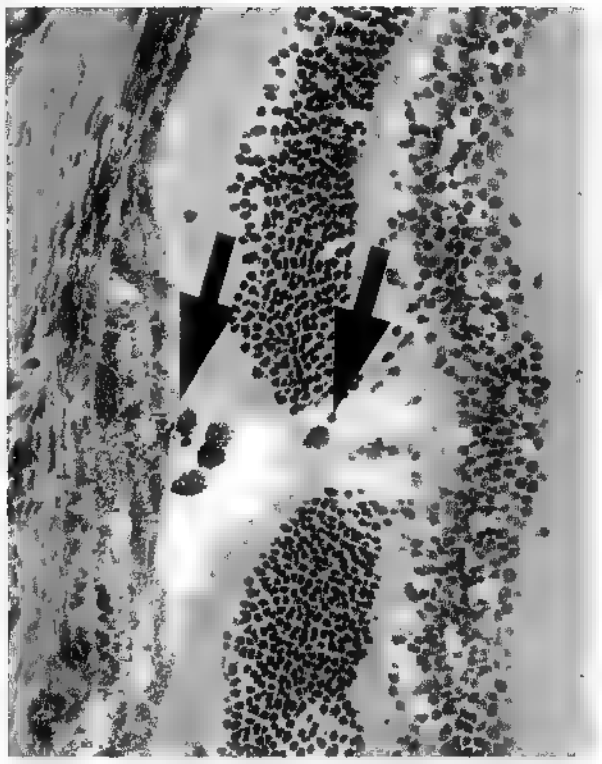

Appendix 2

## Figure 11-

## αB-Crystallin in the posterior segment

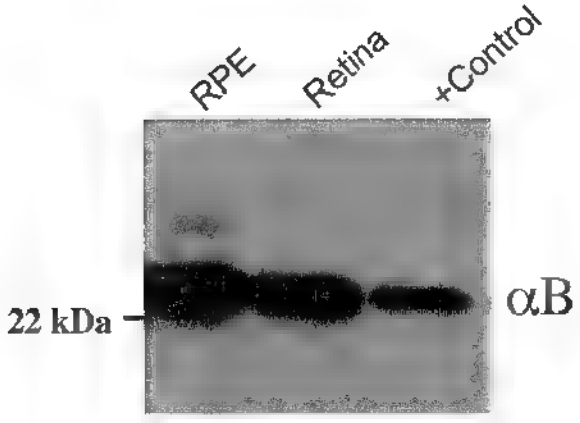

Appendix 2

# Figure 12-
# αB-Crystallin expression in the retina

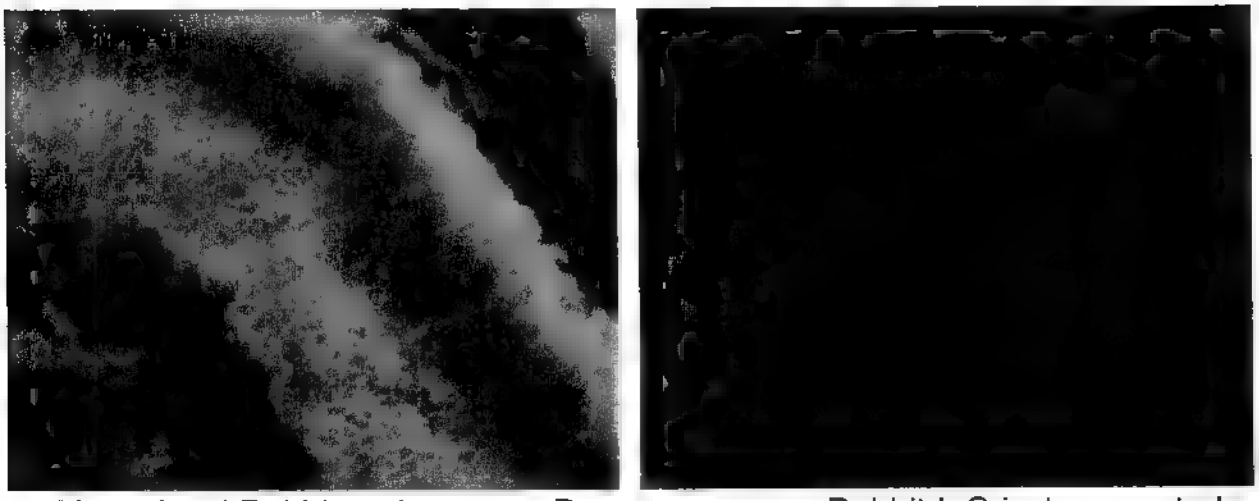

Monoclonal Rabbit anti-mouse αB

Rabbit IgG isotype control

**αB: green**

**Nuclear stain: red**

Appendix 3

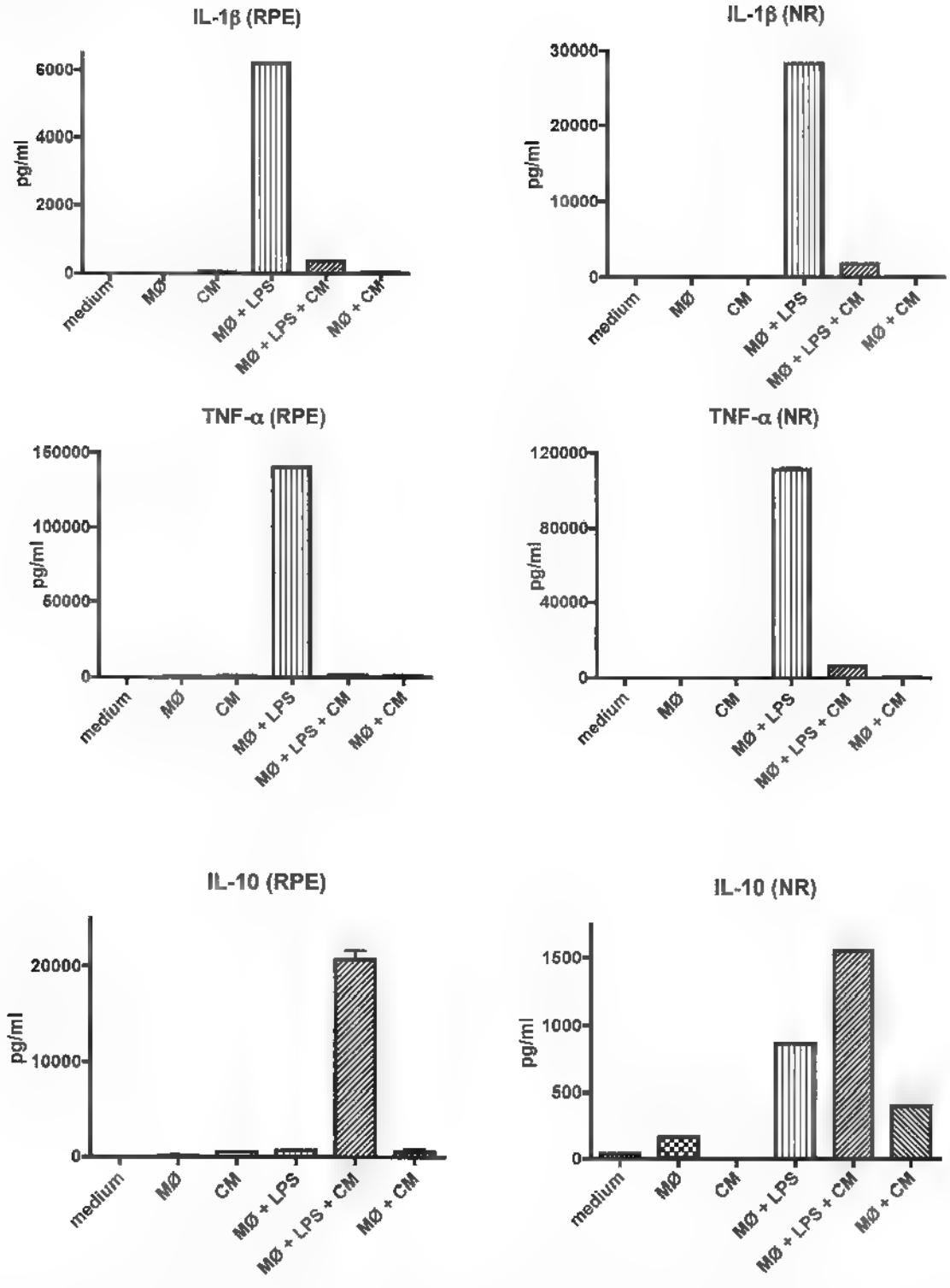


**Figure 1.** The effects of healthy neural retinal (NR) and retinal pigmented epithelial cell eye cup (RPE) conditioned media (CM) on macrophages (MØ) activated with or without endotoxin (LPS). The supernatants of cultured macrophages treated with NR or RPE conditioned media plus 1 μg/ml of LPS were assayed using a multiplex analysis for IL-1beta, TNF-alpha and IL-10 simultaneously. Presented are the mean ± standard error of 5 eyes.

Appendix 3

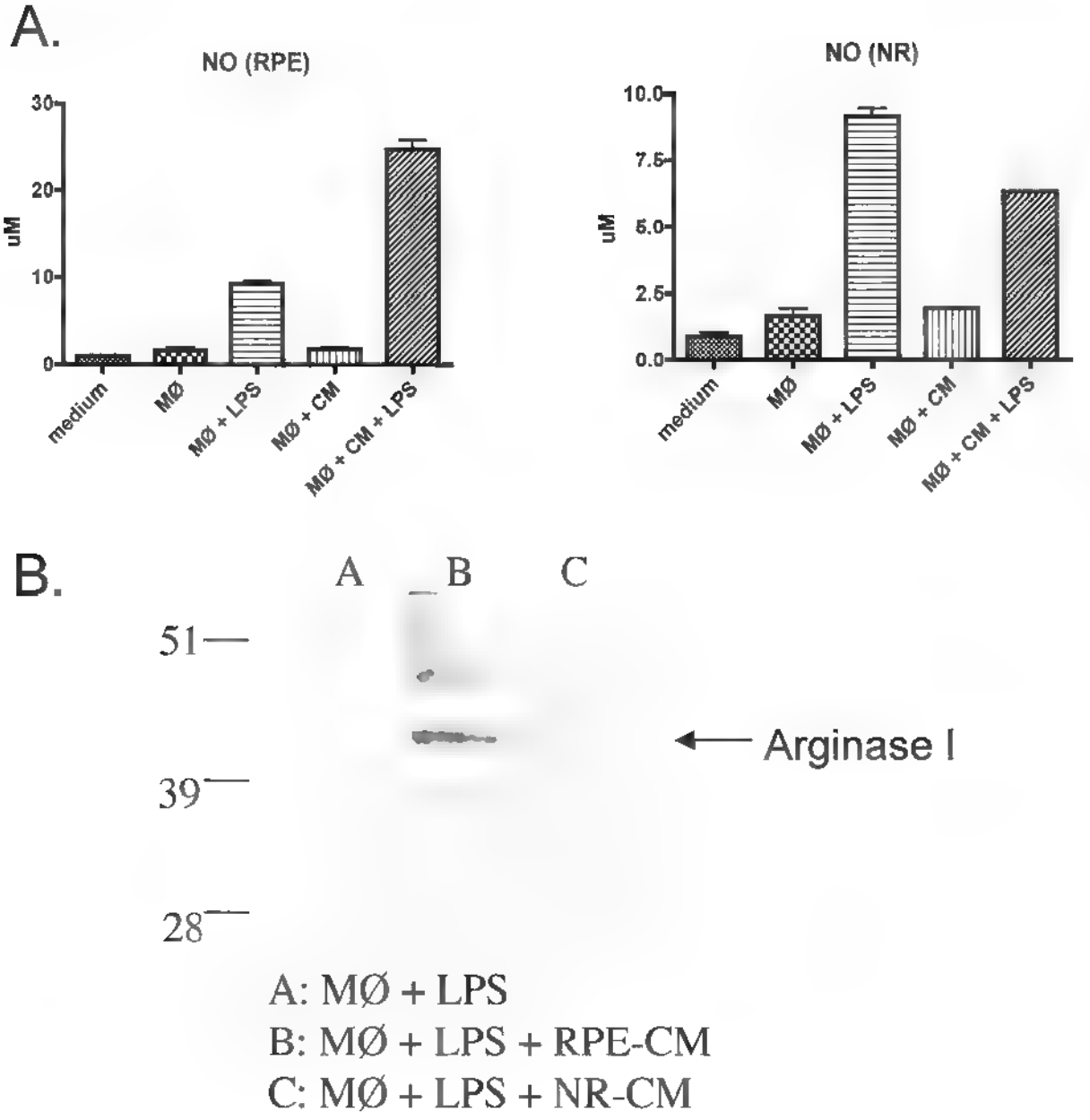


**Figure 2.** The effects of the conditioned media on LPS-stimulated Nitric Oxide (NO) generation and Arginase I expression. A. Macrophages were stimulated with LPS and treated with the conditioned media as described in Figure 1 and the methods. The 24 hour macrophage culture supernatants were assayed with Griess reagent for Nitric Oxide. Presented are the mean ± standard error of 5 eyes. B. This is an immunoblot of lysates of condition media treated, LPS-stimulated macrophages separated by electrophoresis, and transferred to nitrocellulose filter. The nitrocellulose filter was probed using a goat anti-mouse Arginase I antibody, followed by an alkaline phosphatase-conjugated anti-Goat IgG antibody. The bands observed after adding substrate were digitally imaged and presented in the figure. This is representative of two experiments with the same result.

Appendix 3

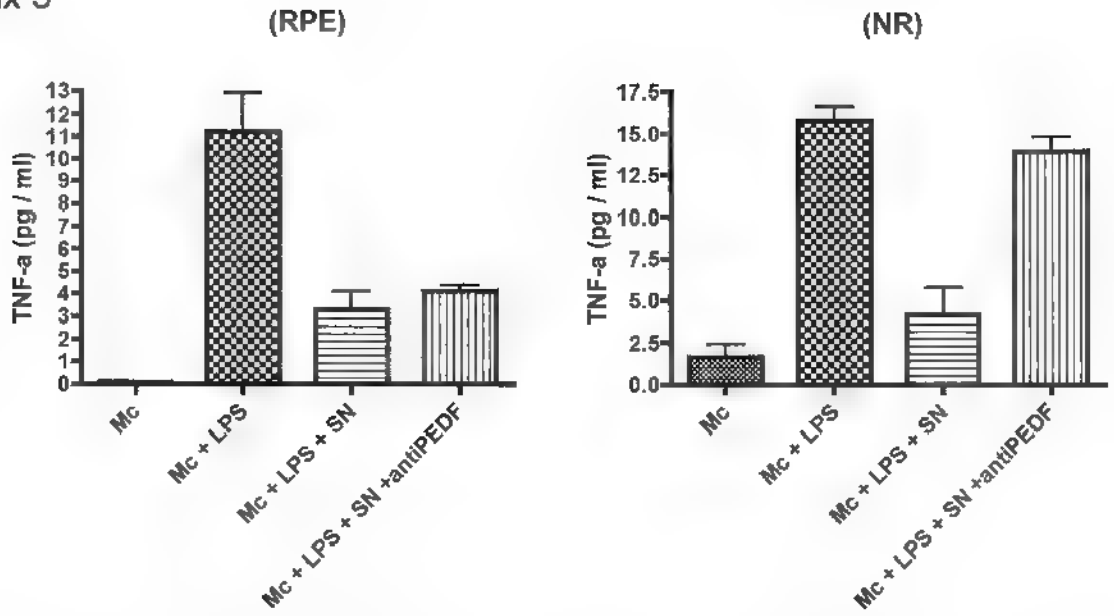


**Figure 3.** The effects of neutralizing PEDF in the condition media on the condition media suppression of TNF-alpha production by LPS-stimulated macrophages. The experimental methods were the same as in Figure 1; however, anti-PEDF was added to the conditioned media. Only TNF-alpha production by the LPS-stimulated macrophages was affected by neutralizing PEDF. Presented are the mean ± standard error of 5 eyes.

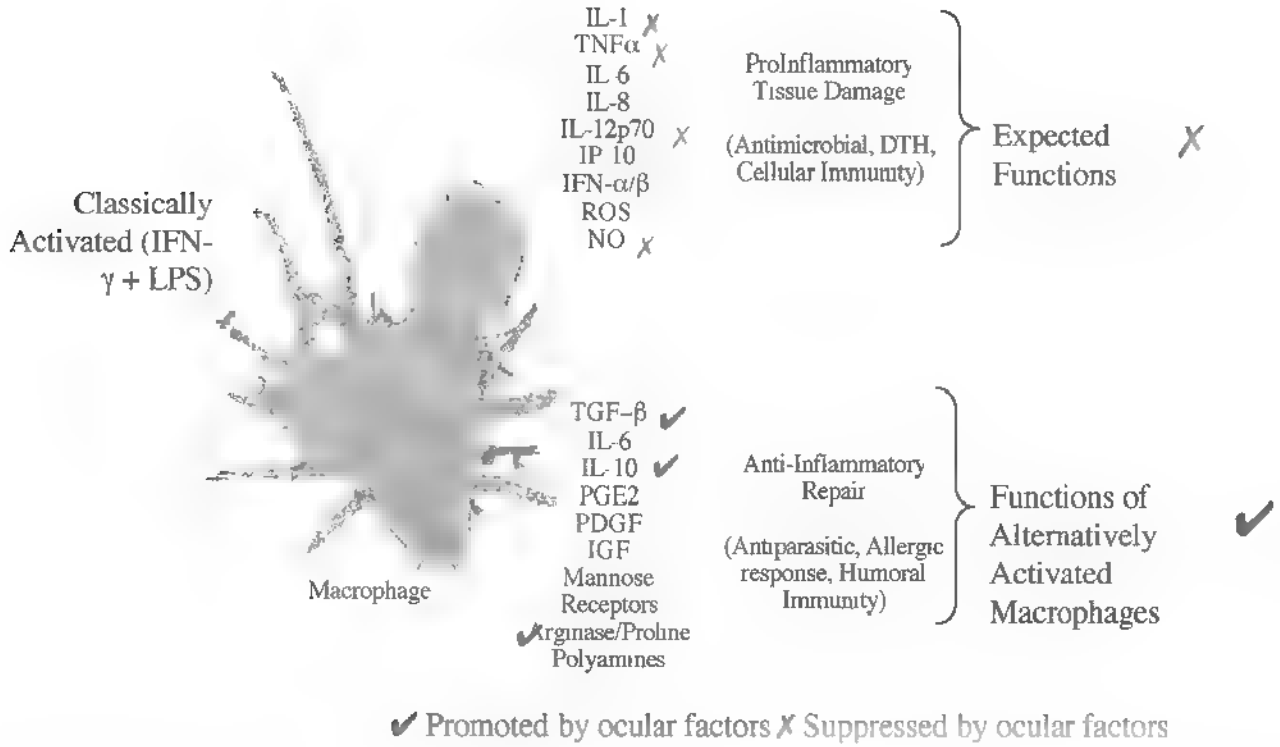


**Figure 4.** Summary of results. The factors produced by the RPE and NR released into the condition media promote an alternative activation of the macrophage away from the expected pro-inflammatory activity mediated by LPS to the alternative response of anti-inflammatory, wound repairing activity.

# Thrombospondin Plays a Vital Role in the Immune Privilege of the Eye

*Parisa Zamiri,*[1] *Sharmila Masli,*[1] *Nobuyoshi Kitaichi,*[1] *Andrew W. Taylor,*[1] *and J. Wayne Streilein*[1,2]

**Purpose.** The role of thrombospondin (TSP)-1 in TGF-β activation and T-cell suppression was studied in the retinal pigment epithelial (RPE) cells, a monolayer of pigmented cells that line the subretinal space, an immune-privileged site in the eye

**Methods.** Posterior eyecups were prepared by excising the anterior segment, lens, and retina from enucleated eyes of C57BL/6, thrombospondin-1 knockout (TSP-1KO), and TGF-β2 receptor II double-negative (TGF-β2 RII DN) mice, leaving behind a healthy monolayer of RPE resting on choroid and sclera. Serum-free medium was added to these RPE eyecups, and, after various time intervals, supernatants (SNs) were removed and tested.

**Results.** SNs of an ex vivo culture of RPE cells from C57BL/6 mice were shown to inhibit both antigen and anti-CD3 activation of T cells, partially due to constitutive production of TGF-β and to the ability of RPE to activate the latent form of TGF-β. Activation of TGF-β was entirely dependent on TSP-1, also produced by RPE. SNs of RPE from TSP-1KO mice failed to inhibit T-cell activation. Ovalbumin (OVA)-specific delayed hypersensitivity (DH) was not impaired when OVA was injected either into the subretinal space or into the anterior chamber of TSP-1KO mice before OVA immunization. Moreover, experimental autoimmune uveoretinitis was significantly more intense in eyes of TSP-1KO mice and failed to undergo spontaneous resolution unlike wild-type mice

**Conclusions.** Production of both TSP-1 and active TGF-β by RPE is essential to the creation and maintenance of immune privilege in the subretinal space and that the immune privilege limits the severity and duration of retinal inflammation due to autoimmunity. (*Invest Ophthalmol Vis Sci.* 2005;46:908–919) DOI:10.1167/iovs.04-0362

Ocular immune privilege is believed to be an important physiological adaptation of the eye that prevents innate and adaptive immune responses from destroying precious ocular cells that are essential for vision and are incapable of regeneration. The immune privilege also prevents immunologically induced inflammation from clouding the ocular media and distorting the visual axis, for when the ocular cells die and/or the visual axis is disrupted, loss of vision (blindness) is the inevitable consequence. Some of the mechanisms that allow the presence of immune privilege in the eye are understood. These include (1) immune deviation to antigens injected into all ocular compartments, the anterior chamber, the subretinal space, and the vitreous cavity; (2) the presence of an immunosuppressive microenvironment in these compartments; and (3) the prolonged survival of solid-tissue allografts placed within ocular compartments.[1] Failure of ocular immune privilege has been associated with disease formation and progression. A notable example is herpes simplex keratitis,[2] an immunopathogenic disease that leads to corneal scarring.

Most studies of ocular microenvironments have concentrated on the properties of the aqueous humor that fills the anterior chamber of the eye. Less attention has been paid to the parenchymal cells in the eye and their contribution to immunosuppressive microenvironments. Recently, our laboratory demonstrated that ocular pigment epithelia of iris, ciliary body, and retina inhibits T-cell proliferation in vitro. Unlike the pigment epithelium of the iris, retinal pigment epithelium (RPE) inhibited T-cell proliferation through soluble factors.[3,4] In the experiments to be described, we sought to determine some of the factors and mechanisms that are responsible for the ability of RPE to inhibit T-cell activation in vitro. We further wanted to determine whether there is a correlation between the T-cell inhibitory capability of RPE and the presence of immune privilege in the posterior segment of the eye.

RPE is a neuroepithelial layer of pigmented cells that lines the outermost boundary of the retina and forms the posterior border of the subretinal space, an immune privileged site in the posterior segment of the eye. The RPE is strategically placed, not only to act as an immunologic barrier by providing the outer blood–retinal barrier, but also by expressing cell surface molecules and by secreting soluble mediators that influence the immune system.[5]

To evaluate the immunomodulatory properties of RPE, we have devised an in vitro experimental system composed of an intact monolayer of RPE (RPE eyecup) resting on the choroid and the sclera. The reasons for this approach are several: (1) The presence of immune privilege in the subretinal space is largely dependent on the presence of an intact and healthy monolayer of the RPE[6]; (2) RPE cells are polarized in vivo and secrete many factors in a polarized manner[5], and (3) cultured monodisperse RPE cells can behave differently from RPE in intact monolayers, both in physical characteristics and in secretory behavior.[7,8]

Our results indicate that the apical surface of RPE in a posterior eyecup constitutively elaborated immunosuppressive factors such as TGF-β that profoundly inhibit T-cell activation in vitro. Thrombospondin (TSP)-1, also produced by RPE, appeared to play a central role in converting latent TGF-β into its active, immune inhibitory form. Eyes of TSP-1 knockout (TSP-1KO) mice with genetic deficiency of TSP-1 failed to promote immune deviation and displayed exaggerated and unresolved experimental autoimmune uveoretinitis (EAU)

From the [1]Schepens Eye Research Institute, Department of Ophthalmology, Harvard Medical School, Boston, Massachusetts

[2]Deceased March 15, 2004

Supported by National Eye Institute Grants EY09595, EY05678, and EY10752, and by a grant from the Massachusetts Lions Eye Research Fund

Submitted for publication April 1, 2004; revised September 20, 2004; accepted November 10, 2004

Disclosure: **P. Zamiri**, None; **S. Masli**, None; **N. Kitaichi**, None; **A.W. Taylor**, None; **J.W. Streilein**, None

The publication costs of this article were defrayed in part by page charge payment. This article must therefore be marked "*advertisement*" in accordance with 18 U.S.C. §1734 solely to indicate this fact.

Corresponding author: Joan Stein-Streilein, Schepens Eye Research Institute, 20 Staniford Street, Boston, MA 02114; jsoffice@vision.eri.harvard.edu

## METHODS

### Animals

Adult male C57BL/6 and DO11.10 mice aged 6 to 10 weeks were obtained from Taconic Laboratories (Germantown, NY) and Jackson Laboratories (Bar Harbor, ME), respectively. TSP-1KO mice were a generous gift from Jack Lawler (Beth Israel Deaconess Medical Center, Boston, MA) and transforming growth factor-β receptor II double negative (TGF-β RII DN) mice were kindly donated by Ron Gress (National Cancer Institute, Bethesda, MD). Mice were housed in a common room of the vivarium. All experimental procedures conformed to the ARVO Statement for the Use of Animals for Ophthalmic and Vision Research.

Inoculations, injections, and clinical examinations were performed under anesthesia induced by intraperitoneal injection of ketamine (Ketalar; Parke Davis, Paramus, NJ) at 0.075 mg/g of body weight and xylazine (Rompun, Phoenix Pharmaceutical, St. Joseph, MO) at 0.006 mg/g of body weight. Enucleation of eyes and removal of spleen and lymph nodes were performed after the animals were euthanatized.

### Preparation of Posterior Eyecups

Eyes from euthanatized C57BL/6 or TSP-1KO mice were enucleated and placed in $Ca^{2+}/Mg^{+}$ free HBSS on ice for 30 minutes. After excision of the muscles, connective tissue, and conjunctiva, a circumferential incision was performed below the level of the ciliary body, and the remainder of the anterior segment (cornea, iris, ciliary body, and lens) was discarded. The remaining tissue was placed in 0.01 U/mL of chondroitinase ABC[9] for 30 minutes at 37°C, placed on ice, and washed three times in HBSS. The neural retina was gently lifted off the RPE layer by microsurgical forceps. Neural retina–deficient posterior eyecups, consisting of sclera, choroid, and a healthy monolayer of RPE, were studied by placing them in individual wells of microculture plates (S plate; Nunc Laboratories, Naperville, IL). The RPE eyecups were partially submerged in serum-free medium (SFM, RPMI 1640, 0.1 M HEPES, 0.1% bovine serum albumin, 1 μg/mL iron-free transferrin, 10 ng/mL linoleic acid, 0.3 ng/mL $Na_2Se$, and 0.2 μg/mL Fe $(NO_3)_3$ for further experimentation. Into each eyecup 10 μL of the SFM medium was placed. Unless otherwise stated, the RPE supernatant (SN) from within the eyecup was removed 24 hours after incubation and further diluted 1:10 in serum-free medium. The diluted SN was then used in the assays. In all studies, the final dilution of SN was 1:40.

### Cultures of Monodisperse RPE Cells

Eyes from adult C57BL/6 mice were enucleated and placed in HBSS on ice for 3 hours. The anterior segment and neural retina were then excised and discarded. The remainder of the posterior segment of the eye was incubated with 0.2% trypsin (BioWhittaker, Walkersville, MD) for 1 hour at 37°C. The eyecups were washed, and the RPE microaggregates were removed. A single-cell suspension, formed by repeated pipetting of microaggregates of RPE, was seeded on six-well plates (Corning-Costar, Corning, NY) in modified DMEM (with 0.1 M HEPES, 20% FCS, 1% L-glutamine, 100 U/mL penicillin, 100 μg/mL streptomycin, and 1% nonessential amino acid [NEAA]), passed once, and cultured until confluence.

### DO11.10 T-Cell Proliferation Assay

T cells from DO11.10 mice express a transgenic T-cell receptor that recognizes ovalbumin (OVA) peptide fragment 323-339 in the context of $I\text{-}A^{d}$.[10] DO11.10 mice were euthanatized, and their lymph nodes were removed. DO11.10 lymph node cells (LNCs, $4 \times 10^5$) in a volume of 25 μL were placed in wells of a 96-well round-bottomed plate (Corning-Costar). SNs of RPE eyecups were collected after appropriate intervals and diluted 1:10 in SFM. DO11.10 LNCs were suspended in the diluted SN, plus 50 μg/mL OVA (Sigma-Aldrich, St. Louis, MO) in a volume of 25 μL and incubated for 96 hours at 37°C. [$^3$H]thymidine (0.5 μCi, NEN Life Sciences Products, Boston, MA) was added to each well on day 4 and incubated overnight. Thymidine uptake was assessed as a measure of T-cell proliferation. Positive control wells contained DO11.10 LNCs and OVA, and negative control wells contained only DO11.10 LNCs. To assess the role of TGF-β, some experimental wells also received either anti-pan TGF-β antibody (R&D Systems, Minneapolis, MN) alone or in combination with soluble TGF-β receptor II (R&D Systems). Three replicate wells were used for each time point, and the experiment was repeated three times.

### Anti-CD3 T-Cell Activation Assay

Spleens and lymph nodes were removed from naïve C57BL/6 mice. T cells were enriched with CD3-enrichment columns (R&D Systems). T cells ($4 \times 10^5$) were added to the wells of 96-well round-bottomed plates at the volume of 25 μL per well (Corning-Costar) together with anti-TCR antibody (2C11, 1 μg/mL [ATCC]) and 50 μL of 1:10 diluted SN of RPE eyecups prepared from the eyes of C57BL/6 or TSP-1KO mice. Some of the cultures were incubated for 24 hours, and 0.5 μCi [$^3$H]thymidine (NEN Life Sciences Products) was added to the wells. The cultures were incubated for a further 24 hours and [$^3$H]thymidine uptake was then measured. Other culture wells were incubated for 48 hours, after which their SNs were removed and used in IFN-γ ELISA assays to measure the amount of IFN-γ produced by T cells.

### Quantification of TGF-β

The concentration of TGF-β in the SNs of RPE eyecups was measured with the standard Mv1Lu (CCL-64, ATCC, Manassas, VA) mink lung epithelial cell proliferation inhibition assay.[11] Before the assay, aliquots of RPE SN underwent transient acidification by addition of 5 μL of 1.0 N HCl to every 100 μL of 1:10 diluted SN of RPE eyecups, lowering the pH to ~2. The acid-treated SN was incubated for 1 hour at 4°C. The acid was neutralized by adding 10 μL of a 1:1 mixture of NaOH (0.01 M) and HEPES (0.04 M, pH 7.4). Acid neutralization was confirmed by samples of the SN's turning the pH indicator paper to the color that indicates 7.4 pH.

Mv1Lu cells from subconfluent cultures were incubated with a serial dilution of unmodified or acid-treated SN of RPE eyecups in 96-well flat-bottomed microtiter plates (Fisher Scientific, Pittsburgh, PA) in EMEM (Invitrogen-Gibco, Gaithersburg, MD) supplemented with 0.05% fetal calf serum. Cultures were incubated for 20 hours at 37°C. At this time 0.5 μCi [$^3$H]thymidine was added to each culture, and 4 hours later the amount of incorporated label was measured. The concentration of TGF-β was determined by comparing the half-maximum inhibition ($IC_{50}$) of the cultures treated with diluted SN of RPE eyecups with a standard curve from the cell cultures treated with known amounts of TGF-β. Specificity of the assay was monitored by treating the cells with the SNs of RPE eyecups in the presence of neutralizing anti-pan-TGF-β antibody (R&D Systems).

### IFN-γ ELISA

IFN-γ production was assayed by using a sandwich ELISA. In brief, a 96-well microtiter plate was coated with capturing mAb to IFN-γ (BD Biosciences, Franklin Lakes, NJ) and incubated overnight at 4°C and blocked with PBS containing 1% BSA. Sample and standard recombinant IFN-γ were applied to the plate and incubated for 3 hours at room temperature. Biotinylated detecting antibody (BD Biosciences) specific to IFN-γ was added for 1 hour. Streptavidin-β-galactosidase was added to the wells and incubated for 30 minutes. The substrate chlorophenylred-β-D-galactopyranoside was then added to the wells. A standard ELISA plate reader was used to read the optical density of the color change at a wavelength of 570 nm.

### RNA Isolation

Total RNA was isolated from RPE cells harvested from eyecups or from the confluent second passage of cultured RPE cells (RNA STAT-60 kit; Tel-Test Inc., Friendswood, TX) according to the manufacturer's in-

structions. This kit utilizes a single-step method by acid guanidinium thiocyanate-phenol-chloroform extraction.

### Reverse Transcription–Polymerase Chain Reaction

cDNA was synthesized by reverse transcribing RNA using random hexamers and AMV RT (Promega). For PCR amplification of TSP, cDNAs were amplified using the following primers. (5′-3′ sequences) forward TSP, GTT CGT CGG AAG GAT TGT TA, reverse TSP TCT ATT CCA ATG GCA ACG AG (733 bp). The TSP intron-spanning primers for specific amplification of selected genes were designed with gene sequences from the public database and a software program (Oligo Primer Analysis software 6.0, Molecular Biology Insights, Inc., Plymouth, MN). PCR reactions were performed in a 50-μL amplification mixture containing 1× polymerase buffer, 2.5 mM $MgCl_2$, 0.2 mM each dNTP, 1 μM forward and reverse primers, 1.25 U *Taq* polymerase (Applied Biosystems, Inc. [ABI], Foster City, CA). After PCR thermal profile was performed in a thermal cycler (GeneAmp PCR System 2400; ABI). One cycle of 5 minutes at 94°C and 5 minutes at 60°C, 40 cycles of 2 minutes at 72°C and 1 minute at 94°C, 1 minute at 58°C, and 1 cycle of 10 minutes at 72°C, hold at 4°C. PCR products were separated by 1.5% agarose gel electrophoresis.

### Immunoblot Analysis

The protein content of RPE eyecup SNs was determined using a bicinchoninic acid (BCA) protein assay (Pierce, Rockford, IL). Commercially available purified platelet-derived TSP protein (MW 450,000; Haematologic Technology, Inc., Essex Junction, VT) was used as a positive control. In the presence of reducing agent, equivalent amounts of RPE eyecup SN protein were subjected to SDS-PAGE in 3% to 8% Tris-acetate gradient gel (Invitrogen, Inc., Carlsbad, CA) followed by electrophoretic transfer of the separated proteins to nitrocellulose membranes (Pierce). Immunoblot analysis was performed using anti-TSP-1 antibody (Santa Cruz Biotechnology, Inc., Santa Cruz, CA). Antibodies bound to proteins on the membrane were identified using horseradish peroxidase–conjugated secondary antibody (Santa Cruz Biotechnology, Inc.) and detected with chemiluminescent substrate (ECL detection reagents, Amersham Pharmacia Biotech, Piscataway, NJ). The immunoblot membranes were then exposed to autoradiograph film (Biomax Light Film, Kodak, Rochester, NY) to detect the chemiluminescent signal. Under reducing conditions TSP-1 polypeptides are known to migrate at 185 and 160 kDa. Both forms of TSP polypeptides were detectable as shown in Figure 5.

### Injections into the Anterior Chamber and Subretinal Space

For anterior chamber injection, anesthetized mice received a 0.3-mm penetrating wound in the peripheral portion of the cornea, 1 mm anterior to the limbus, using a 30-gauge needle. OVA in a volume of 2 μL, was slowly injected into the anterior chamber with a glass micropipette connected to a 10-μL syringe. The subretinal injections were performed according to the procedure of Whiteley et al.[12] on anesthetized animals that, in addition, received topical proparacaine to anesthetize the ocular surface and tropicamide 1% to dilate the right pupil. Injection into the subretinal space was performed using very fine, bevelled, pulled glass micropipettes that were connected to a 10-μL syringe (Hamilton, Reno, NV) through a fine polyethylene tube. The entire apparatus was filled with HBSS, but an airlock was produced before the volume to be injected, thus preventing dilution of the injected material. The bore of the glass needle was coated with silicon (Sigma coat) to prevent adherence of the cells. The injections were made via a transscleral approach under direct visualization, using a binocular surgical microscope and a coverslip held on the cornea. The glass needle was advanced carefully until it reached the subretinal space where 1 μL OVA (50 ng) was injected.

### Induction and Assessment of Immune Deviation

The expression of delayed hypersensitivity (DH) to OVA antigen was evaluated in mice that received an anterior chamber or subretinal injection of 50 μg/mL OVA. Seven days after intracameral injections, the animals, together with a group of naïve animals (positive control), were immunized subcutaneously with 1:1 mixture of 100 μg of OVA and complete Freund's adjuvant (CFA). An ear-swelling analysis was performed 7 days later on all experimental animals, together with a group of naïve animals that served as the negative control. Each group consisted of five mice. Delayed hypersensitivity was measured based on ear swelling, as previously described.[15] Briefly, 200 μg of OVA in 10 μL of HBSS were injected into the right ear pinnae of the mice. The left ear served as the untreated control. Both ear pinnae were measured with an engineer's micrometer (Mitutoyo, Tokyo, Japan) immediately before and 24 hours after the ear injection. The measurements were performed in triplicate. Anterior chamber–associated immune deviation (ACAID) was detected as the suppression in DH, which was measured as change in ear swelling [(24-hour measurement − 0-hour measurement in the experimental ear) − (24-hour measurement − 0-hour measurement in the negative control ear)] of experimental groups was expressed relative to positive control animals. A two-tailed Student's *t*-test was used, with significance assumed at $P \leq 0.05$.

### Induction and Evaluation of EAU

To induce EAU in C57BL/6 and TSP-1KO mice (H-$2^b$) mice, five mice in each group were immunized subcutaneously in the back with 200 μg human interphotoreceptor retinoid-binding protein (IRBP) peptide 1-20 (GPTHLFQPSLVLDMAKVLLD; Invitrogen, Inc.) emulsified into CFA, which contains 6.0 (final 3.0) mg/mL *Mycobacterium tuberculosis* (H37RA, Difco Laboratories, Detroit, MI). The mice were also injected intraperitoneally with 0.1 μg purified *Bordetella pertussis* toxin (PTX, Sigma-Aldrich).[14] Disease severity was clinically assessed by ocular fundus examinations performed in animals under anesthesia. Pupils were dilated with 1% tropicamide ophthalmic solution (Akorn, Buffalo Grove, IL) before examination. Clinical scoring of EAU was based on retinal vessel dilatation, the number of white, focal, perivascular lesions; and the extent of retinal vessel exudates, hemorrhage, and detachment. Clinical severity was graded on a 0 to 5, as described previously.[15]

The difference between the clinical scores of the two groups was analyzed statistically by the nonparametric Mann-Whitney test for the comparison of two independent populations. Differences were deemed significant when $P < 0.05$.

### Histologic Examinations

The C57BL/6 or TSP-1KO mice were euthanatized 120 days after they were immunized with IRBP, and their eyes were enucleated, fixed immediately in 10% formalin, and embedded in methacrylate. Five-micrometer sections were cut and stained with hematoxylin and eosin. Tissue sections were then examined by light microscopy.

## Results

### Ability of SNs of RPE Eyecups to Suppress T-Cell Activation In Vitro

SNs from cultured RPE cells have been shown to inhibit T-cell proliferation by elaborating soluble factors.[3] However, proliferation is only one parameter that expresses the state of T-cell activation. Ocular immune privilege has been found to suppress T cells that secrete Th1 type cytokines, such as IFN-γ,[15] and we wondered whether the SN harvested from RPE eyecups is capable of inhibiting both proliferation and IFN-γ production by antigen-activated T cells. LNCs from DO11.10 mice, with T cells carrying a *Tcr* transgene specific for OVA, were incubated with diluted 24-hour RPE SN and OVA. T-cell proliferation and

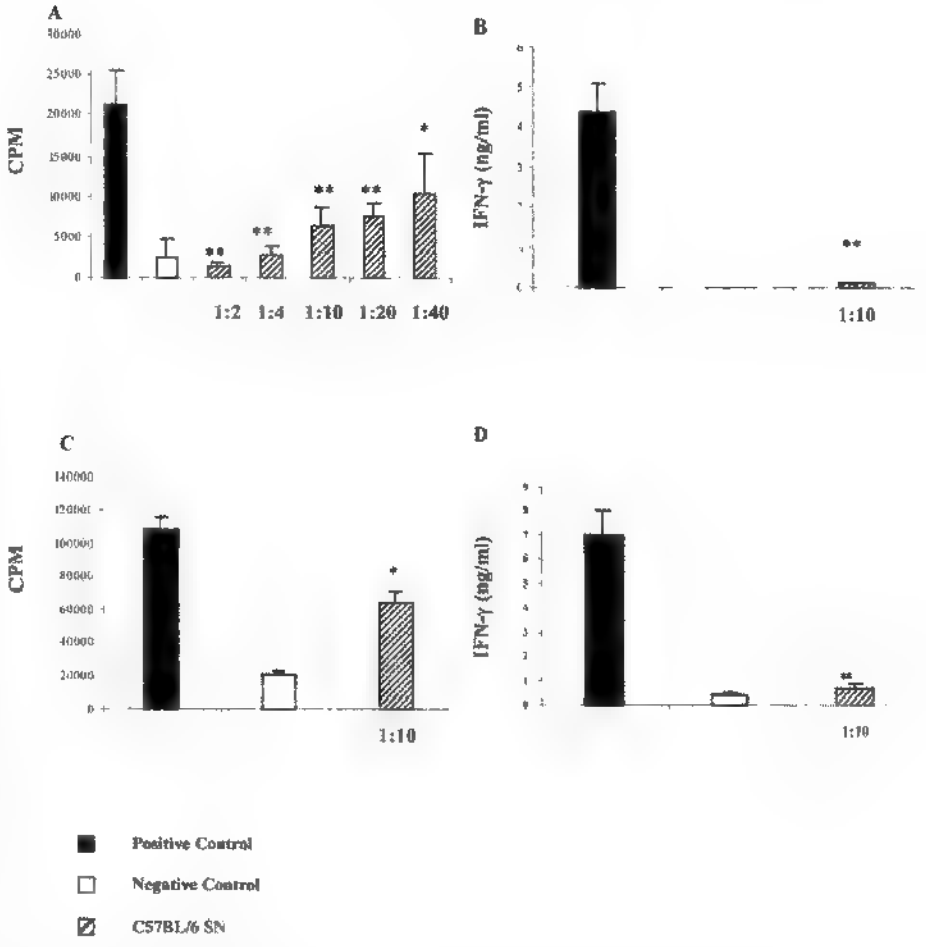


FIGURE 1. Effect of SN from C57BL/6 RPE eyecups on T-cell activation (A, B) DO11 10 LNCs were incubated with OVA and serially diluted SNs of RPE eyecups for 96 hours. Positive control cultures were DO11 10 LNCs and OVA and negative control cultures were DO11 10 LNCs alone. T-cell proliferation (A) and IFN-γ production (B) were measured at 96 hours. (C, D) Twenty-four-hour SNs of eyecups from eyes of C57BL/6 mice were incubated with enriched T cells and anti-CD3 Ab for 24 hours. T-cell proliferation (C) and IFN-γ production (D) were measured after 48 hours. Positive control wells contained T cells and anti-CD3 Ab, and negative control wells contained T cells only. Data represent the mean ± SEM of results in triplicate wells in a representative experiment. $^*P < 0.05$ and $^{**}P < 0.01$ significantly less than the positive control.

IFN-γ production were measured at 96 hours. Positive control cultures contained DO11 10 LNC and OVA and negative control cultures contained only DO11.10 LNC. Figure 1A shows that DO11 10 T cells are capable of mounting strong proliferative responses to OVA and that RPE SN inhibited this proliferation in a concentration-dependent manner. Even at a dilution of 1 40 the antiproliferative capacity of RPE SN was significant. Our results displayed in Figure 1B reveal that DO11 10 T cells are capable of producing appreciable amounts of IFN-γ in response to OVA, and that IFN-γ production is significantly suppressed when the T cells are stimulated in the presence of SN of RPE eyecups. Thus, SN from RPE eyecups contains a soluble factor(s) that suppresses T-cell activation in vitro by two parameters.

In the DO11.10 T-cell activation assay just described, unfractionated LNCs, containing both T cells and antigen-presenting cells (APCs), were used as responders. To determine the extent to which RPE-derived immunosuppressive factors act directly on T cells, we tested RPE SN on T cells activated in vitro by mitogenic anti-CD3 antibodies (Ab). In this assay, enriched T cells prepared from spleens of normal C57BL/6 mice were stimulated in vitro with anti-CD3 Ab in the presence of 24-hour SN obtained from RPE eyecups of normal C57BL/6 mice. T-cell proliferation and IFN γ production were measured at 48 hours. Cultures with only T cells and anti-CD3 antibody served as positive controls, and those containing T cells alone served as negative controls.

Stimulated T cells mounted an appreciable proliferative response to anti-CD3 Ab (Fig. 1C) and produced significant amounts of IFN-γ (Fig. 1D). T cells stimulated by anti-CD3 Ab in the presence of SN from normal C57BL/6 RPE eyecups proliferated poorly and produced virtually no IFN γ. These results reveal that factors produced by normal RPE eyecups directly suppress T-cell activation, independent of their capacity to alter APC function.

## Role of TGF β in T-Cell Suppression by RPE Eyecup SN

Because RPE cells constitutively express mRNA for TGFβ[16] and, when activated, TGF-β profoundly inhibits both proliferation and lymphokine production by T cells,[17] we wanted to determine whether TGF-β is present in RPE eyecup SN, and if so, whether it was responsible for the capacity of these SNs to suppress T-cell activation.

To identify the presence of TGF-β, we used the mink lung epithelial cell proliferation inhibition assay. The SN was harvested from RPE eyecups after 0, 1, 6, 12, 24, and 48 hours of incubation. Mink lung cells were incubated with transiently acidified SN (to reveal the total amount of TGFβ present) or untreated SN (to reveal the amount of active TGF-β present) diluted SN for 20 hours. Then, [$^3$H]thymidine was added, and the amount of isotope incorporated was assessed. Figure 2A demonstrates that within 1 hour of incubation of RPE eyecups in SFM, latent (but not active) TGF-β was detected. Maximum levels of TGF-β were found in RPE eyecup SN at 12 hours. Active TGF-β was first detected at 12 hours, with the peak levels at 24 hours of incubation and declining at 48 hours. We interpret these results to mean that RPE eyecups elaborate

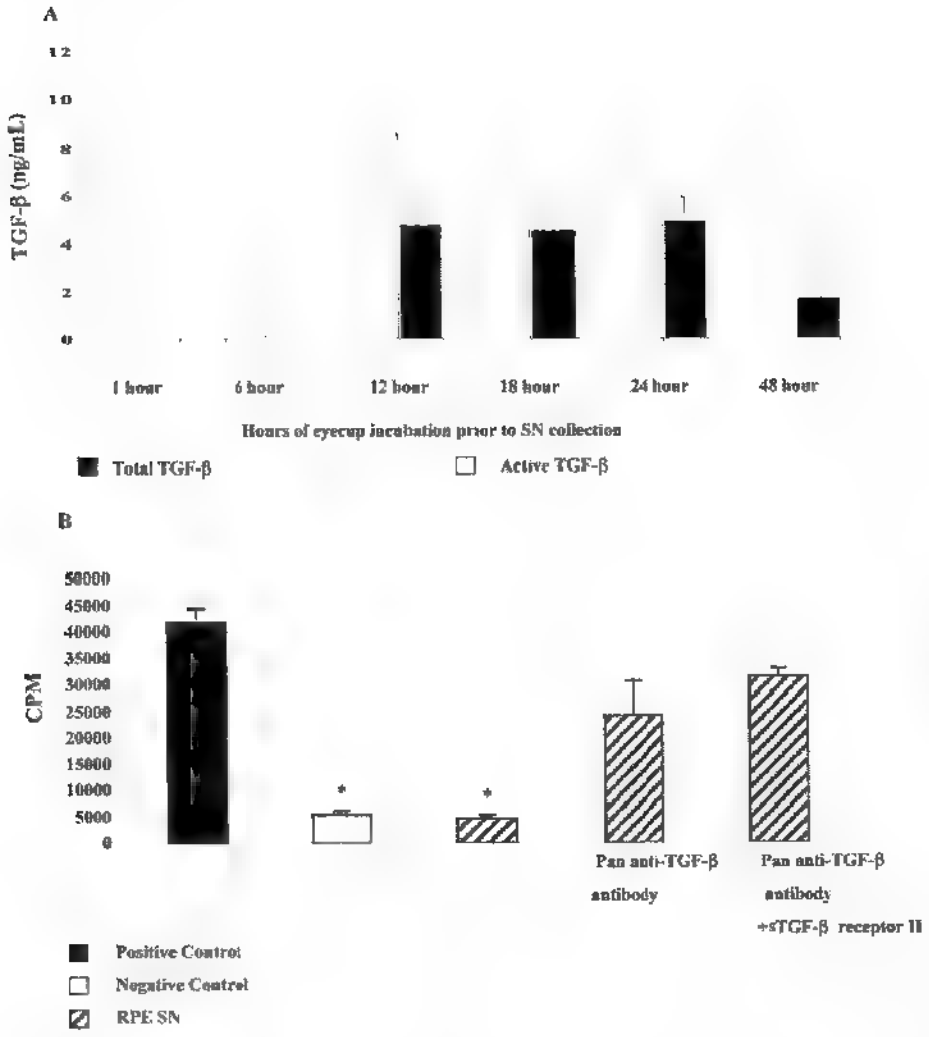


FIGURE 2. Kinetics of TGF-β production and activation in SN of RPE eyecups and role of TGF-β in DO11.10 T-cell proliferation in the presence of RPE SN. (A) Posterior eyecups were incubated with SFM for 1, 6, 12, 18, 24, and 48 hours. Mv1Lu cells were incubated with unmodified or acid-treated SNs of the RPE eyecups. A mink lung cell proliferation inhibition assay was performed by measuring incorporated [$^3$H]thymidine. The final dilution of SN in all wells was 1:40. (B) Experimental wells contained 24-hour untreated RPE SN, SN treated first with anti-pan-TGF-β antibody, or SN treated first with both anti-pan-TGF-β and sTGF-βRII. Positive control wells contained LNCs and OVA, and negative control wells contained only LNCs. Thymidine uptake was measured at 96 hours. Data represent the mean ± SEM of results in triplicate wells in a representative experiment. *Significantly less than the positive control ($P < 0.05$).

latent TGF-β, which they then convert into the active form by a mechanism yet to be revealed.

To determine whether the active TGF-β present in RPE eyecup SN was responsible for inhibiting T-cell activation in vitro, we next added a pan-anti-TGF-β Ab reagent to 24-hour RPE eyecup SN before suspending DO11.10 lymph node cells in the medium in the presence of OVA. As a control, DO11.10 lymph node cells were incubated with OVA alone, with SFM alone, or with OVA and untreated SNs of RPE eyecups. Figure 2B demonstrates that neutralization of active TGF-β by the antibody reversed the inhibitory effect of 24-hour RPE SN on DO11.10 T-cell proliferation, but only partially. In case the anti-TGF-β Ab failed to neutralize all TGF-β, we performed an additional experiment in which soluble TGF-β receptor II (sTGF-βRII) was also added to SN containing anti-TGF-β antibodies. As revealed in Figure 2B, addition of sTGF-β RII further neutralized the suppression inherent in the RPE SN, but still not completely. These results confirm that TGF-β contributes to the ability of RPE eyecup SN to suppress T-cell activation.

## Effectiveness of SN of RPE Eyecup in Inhibiting Activation of T Cells from TGF-β RII DN Mice

To confirm the role of the TGF-β present in the SN of RPE in T-cell inhibition, we used T cells from TGF-β RII DN mice (Fig. 3). These transgenic mice express a dominant negative TGF-β type II receptor selectively on T cells, allowing direct study of the role of TGF-β in T-cell function.[18] T cells enriched from lymph nodes and spleens of naïve C57BL/6 or TGF-β RII DN mice were cocultured with anti-CD3 Ab and 24-hour SN of eyecups from C57BL/6 eyes. T-cell proliferation and IFN-γ production were measured, as described earlier. The positive control was cultures of T cells and anti-CD3 Ab without RPE eyecup SN, and the negative control was cultures containing only T cells. T cells from both wild-type and TGF-β RII DN mounted comparable proliferative responses to anti-CD3 Ab (Fig. 3A), and produced similar levels of IFN-γ (Fig. 3B). Whereas SN of RPE eyecups significantly inhibited both proliferation and IFN-γ production by wild type C57BL/6 T cells, the SN failed to inhibit proliferation of TGF-β RII DN T cells (Fig. 3A). The ability of RPE SN to inhibit IFN-γ production was less affected. We conclude that the TGF-β present in the SN is the major inhibitor of T-cell proliferation, but that factors in addition to TGF-β suppress IFN-γ production.

## Correlation of the Capacity of RPE SN to Suppress T-Cell Activation with the Presence of Active TGF-β

To ascertain what role the activation of TGF-β plays in T-cell inhibition by RPE SN, SNs were collected from the eyecups at 0, 1, 6, and 24 hours after incubation. These SN were diluted and placed in T-cell proliferation and IFN-γ production assays as previously described. As shown in Figure 4A, the SN of RPE eyecups collected after 0 and 1 hour of incubation failed to

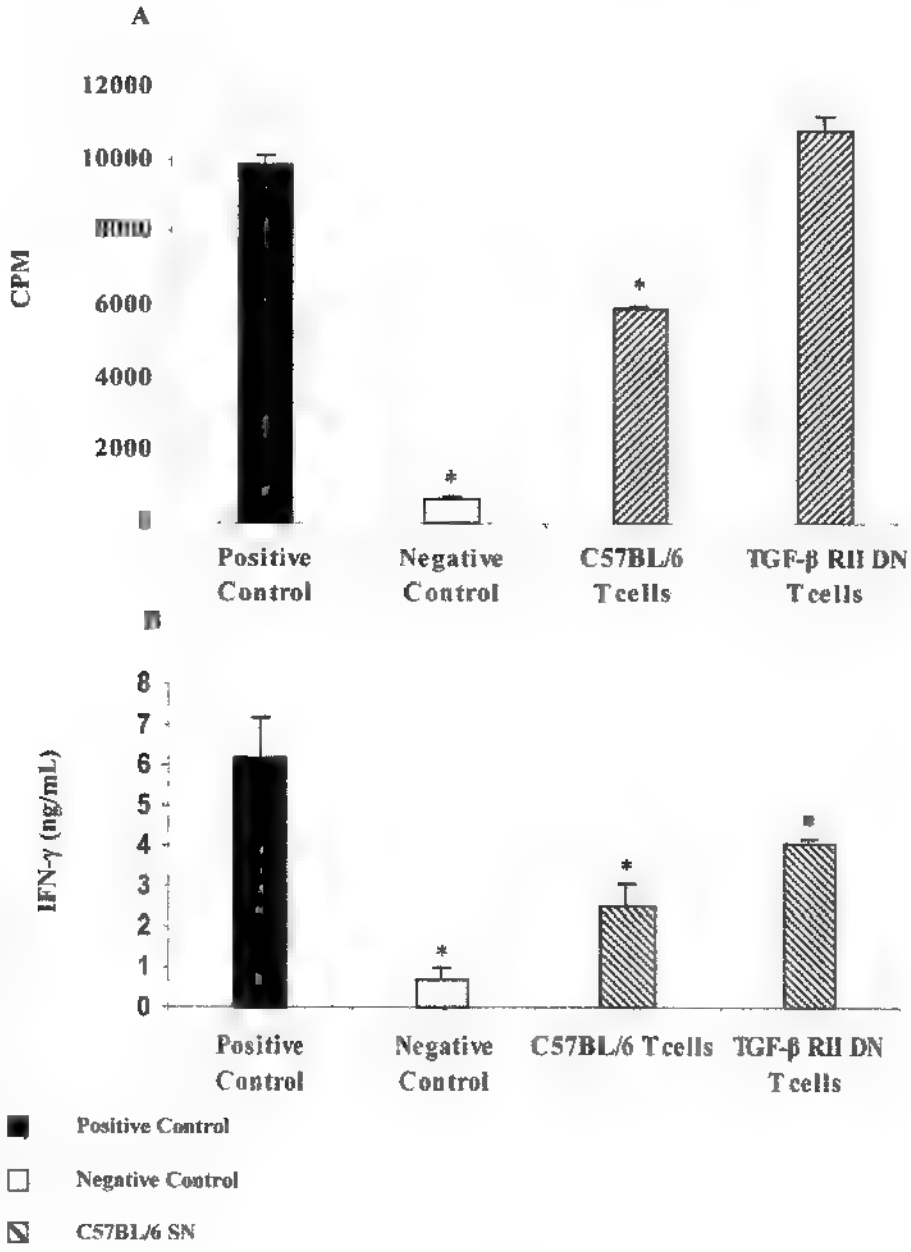


FIGURE 3. Effect of SNs of RPE eyecups from C57BL/6 and TGF-β RII DN mice on anti-CD3 activation of T cells. T cells from either C57BL/6 or TGF-β RII DN mice were incubated with 24-hour SN of the C57BL/6 RPE eyecup and anti-CD3 Ab. Positive control wells contained TGF-β RII DN T cells and anti-CD3 Ab, and negative control wells contained only TGF-β RII DN T cells. T-cell proliferation (A) and IFN-γ production (B) were measured after 48 hours. Data represent the mean ± SEM of results in triplicate wells in a representative experiment. *Significantly less than the positive control ($P < 0.05$).

inhibit T-cell proliferation. Only the RPE SN collected after 6 hours and thereafter suppressed T-cell proliferation, and these time points correspond to the presence of active TGF-β. IFN-γ production was also inhibited by the RPE SN collected after 6 hours of incubation and beyond, but it was also reduced at 1 hour compared with the positive control (Fig. 4B). These results provide some evidence for the view that the activation of TGF-β in RPE SN is necessary for T-cell proliferation to be suppressed. However, the results also imply that another immunosuppressive agent(s) is present to inhibit IFN-γ production.

### Effect of TSP-1 Produced by RPE on Latent TGF-β in Eyecup SN

Our attention was drawn to TSP-1 as the activator of TGF-β in RPE eyecup SN, because (1) TSP-1 is the major activator of TGF-β, both in vivo and in vitro[19]; (2) cultured RPE cells express mRNA for TSP[20]; (3) cultured human RPE cells secrete TSP-1[21]; and (4) TSP-1 has the ability to alter directly the functional properties of Th1 cells otherwise destined to become Th1 like.[22] To demonstrate that RPE eyecups contain mRNA for TSP-1 and secrete TSP-1 protein, RT-PCR and immunoblot analysis for TSP-1 was performed. The RPE eyecups of C57BL/6 mice contained easily detectable TSP mRNA transcripts and TSP-1 protein (Fig. 5).

To determine whether TSP-1 plays an important role in activating TGF-β found in RPE SN, eyecups were prepared from eyes of TSP-1KO mice (TSP 1KO). The SN was collected from the eyecups after 24-hour incubation and assayed for the presence of active and total TGF-β. The results presented in Figure 6 indicate that SN of RPE eyecups of TSP 1KO mice contained amounts of total TGF-β comparable to that found in

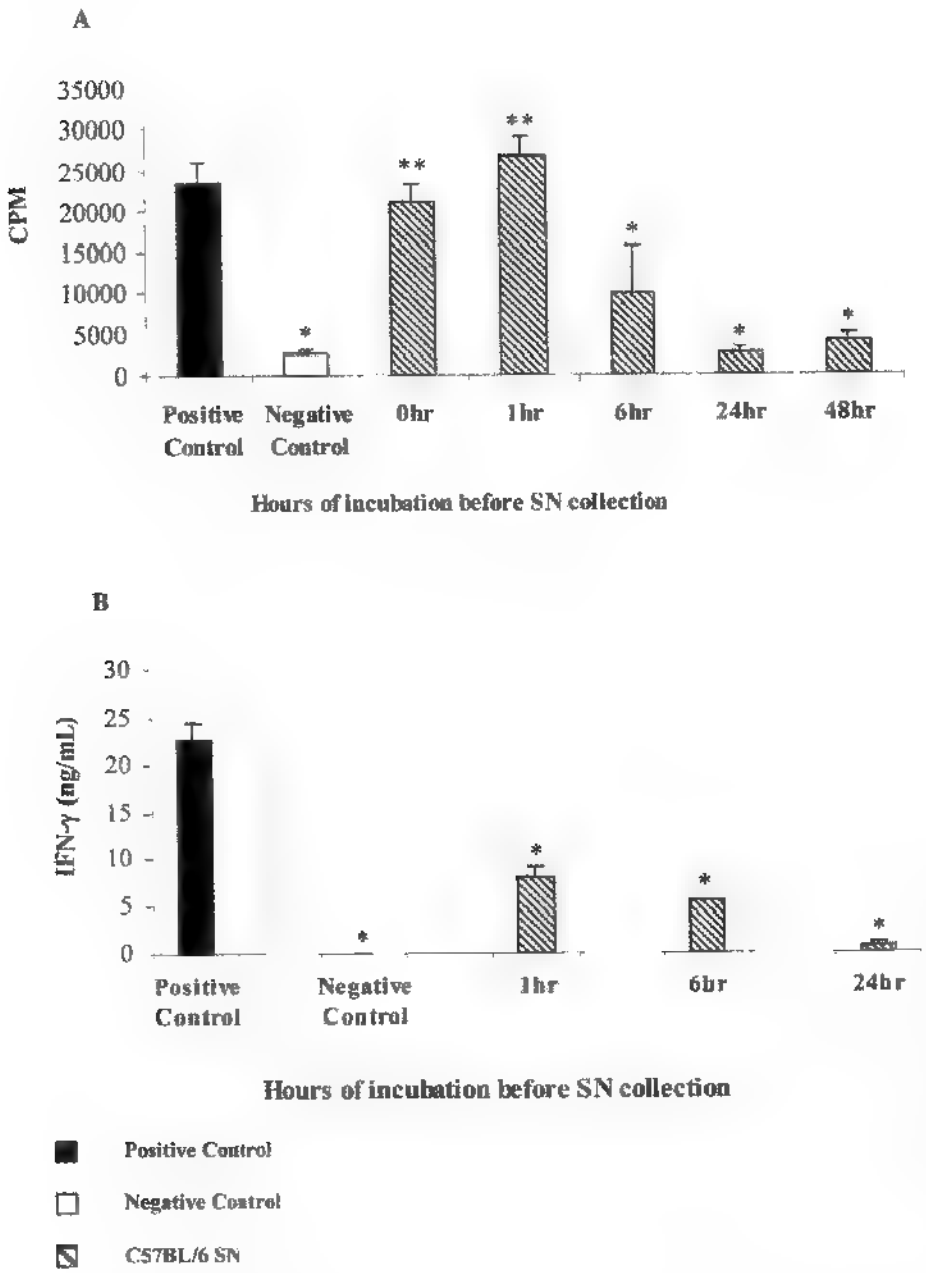


FIGURE 4. Correlation between the duration of RPE eyecup incubation and ability of SNs to suppress T-cell activation. RPE eyecups were incubated with serum-free medium for 1, 6, 24, and 48 hours. DO11.10 LNCs were incubated with OVA and different SN. Positive control cultures contained DO11.10 LNCs and OVA and negative control cultures contained only DO11.10 LNCs. T-cell proliferation (A) and IFN-γ production (B) were measured at 96 hours. Data represent the mean + SEM of triplicate wells from a representative experiment. $^*P < 0.05$ significantly less than positive control and $^{**}P < 0.05$ significantly greater than 24-hour-SN effect.

SN of wild-type C57BL/6 RPE eyecups. However, virtually no active TGF-β was found in TSP-1KO SN.

To reveal the functional importance of TSP-1-dependent TGF-β activation in these studies, TSP-1KO RPE SNs were tested for their capacity to suppress the activation of DO11.10 T cells as well as anti-CD3 stimulated T cells in vitro, as described earlier. The RPE SN from wild-type C57BL/6 eyecups suppressed T-cell proliferation and IFN-γ production (Fig. 7). The RPE SN from TSP-1KO eyecups did not inhibit anti-CD3 driven T-cell proliferation or IFN-γ production and were significantly less effective, compared with the RPE SN from wild-type C57BL/6 eyecups, in suppressing proliferation and IFN-γ production by DO11.10 T cells (Fig. 7). However, compared with the positive control, the SN from TSP-1KO eyecups still inhibited partially both proliferation and IFN-γ production by DO11.10 T cells (Fig. 7).

## Ability of Eyes from TSP-1KO Mice to Promote Immune Deviation

Immune deviation, an essential component of immune privilege, diminishes DH responses mediated by Th1 cells.[1] Because the RPE SN of TSP-1KO eyecups did not inhibit T-cell activation to the same degree as that of wild-type eyecups, we wanted to see whether the eyes of these mice would support the induction of immune deviation. Immune deviation was elicited according to the procedures described in the Methods section. Figure 8 demonstrates that the positive control TSP-1KO mice that received a subcutaneous injection of OVA and CFA mounted intense DH responses. In contrast to wild-type C57BL/6 mice, TSP-1KO mice that first received an inoculation of OVA in the subretinal space or the anterior chamber of the eye also displayed an intense DH responses. Our results demonstrate that lack of TSP-1 production by RPE in TSP-1KO mice

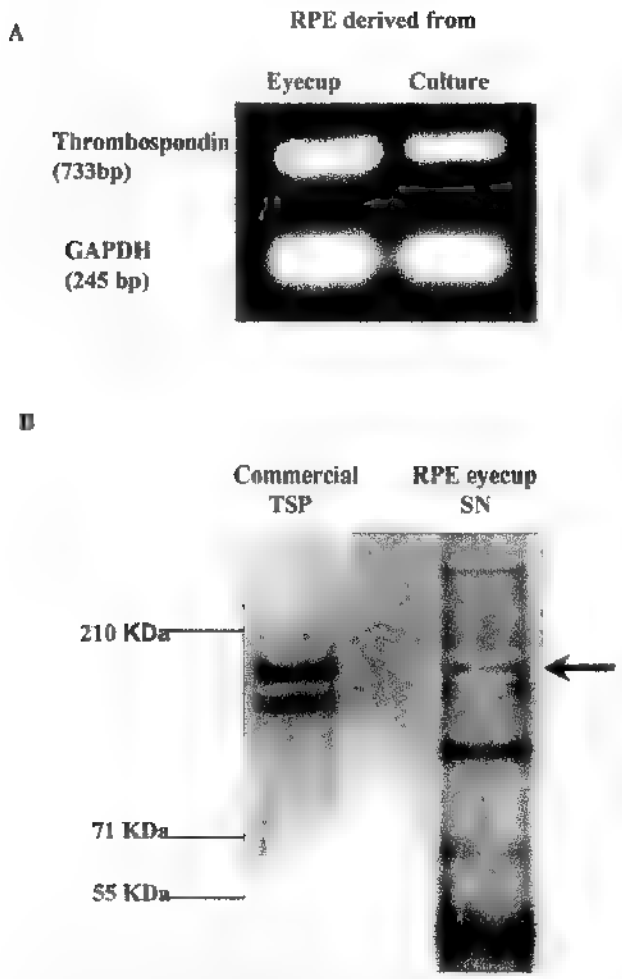


FIGURE 5. Expression of TSP-1 mRNA and presence of TSP-1 protein by RPE eyecups. (A) TSP-1 mRNA. total RNA extracted from freshly isolated or cultured RPE cells was subjected to RT-PCR analysis using primers for TSP-1 and GAPDH. PCR products were detected by ethidium bromide/agarose gel electrophoresis. (B) TSP-1 protein in 24-hour RPE SN was determined by immunoblot analysis. Total protein from SN samples and commercial TSP (positive control) was used for this analysis. TSP protein was detected with anti-TSP-1 Ab and chemiluminescence detection. *Arrow* TSP-1 band in SN from the eyecup

prevents their eyes from promoting immune deviation via the anterior chamber and the subretinal space.

## Development of Experimental Autoimmune Uveoretinitis in C57BL/6 and TSP-1KO Mice

We next explored the role of TSP-1 and active TGF-$\beta$ in the ability of C57BL/6 mice to withstand autoantigen-induced inflammation in the ocular posterior segment. Given that experimental autoimmune uveitis (EAU) is mediated by Th1 cells,[23] and because we found that the RPE from TSP-1KO mice did not inhibit IFN-$\gamma$ production by activated Th1 cells, we hypothesized that TSP-1KO mice might experience exaggerated EAU compared with control mice. Both wild-type C57BL/6 and TSP-1KO mice were immunized subcutaneously with IRBP peptide and CFA and intraperitoneally with PTX. Their retinas were examined clinically at regular intervals, and the degree of uveitis was measured and scored. Wild-type C57BL/6 mice displayed significant retinal inflammation with the average maximum score reaching 2.5 ± 0.6 on day 18 after immunization (Fig. 9, circles). One hundred twenty days after immunization, the disease abated and eyes reached the score of zero. In contrast, TSP-1KO mice had a significantly higher average score of 3.5 ± 0.5 at the peak of EAU, and these mice continued to display severe inflammation throughout the examination period (Fig. 9, squares). Our results indicate that expression of TSP is essential in diminishing the severity and duration of uveitis in EAU.

## Retinal Recovery of C57BL/6 and TSP-1KO Mice from EAU

To examine the histologic status of the retina in eyes of C57BL/6 mice and TSP-1KO mice, immunized mice from both groups were euthanatized after 120 days, and their eyes were prepared for histologic evaluation. Figure 10D demonstrates a retina taken from a naive 6-week-old TSP-1KO mouse. All retinal layers are present in normal thickness and configurations with an intact RPE layer. The retinas of C57BL/6 mice that recovered clinically from EAU, retained normal retinal architecture, although minor irregularities were detected over a small section of the RPE and there was slight thinning of the outer and inner nuclear layers (Fig. 10A). In contrast, the retina of immunized TSP-1KO mice displayed severe abnormalities (Figs. 10B, 10C): The RPE layer was discontinuous, and in fact totally destroyed in places. There were few photoreceptor outer segments remaining, and the inner nuclear layer was reduced to half of its original thickness. There was a complete loss of the outer plexiform layer with disorganization of the inner plexiform and ganglion cell layers. Areas of hemorrhage

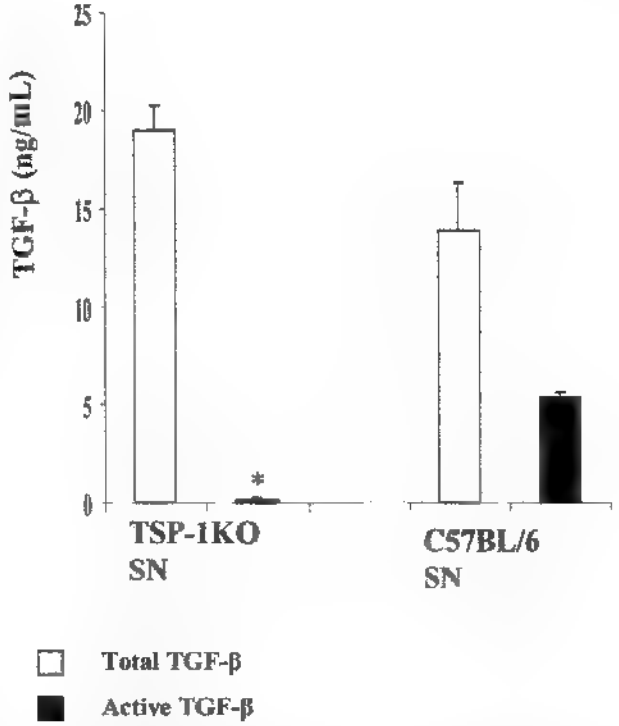


FIGURE 6. Total and active TGF-$\beta$ content of SN of eyecups prepared from C57BL/6 and TSP-1 KO mice. Mv1Lu cells were incubated with unmodified or acid treated 24-hour SN of eyecups prepared from either C57BL/6 or TSP-1KO mice. [$^3$H]thymidine was added to each well, and 4 hours later the amount of incorporated label was measured. Data are expressed as the mean ± SEM of results in triplicate wells in a representative experiment. *Significantly less than the SN effect in C57B/6 mice ($P < 0.01$).

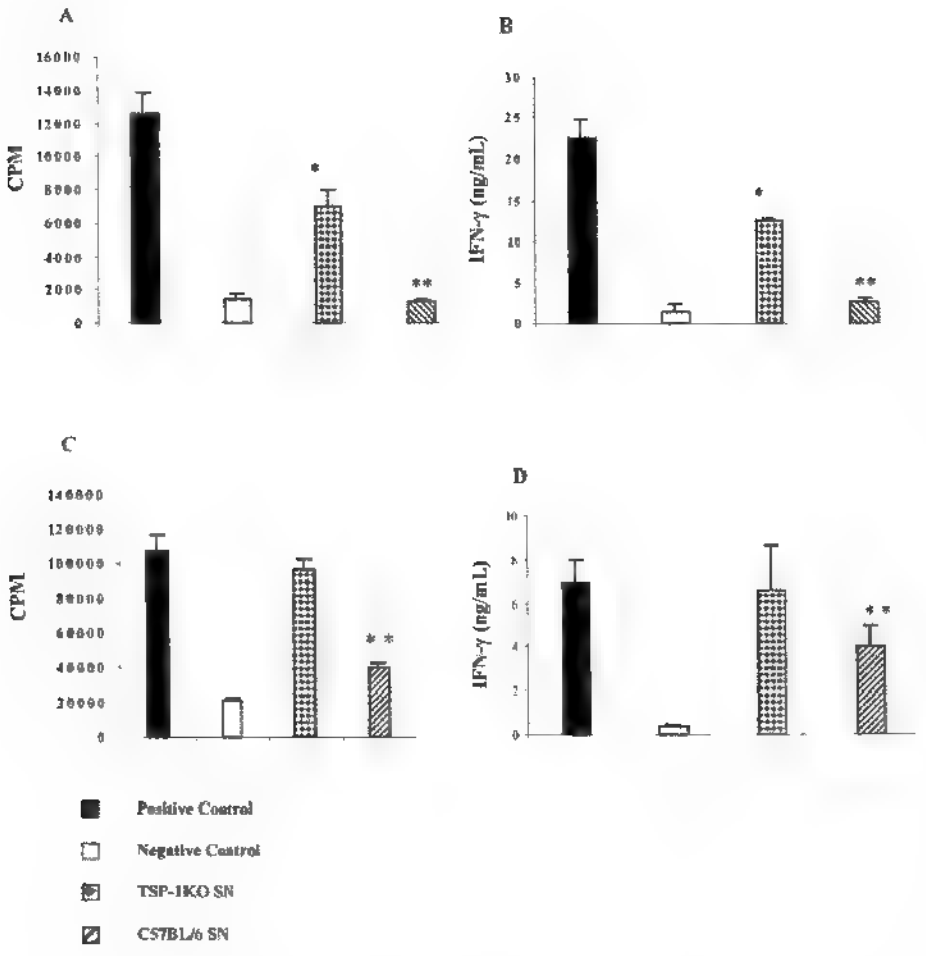


FIGURE 7. Effects of SNs of RPE eyecups from TSP-1KO and C57BL/6 mice on antigen and anti-CD3 stimulated T-cell proliferation. After 24 hours of incubation of RPE eyecups from TSP-1KO or C57BL/6 mice, SNs were collected. (A, B) DO11.10 LNCs were incubated with OVA and serially diluted SNs of RPE for 96 hours. Positive control cultures contained DO11.10 LNCs and OVA, and negative control cultures contained only DO11.10 LNCs. T-cell proliferation (A) and IFN-γ production (B) were measured at 96 hours. (C, D) Twenty-four-hour SNs from eyecups prepared from eyes of C57BL/6 mice were incubated with purified T cells and anti-CD3 Ab for 24 hours. T-cell proliferation (C) and IFN-γ production (D) were measured 48 hours later. Positive control cultures contained T cells with anti-CD3 Ab, and negative control wells contained only T cells. Data are expressed as the mean ± SEM of results in triplicate wells in a representative experiment. $^{*}P < 0.05$, $^{**}P < 0.01$: significantly less than the positive control.

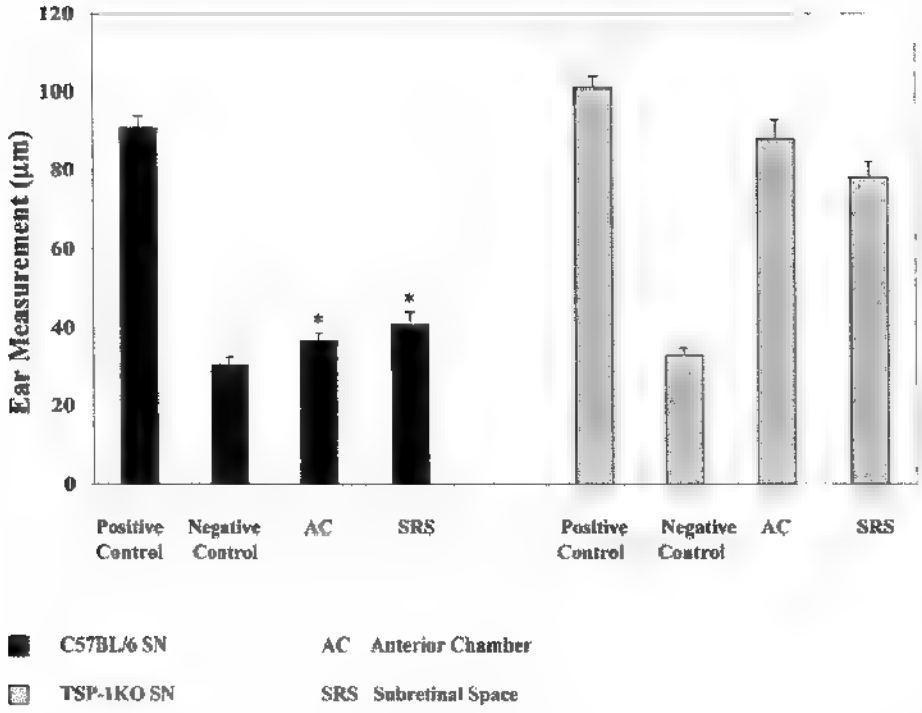


FIGURE 8. Capacity of eyes of TSP-1KO and C57BL/6 mice to support immune deviation to intracameral OVA antigen. All control and experimental animals underwent an ear challenge on day 14, and ear thickness was measured by micrometer 24 hours later. Experimental TSP-1KO and C57BL/6 mice received injections of OVA into the anterior chamber or the subretinal space on day 1, followed by subcutaneous immunization with OVA and CFA 7 days later. Positive control groups also received subcutaneous immunization. The data depicted are expressed as a percentage of the positive control percentage. *Significant difference between ear swelling in either anterior chamber– or subretinal space–injected animals and the positive control ($P < 0.05$).

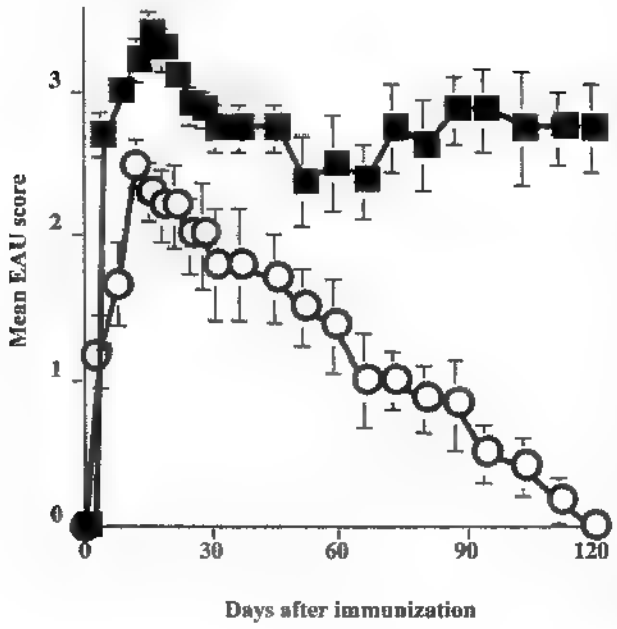


FIGURE 9. Expression of EAU in C57BL/6 and TSP-1KO mice. Groups of C57BL/6 and TSP-1KO mice were immunized subcutaneously with IRBP peptide and CFA and received simultaneous intraperitoneal injection of PTX. Retinas were examined at regular intervals throughout a 120-day period. The extent of uveitis is represented as the mean EAU score for both eyes on the day of examination.

were found within the outer retina. New vessels were seen to stretch between the ganglion cell layer and the inner nuclear layer (Fig. 10B) as well as between the choroid and the RPE layers (Fig. 10C).

Our results reveal that remarkable histologic recovery from inflammation occurred in the retinas of C57BL/6 mice that recovered clinically from EAU. Alternatively, mice deficient in TSP-1 displayed a devastating and prolonged inflammatory response that destroyed the organization of the retina and many cells in the various layers.

## Discussion

Data recently published[4] and our results (Fig. 1) indicate that T cells that receive activation signals, either through APCs or through their T-cell receptors for antigen, fail to respond in the presence of soluble factors produced by the RPE—that is, these T cells fail to proliferate and secrete proinflammatory cytokines such as IFN-γ. In the present experiments, active TGF-β played an essential role in conferring immunosuppressive properties on RPE SNs. A sensitive bioassay showed latent TGF-β, produced constitutively by the monolayer of RPE and present in the SN of RPE eyecups. However, latent TGF-β in RPE SN did not inhibit T-cell proliferation; only on activation did TGF-β suppress T-cell activation. We have also demonstrated that SN of RPE did not inhibit activation of purified T cells taken from TGF-β RII DN mice, illuminating the fundamental role that TGF-β plays in T-cell inhibition.

As alluded to in the Results section, inhibition of TGF-β by its neutralizing antibody or by TGF-β receptor II did not fully reverse the effectiveness of the SN of RPE in inhibiting T-cell activation. In addition, inhibition of IFN-γ production persisted when there was no active TGF-β (Fig. 4B) and T cells from TGF-β RII DN mice were used (Fig. 3B). We conclude that although active TGF-β has an essential role in inhibition of T-cell activation, it is not the sole factor responsible. A search for other factors that may play a part in conferring immune-privilege properties on RPE SN is under way.

Other laboratories have shown that RPE cells inhibit T cells.[24,25] Liversidge et al.[24] have reported that RPE cells use both soluble and membrane-bound mechanisms to suppress lymphocyte proliferation stimulated by antigen, mitogen, and IL-2. They did not find TGF-β in the SN of cocultured T cells and RPE by Western blot, leading them to conclude that TGF-β did not play a role in suppression of T-cell activation. Rezai et al.[25] subsequently corroborated the ability of human fetal RPE (HFRPE) cells to suppress, through apoptosis, T-cell activation across a migration assay membrane (Transwell, Corning-Costar). Their search for the factor secreted by HFRPE cells excluded TGF-β, TNF-α, and IL-10, since these factors were not found by ELISA, and their addition to T-cell cultures did not lead to T-cell apoptosis.[26] It is possible that in these studies,

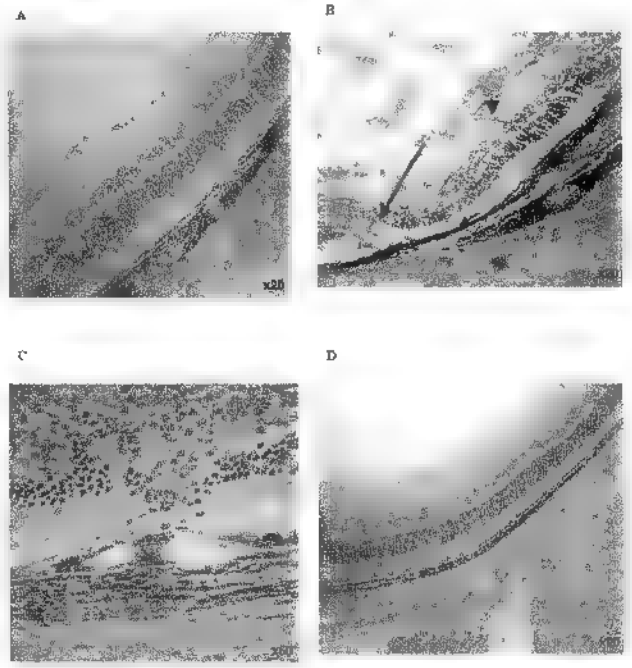


FIGURE 10. Histology of eyes from C57BL/6 and TSP-1KO mice 120 days after induction of EAU. (A) Retina of C57BL/6 mouse at day 120 after induction of EAU. Punctate neuron loss was noted in both the inner nuclear and photoreceptor cell layers. The normal architecture of the retina was preserved. (B) Retina from TSP-1KO mouse 120 days after IRBP immunization, at which time the average clinical uveitis score was 3. The RPE layer appeared discontinuous and was totally destroyed in places (*short arrow*). Photoreceptor outer segments were barely visible, and there was complete loss of the outer plexiform layer and profound disorganization of the inner plexiform and ganglion cell layers. An area of hemorrhage (*long arrow*) and a new vessel (*arrowhead*) stretched between the ganglion cell and inner nuclear layers. (C) A higher magnification of TSP-1KO retina 120 days after immunization. A new vessel arose from the choroidal circulation incorporating the RPE. (D) Retina of a naive 6-week-old TSP-1KO mouse.

TGF-β was present but was latent or that an intact monolayer of RPE is essential for RPE production of appreciable levels of active TGF-β.

We have also demonstrated that eyecups from TSP-1KO mice were ineffective in inhibiting T-cell activation. RPE SN from TSP-1KO animals contained levels of latent TGF-β comparable to that of wild-type C57BL/6 eyecups, but lacked active TGF-β. The mechanisms of TGF-β activation in the eye are not fully understood. Activation of TGF-β in vitro is achieved by treating the latent TGF-β with extremes of heat and pH, whereas, in vivo the activation of TGF-β is largely enzymatic through proteolytic activities of plasmin, cathepsin, and others.[26] TSP can activate TGF-β by binding the latent TGF-β complex,[27] and the effectiveness of TSP in activating TGF-β is usually enhanced in the presence of proteolytic enzymes. Although RPE produce plasminogen activators[28] and display receptors for urokinase,[29] there was no indication that RPE from TSP-1KO mice mediates TGF-β activation through enzymatic mechanisms alone. To our knowledge, this is the first report to show that RPE activates TGF-β and to demonstrate that the mechanism of this activation is solely through TSP-1. SNs of eyecups from TSP-1KO mice failed entirely to inhibit T-cell activation if the purified T-cell populations were stimulated through anti-CD3, but when lymph node cells were stimulated with OVA, SN of RPE from TSP-1KO mice inhibited T-cell activation partially. The reason for this partial response could be that lymph node mixtures contain other factors, such as proteases, that can activate TGF-β despite the absence of TSP-1, leading to inhibition of T-cell activation. We conclude that it is essential that TSP-1 be expressed by RPE to create and maintain the immunosuppressive microenvironment of the subretinal space, probably through the ability of TSP to activate latent TGF-β.

Both the anterior chamber and the subretinal space of eyes of TSP-1KO mice, in contrast to the wild-type mice, failed to support induction of OVA-specific immune deviation. This result demonstrates that the presence of TSP-1 is essential in the ability of the eye to divert the immune response away from a proinflammatory Th1 course. To our knowledge, this is the first report to demonstrate an essential role for TSP-1 in promoting ocular immune deviation.

Moreover, TSP-1KO mice that were immunized with IRBP to induce EAU experienced significantly enhanced uveitis that failed to resolve. Our findings in TSP-1KO mice that were immunized with IRBP reveal that the absence of TSP, and therefore of a potential mechanism of TGF-β activation, resulted in destructive and sustained autoimmune inflammation of the uveal tract and retina. Our laboratory has shown that preemptive induction of IRBP-specific ACAID can prevent the onset of EAU, and that induction of ACAID once EAU is established abruptly terminates the disease.[30] Others have shown that regulatory mechanisms come into play as EAU wanes after its initial clinical expression.[11] Because we also demonstrated that the subretinal space of TSP-1KO mice does not support immune deviation, we infer that induction of immune deviation is responsible, at least in part, for the suppression of autoimmunity that limits both the extent and the duration of EAU in normal mice.

Unlike the retina of normal C57BL/6 mice, the retina of TSP-1KO mice subjected to EAU revealed new vessel formation from both the choroidal and retinal circulations. Under normal circumstances, spontaneous neovascularization was not noted in the retinas of TSP-1KO mice, but once their retinas received an insult, such as EAU, there were multiple new vessels in evidence. TSP-1 has been shown to inhibit angiogenesis in vivo and in vitro assays,[31] and overexpression of TSP-1 in tumor cells leads to inhibition of angiogenesis.[32] The antiangiogenic activity of TSP has been attributed by various investigators to its ability to activate latent TGF-β,[33] to bind to CD36,[34] or to interact with heparan sulfate proteoglycans.[35] The presence of new vessels in the retina of TSP-1KO mice that had uveitis points to an important role that TSP-1 plays as an antiangiogenic factor in the retina.

We have demonstrated that TSP-1, possibly through activation of TGF β, provides a molecular mechanism by which the immune privilege of the posterior segment of the eye can be maintained. We have also shown a direct link between the recovery of the retina from a severe inflammatory insult and the presence or resurgence of immune privilege in the posterior segment of the eye. Therapeutic attempts to restore immune privilege may aid recovery from autoimmune diseases and limit inflammation-induced damage.

## Acknowledgments

The authors thank Jack Lawler and Daniel Buros for helpful advice, Bruce Turpie, David Yee, and Jiang Gu for technical assistance; Jacqueline Doherty for expert laboratory management, and Marie Ortega for excellent management of the animal facility.

## References

1 Streilein JW. Immunoregulatory mechanisms of the eye. *Prog Retin Eye Res.* 1999;18:357–470.
2 Streilein, JW, Dana MR, Ksander BR. Immunity causing blindness: five different paths to herpes stromal keratitis. *Immunol Today.* 1997;8:443–449.
3 Ishida K, Panjwani N, Cao Z, et al. Participation of pigment epithelium of iris and ciliary body in ocular immune privilege. 3. Epithelia cultured from iris, ciliary body, and retina suppress T cell activation by partially non-overlapping mechanisms. *Ocul Immunol Inflam.* 2003;11:9–105.
4 Sugita S, Streilein JW. Iris pigment epithelium expressing CD86 (B7–2) directly suppresses T cell activation in vitro via binding to cytotoxic T lymphocyte-associated antigen 4. *J Exp Med.* 2003; 198:161–171.
5 Holtkamp GM, Kijlstra A, Peek R, et al. RPE-immune system interactions: cytokine production and cytokine-induced changes. *Prog Retin Eye Res.* 2001;20:29–48.
6 Wenkel H, Streilein JW. Analysis of immune deviation elicited by antigens injected into the subretinal space. *Invest Ophthalmol Vis Sci.* 1998;39:1823–1834.
7 Fröhlich E, Klessen C. Enzymatic heterogeneity of bovine retinal pigment epithelial cells in vivo and in vitro. *Graefes Arch Clin Exp Ophthalmol.* 2001;239:25–34.
8 Gundersen D, Powell SK, Rodriguez-Boulan E. Apical polarization of N-CAM in RPE is dependent on contact with the neural retina. *J Cell Biol.* 1993;121:335–343.
9 Yao XY, Hageman GS, Marmor MF. Recovery of retinal adhesion after enzymatic perturbation of the interphotoreceptor matrix. *Invest Ophthalmol Vis Sci.* 1992;33:498–503.
10 Shimonkevitz R, Colon S, Kappler JW, et al. Antigen recognition by H-2-restricted T cells. II. A tryptic ovalbumin peptide that substitutes for processed antigen. *J Immunol.* 1984;133:2067–2074.
11 Namba K, Kitaichi N, Nishida T, et al. Induction of regulatory T cells by the immunomodulating cytokines alpha-melanocyte-stimulating hormone and TGF-$\beta_2$. *J Leukoc Biol.* 2002;72:946–952.
12 Whiteley SJ, Klassen H, Coffey PJ, et al. Photoreceptor rescue after low-dose intravitreal IL-1beta injection in the RCS rat. *Exp Eye Res.* 2001;73:557–568.
13 Jiang LQ, Jorquera M, Streilein JW. Immunologic consequences of intraocular implantation of retinal pigment epithelial allografts. *Exp Eye Res.* 1994;58:719–728.
14 Avichezer D, Silver PB, Chan CC, et al. Identification of a new epitope of human IRBP that induces autoimmune uveoretinitis in mice of the H-2b haplotype. *Invest Ophthalmol Vis Sci.* 2000;41: 127–131.
15 Taylor AW, Ye, DG, Nishida T, et al. Neuropeptide regulation of immunity: the immunosuppressive activity of alpha-melanocyte-

stimulating hormone (alpha-MSH). *Ann NY Acad Sci* 2000;917:239–247.

16. Tanihara H, Yoshida M, Matsumoto M, Yoshimura N. Identification TGF-β expressed in cultured human retinal pigment epithelial cells. *Invest Ophthalmol Vis Sci* 1993;34:413–419.
17. Cousins SW, McCabe MM, Danielpour D, et al. Identification of TGF-β as an immunosuppressive factor in aqueous humor. *Invest Ophthalmol Vis Sci* 1991;32:2201–2211.
18. Lucas PJ, Kim SJ, Melby SJ, et al. Disruption of T cell homeostasis in mice expressing a T cell-specific dominant negative TGF-β II receptor. *J Exp Med* 2000;191:1187–1196.
19. Crawford SE, Stellmach V, Murphy-Ullrich, JE, et al. TSP-1 is a major activator of TGF-$\beta_1$ in vivo. *Cell*. 1998;93:1159–1170.
20. Carron JA, Hiscott P, Hagan S, et al. Cultured human RPE cells differentially express TSP-1, -2, -3, and -4. *Int J Biochem Cell Biol* 2000;32:1137–1142.
21. Miyajima-Uchida H, Hayashi H, Beppu R, et al. Production and accumulation of TSP-1 in human RPE cells. *Invest Ophthalmol Vis Sci* 2000;41:561–567.
22. Avice MN, Rubio M, Sergerie M, et al. CD47 ligation selectively inhibits the development of human naive T cells into Th1 effectors. *J Immunol* 2000;165:4624–4631.
23. Saoudi A, Kuhn J, Huygen K, et al. TH2 activated cells prevent experimental autoimmune uveoretinitis, a TH1-dependent autoimmune disease. *Eur J Immunol* 1993;23:3096–3103.
24. Liversidge J, McKay D, Mullen G, et al. RPE cells modulate lymphocyte function at the blood-retina barrier by autocrine PGE2 and membrane-bound mechanisms. *Cell Immunol* 1993;149:315–330.
25. Rezai KA, Semnani RT, Farrokh-Siar L, et al. Human fetal RPE cells induce apoptosis in allogenic T-cells in a Fas ligand and PGE2 independent pathway. *Curr Eye Res*. 1999;18:430–439.
26. Lyons RM, Gentry LE, Purchio AF, et al. Mechanism of activation of latent recombinant TGF-$\beta_1$ by plasmin. *J Cell Biol* 1990;110:1361–1367.
27. Murphy-Ullrich JE, Poczatek M. Activation of latent TGF-β by TSP-1: mechanisms and physiology. *Cytokine Growth Factor Rev* 2000;11:59–69.
28. Siren V, Stephens RW, Salonen EM, A, et al. RPE cells secrete urokinase-type plasminogen activator and its inhibitor PAI-1. *Ophthalmic Res* 1992;24:203–212.
29. Elner SG. Human RPE lysis of extracellular matrix: functional urokinase plasminogen activator receptor, collagenase, and elastase. *Trans Am Ophthalmol Soc* 2002;100:273–299.
30. Hara Y, Caspi RR, Wiggert B, et al. Use of ACAID to suppress interphotoreceptor retinoid binding protein-induced experimental autoimmune uveitis. *Curr Eye Res* 1992;11(suppl):97–100.
31. Tolsma SS, Volpert OV, Good DJ, et al. Peptides derived from two separate domains of the matrix protein TSP-1 have anti-angiogenic activity. *J Cell Biol*. 1993;122:497–511.
32. Bleuel K, Popp S, Fusenig NE, et al. Tumor suppression in human skin carcinoma cells by chromosome 15 transfer or TSP-1 overexpression through halted tumor vascularization. *Proc Natl Acad Sci USA* 1999;96:2065–2070.
33. Schultz-Cherry S, Chen H, Mosher DF, et al. Regulation of TGF-β activation by discrete sequences of TSP-1. *J Biol Chem* 1995;270:7304–7310.
34. Dawson DW, Pearce SF, Zhong R, et al. CD36 mediates the In vitro inhibitory effects of TSP-1 on endothelial cells. *J Cell Biol*. 1997;138:707–717.
35. Guo NH, Krutzsch HC, Negre E, et al. Heparin-binding peptides from the type I repeats of TSP: structural requirements for heparin binding and promotion of melanoma cell adhesion and chemotaxis. *J Biol Chem* 1992;267:19349–19355.

# FOCIS 2005

**Abstract Number:** 850864

**Presenting Author:** C H Lau

**Author for Correspondence** Chun H Lau, MB,MSc,MD, FRCS

**Department/Institution:** Ophthalmology, Schepens Eye Research Institute, Harvard Medical School

**Address:** 20 Staniford Street

**City/State/Zip/Country:** Boston, MA, 02114-2500, United States

**Phone:** 617-912-7456 **Fax:** 617-912-7456 **E-mail:** chunlau@vision.eri.harvard.edu

**Abstract Categories:** 13. Immunology of the Eye

**Abstract Theme:** 4. Immunoregu ation

**Title:** Mechanisms of ret nal immune privilege

C H Lau and A W Taylor. [1]Schepens Eye Research Institute and Department of Ophthalmology, Harvard Medical School, Boston, MA, United States.

**Body:** The eye is an immune privileged tissue that constitutively produces neuropeptides, cytokines, and factors that actively suppress inflammation mediated by innate and adaptive immunity. The neural retina (NR) and retinal pigmented epithelial (RPE) cells are documented to support immune privilege; however, most of our understanding of the mechanisms of ocular immunity has been from analyzing the anterior chamber of the eye. Therefore, to begin to identify factors important in regulating immunity in the retina, we investigated the effects of secreted factors from the NR and the RPE on the activity of resting and activated macrophages. The NR from healthy C57BL/6J mice was dissected and placed in culture for 24 hours. Culture media was placed into the resulting posterior eye cup containing RPE and incubated for 24 hours. These conditioned media (CM) was used to treat resting or endotoxin-stimulated macrophages (J774A.1 cell line). After 48 hours, the macrophage supernatants were assayed by multiplex analysis for IL-1beta, IL-6, IL-10, TNF-alpha, GM-CSF. In addition, the RPE-CM and NR-CM were assayed by multiplex analysis. We found IL-6, GM-CSF in RPE-CM, and IL-6 in the NR-CM. The NR-CM stimulated GM-CSF production by resting macrophages, but was suppressed in endotoxin-stimulated macrophages. Both the RPE-CM and NR-CM suppressed IL-1beta and TNF-alpha production by the endotoxin-stimulated macrophages, while they induced significant levels of IL-10 production by the macrophages. While the NR may support macrophage differentiation through GM-CSF, both the NR and the RPE suppress the production of inflammatory cytokines (IL-1beta and TNF-alpha) by endotoxin-stimulated macrophages, while causing the same macrophages to produce the anti-inflammatory cytokine, IL-10. Such results suggest that the mechanisms of immunosuppression by the retina may involve factors that suppress classical activation while promoting alternative activation of macrophages. Therefore, both the neuroretina and RPE contribute to the mechanisms of retinal immune privilege.
Supported by grants from the USAMRMC.

| | |
|---|---|
| **Program#/Poster#:** | 970/B944 |
| **Abstract Title:** | **Contribution of Neuroretinal and Pigmented Epithelial Cell Factors to Subretinal Immunity** |
| **Presentation Start/End Time:** | Sunday, May 01, 2005, 2:30 PM - 4:15 PM |
| **Location:** | Hall B/C |
| **Reviewing Code:** | 219 ocular immune responses - IM |
| **Author Block:** | *C.H. Lau, A.W. Taylor.* Schepens Eye Research Institute and Department of Ophthalmology, Harvard Medical School, Boston, MA. |
| **Keywords:** | 544 immunomodulation/immunoregulation, 546 inflammation, 485 cytokines/chemokines |

**Purpose:** Previous studies by Streilein et al revealed that the subretinal space is an immunosuppressive microenvironment. Since both the neuroretinal cells (NR) and the pigmented epithelial cells (RPE) have the potential to contribute factors into the subretinal space, we investigated the expression of cytokines produced by the NR and RPE and their effect on inflammatory macrophage activity. **Methods:** RPE eyecups and NR from healthy C57BL/6J mice were prepared and cultured for 24 hours. The eyecup supernatant (RPE-SN) and NR conditioned media (NR-SN) were transferred to macrophage cultures with or without lipopolyssacharide activation. After 48 hours culture, the macrophage culture supernatants were analyzed using a Bio-Rad multiplex analyzer for IL-1β, IL-6, Il-10, IL-12 (p70), TNF-α, G-CSF, GM-CSF, MIP-1α, RANTES and KC. The RPE-SN and NR-SN were also analyzed by the multiplex analysis. **Results:** We found IL-6, IL-10, TNF-α, GM-CSF and KC in RPE-SN and G-CSF and KC in the NR-SN. In the presence of resting macrophage, KC levels were reduced in both RPE-SN and NR-SN. RPE-SN suppressed G-CSF, while NR-SN increased GM-CSF production by resting macrophage For LPS-activated macrophages, the RPE-SN did not suppress any LPS-induced factor, but did induce significant production of IL-10. The NR SN significantly promoted TNF-α production, and significantly suppressed IL-1β production by the activated macrophages **Conclusions:** Both RPE and NR supernatants did not activate the macrophages, however, RPE-SN and NR-SN had differential effects on LPS-activated macrophages. Therefore neuroretinal and RPE cells contribute differently to the subretinal microenvironment. This implies that the mechanism of immunosuppression observed in the subretinal space is a combined effort of the RPE and neuroretina.

| | |
|---|---|
| **Commercial Relationship:** | **C.H. Lau**, None; **A.W. Taylor**, None |
| **Support:** | NIH Grant EY10752 and Department of Defense/USAMRMC |

Appendix 4

Available online at www.sciencedirect.com
SCIENCE DIRECT®
Biomaterials 26 (2005) 3187–3196
Biomaterials
www.elsevier.com/locate/biomaterials

# Fabrication of degradable polymer scaffolds to direct the integration and differentiation of retinal progenitors

E.B. Lavik[a,*], H. Klassen[b], K. Warfvinge[c], R. Langer[d], M.J. Young[e]

[a]Biomedical Engineering, Yale University, 15 Prospect Street, Becton Center 229, New Haven, CT 06511, USA
[b]Stem Cell Research, Children's Hospital of Orange County, Orange, CA
[c]Department of Ophthalmology Lund, Sweden
[d]Chemical Engineering, MIT
[e]Schepens Eye Research Institute, Harvard Medical School, Boston, MA

Received 15 June 2004; accepted 10 August 2004
Available online 28 September 2004

**Abstract**

Retinal progenitor cells (RPCs) are self-renewing cells capable of differentiating into the different retinal cell types including photoreceptors, and they have shown promise as a source of replacement cells in experimental models of retinal degeneration. We hypothesized that a biodegradable polymer scaffold could deliver these cells to the subretinal space in a more organized manner than bolus injections, while also providing the graft with laminar organization and structural guidance channels. We fabricated highly porous scaffolds from blends of poly(L-lactic acid) and poly(lactic-*co*-glycolic acid) using a variety of techniques to produce pores oriented normal to the plane of the scaffold. RPCs were seeded on the polymer scaffolds and cultured for 14 days. Seeded scaffolds were then either fixed for characterization or used in an explant or in vivo rat model. The scaffolds were fully covered by RPCs in 3 days. Attachment of RPCs to the polymer scaffold was associated with down regulation of immature markers and up-regulation of markers of differentiation. This suggests that the scaffold may promote differentiation of RPCs. The seeded cells elaborated cellular processes and aligned in the scaffold in conjunction with degenerating retinal explants. The cells also exhibited morphologies consistent with photoreceptors including a high degree of polarization of the cells. This data suggests that the scaffold may be a means to assist in the promotion of photoreceptor phenotypes. Implantation of the seeded scaffold into the rat eye is associated with increased RPC survival. Taken together, these data suggest that these polymer scaffolds provide a useful means for delivering RPCs to the subretinal space and may assist in the formation of retinal cell phenotypes, although it is clear that more cues are needed to direct the differentiation of RPCs into functional photoreceptors.


*Keywords*: Polymer; Scaffold; PLGA; Retina; Retinal progenitor cells

## 1. Introduction

Conditions of retinal degeneration including retinitis pigmentosa (RP) and age-related macular degeneration (AMD) affect over a million people in the US alone, where they comprise the leading cause of irreversible visual disability [1]. Outer retinal degeneration involves the loss of photoreceptor cells and may also involve the cells of the inner nuclear layer which connect to and support the photoreceptors. Neural progenitor cells (NPCs) have been shown to integrate morphologically into the inner nuclear layer in injury models but have not been seen to replace photoreceptors [2–4]. Recently, retinal progenitor cells (RPCs) have been isolated from the mature eye [5,6] and developing retina [7,8] and these cells may have promise for replacing photoreceptors [9].

The retina has a complex, multilayered architecture that is polarized with respect to the photoreceptors which are located at the back of the retina and

*Corresponding author. Tel.: +1 203-432-4265.
*E-mail address:* erin.lavik@yale.edu (E.B. Lavik).

0142-9612/$ - see front matter © 2004 Elsevier Ltd. All rights reserved.
doi:10.1016/j.biomaterials.2004.08.022

intimately associated with the retinal pigment epithelium (RPE). Light must travel through the retinal processing layers before reaching the photoreceptor outer segments where phototransduction occurs. The integrity of the RPE layer is critical to the survival and function of photoreceptors and hence patterned vision. RPC grafts alone may be insufficient to recreate this complex cytoarchitecture on a large scale, particularly when multiple retinal layers have been lost or disrupted [10,11]. A second challenge for the use of RPCs is the delivery and survival of the cells. Studies indicate that the typical bolus injection of RPCs leads to a large degree of cell death. Another concern is reflux of cells from the subretinal space into the vitreous cavity at the time of injection. Vitreal cells can obscure the light path or in some instances even result in retinal detachment [12]. In addition, the widespread intraretinal migration frequently observed with these cells may not be desirable in all settings. For instance, the organized reconstruction of specific cellular layers may require that precise constraints be placed upon grafted cells.

We hypothesized that a tissue engineering approach, namely, using a degradable polymer scaffold with the appropriate architecture, might improve the survival and promote the organized differentiation of grafted RPCs in models of retinal degeneration and injury. In the intact retina, the orientation of photoreceptors and retinal bipolar cells is radial with respect to the curvature of the globe. To approximate the physical characteristics of this microenvironment, we experimented with a variety of techniques, including phase-inversion casting [13] and solid liquid phase separation [14], to create porous scaffolds with pores oriented normal to the plane of the scaffolds. These scaffolds were then seeded with cells, the cells were characterized via RT-PCR and immunohistochemistry, and seeded scaffolds were co-cultured with degenerating retinal explants or implanted in vivo in models of retinal degeneration. The results of this work indicate that degradable polymer scaffolds improve the survival of RPCs in retinal degeneration models, promote differentiation of RPCs, and provide physical guidance to the RPCs resulting in a more normal anatomical organization.

## 2. Experimental

### 2.1. Polymer fabrication

#### 2.1.1. Materials

Poly(lactic-*co*-glycolic acid) (PLGA) with a lactic to glycolic acid ratio of 50:50 and a number average molecular weight of Mn ~35,000 g/mol, noted here as PLGA 504, PLGA with a lactic to glycolic acid ratio of 50:50, a carboxylic acid end group, and a number average molecular weight of Mn ~25,000 g/mol, noted as PLGA 503H here, and PLGA with a lactic to glycolic acid ratio of 75:25 and a number average molecular weight of Mn ~45,000 g/mol, referred to as PLGA 755, were obtained from Boehringer Ingelheim GmbH (Germany). Poly(L-lactic acid) (PLLA) with a number average molecular weight of Mn ~100,000 g/mol, referred to here as PLLA 100k, and PLLA with a number average molecular weight of Mn ~50,000 g/mol, referred to here at PLLA 50k, were obtained from Polysciences (Warrington, PA). All solvents were from Aldrich (St. Louis, MO) (ACS Grade).

#### 2.1.2. Phase-inversion membrane formation

Solutions were prepared with concentrations of 10, 20, 25 and 30% (w/v) polymer (either PLGA 504 or PLGA 503H) in dimethylsulfoxide (DMSO). 5–10% (v/v) of glycerol was added to the solutions to promote the formation of larger and less asymmetric pore structures. 0.4 ml of the complete solution was added to a glass slide (dimensions) and allowed to spread evenly over the entire surface of the slide. The glass slide was then immersed in 18 MΩ water (MilliQ system, Millipore, Billerica, MA) at room temperature and the solvent transfer process initiated. Slides were removed from the water once the transfer process was complete, approximately 10 min after immersion. The completion of the transfer was indicated by the absence of solution at the glass-slide interface. Samples that completed the transfer were easily removed from the glass slides without any apparent sticky residue. Membranes were then dried with blotting paper and lyophilized overnight to remove residual water and solvent.

#### 2.1.3. Solid-liquid phase separation

Five percent (w/v) solutions of PLGA, PLLA, or blends of PLGA/PLLA in dioxane were prepared. 0.3–0.5 ml of solution was added to a glass slide and allowed to spread uniformly across the slide. The slide was then placed on an ice bath so that the slide was in good contact with the ice, but residual water was not allowed to interact with the solution. After 1 min, a 20-gauge piece of copper wire, which had been sitting in dry ice, was touched to the surface of the slide. This initiated nucleation of dioxane crystals. The growth front spread along the surface of the slide and then moved normal to the slide, growing towards the solution–air interface. Once the dioxane had completely solidified, the slide was transferred to a freezer at −20 °C for at least 1 h. Slides were then placed on a lyophilizer to sublimate the dioxane, leaving behind the polymer scaffolds whose pore structure was a direct artifact of the freezing process.

During the above procedure, slides would occasionally become immersed in the ice water solution before the dioxane crystallization process was nucleated. These samples were placed in the freezer and lyophilized

separately. The architectures formed as a result of this immersion were found to be novel. To initiate this procedure in a controlled and reproducible manner, slides were placed on the ice, cooled to 0 °C, and nucleation was initiated via the introduction of water through atomization from a spray bottle. The procedure, a hybrid of the solid–liquid phase separation technique and the phase-inversion technique, produced unique and reproducible scaffolds.

### 2.2. Scanning electron microscopy

Polymer samples were mounted and gold coated using a sputtering apparatus at 25 mA for 30 s. Samples containing cells were dehydrated through a graded series of ethanol steps to 100% ethanol followed by transfer to hexamethyldisilazane (Polysciences) and evaporation of the residual solvent in a chemical hood, followed by gold coating as before.

### 2.3 Mechanical testing

Samples were cut to the following dimensions: 4 cm by 0.75 cm. Each scaffold was approximately 0.3 mm thick. Exact measurements for each scaffold were found prior to testing using digital calipers. Porous scaffolds were used instead of solid sheets to permit a more direct comparison with the in vitro and in vivo experiments. The scaffolds were tested at a strain rate of 0.05 mm/s until failure. Five samples of each blend of polymer scaffold were successfully tested. One sample failed in the grips and was excluded from the analysis.

### 2.4. Cell seeding

Briefly, RPCs were isolated from pooled retinae of postnatal day 1 eGFP transgenic C57Bl/6 mice (gift from Dr. Okabe, University of Osaka, Japan). Retinae were dissected free from the posterior eyecup and the ciliary marginal zone and optic nerve head removed under microscopic visualization. Pooled retinal tissue was finely minced and digested with 0.1% Type 1 collagenase (Sigma, St. Louis, MO) for 20 min. The supernatant containing liberated cells was forced through a 100 μm mesh strainer, centrifuged and seeded into culture vessels in Neurobasal medium (GIBCO BRL Life Technologies, Rockville, MD) supplemented with 2 mM L-glutamine, 100 μg/ml penicillin–streptomycin, 20 ng/ml epidermal growth factor (EGF, Promega, Madison, WI) and B27 neural supplement (GIBCO). This cycle was repeated until all retinal tissue was digested. Cells were re-fed on alternating days. Within 2–3 weeks, RPCs were visible as non-adherent spheres and continued to expand in the presence of EGF. Cultures were split 1:5 every 7–10 days. Although capable of expansion through >60 passages, cells of <20 passages were used in this study. Scaffolds were sterilized by soaking overnight in 70% ethanol. Under aseptic conditions, the scaffolds were then rinsed three times in PBS. Rinsed scaffolds were transferred to 6-well plates where RPCs were added to the scaffolds as spheres or dissociated cells in medium. RPCs seeded on the polymers were cultured under expansion conditions (20 ng/ml EGF) for 14 days prior to transplantation.

### 2.5. Histology and immunohistochemistry on seeded scaffolds

At specific times following seeding of the RPCs, scaffolds were fixed in 4% paraformaldehyde and cryosectioned. Sections were then stained with hemotoxylin and eosin (H&E) or antisera directed against neurofilament (NF), glial fibrillary acidic protein (GFAP), Hes1, Hes5, proliferative cellular nuclear antigen (PCNA), NUMB, Cyclin D3 or Oligo1.

### 2.6. RT-PCR

The cells were seeded and maintained on the polymers in EGF-containing medium for 7 days, after which the medium was removed and the polymer transferred to a new culture dish to avoid extracting RNA from stray cells adhering to the original dish. With the cells still adherent to the polymer, a Purescript RNA Isolation Kit (Gentra) was used to extract total RNA according to the manufacturer's instructions. Extracted RNA was treated with DNase (DNA-*free*, Ambion) to eliminate any contaminating DNA. M-MLV (Moloney Murine Leukemia Virus) reverse transcriptase (Invitrogen) was used to perform reverse transcription using 2 μl of RNA in a final volume of 20 μl. To further select for amplification of transcripts, as opposed to genomic sequences, primers were chosen to flank at least one intron whenever possible. Amplification was performed with 2.7 μl of cDNA template, 0.7 μl of forward and reverse primers (0.5 μg/μl, Qiagen), and 1.25 units of *Taq* DNA Polymerase (Amersham) on a Techne Genius thermocycler. The PCR program consisted of 4 min at 94 °C, followed by 30 cycles that consisted of 1 min at 94 °C, 1 min at the annealing temperature corresponding to the primers used, and 1 min at 72 °C. The final extension reaction lasted for 7 min and was carried out at 72 °C. Amplified products were visualized on a 2% agarose gel against a 100 base pair ladder. Negative controls were run with RNA, but no reverse transcriptase, to ensure that the PCR product was not amplified from genomic DNA.

### 2.7. Explant studies

Scaffolds were seeded with RPCs and cultured for 7 days at 37 °C and 5% $CO_2$. At 7 days, the seeded

scaffolds were co-cultured with degenerating mouse retinal explants. The explants were obtained from the C3H rd/rd mouse model, in which photoreceptors are rapidly lost during the first 3 weeks of postnatal development. Three-week-old mice were used for these studies. Retinae were isolated from each eye and placed into culture in Millicell well tissue culture inserts (Becton Dickenson) with the retinal ganglion cell layer down. Polymers seeded with RPCs as described above were then placed onto the upper surface of the explant in direct apposition to the degenerating photoreceptor layer. These explant/polymer composites were then cultured for 7–14 days, after which they were fixed in 4% paraformaldehyde and prepared for histological examination.

### 2.8. In vivo studies

Polymer scaffolds seeded with RPCs were also injected into the subretinal space of 5 adult Sprague-Dawley rats. The seeded scaffolds were trimmed to ~1 × 2 mm, and injected into the subretinal space via a 50 μl Hamilton syringe connected to a glass capillary tube. The subretinal space was accessed through a transceral incision 1 mm posterior to the ora serrata. The graft was imaged in vivo with a fluorescent fundus camera and the recipients sacrificed after 2 weeks.

## 3. Results and discussion

### 3.1. Fabrication of scaffolds

Scaffolds were fabricated using either the phase-inversion technique or the solid–liquid phase separation technique. Both techniques resulted in scaffolds with pores oriented normal to the plane of the scaffold as desired for mimicking the polarized nature of the retina. Fig. 1A–C demonstrates the architecture of scaffolds made using the phase-inversion technique. Fig. 1D–F are examples of those made using the solid–liquid phase separation technique, and Fig. 1G–I are examples of those made using a non-solvent plus solid–liquid phase separation technique.

The phase-inversion technique led to asymmetric pores as is typically the case [13]. Fig. 1A is an SEM micrograph of the water-exposed side in which the polymer precipitates out of solution very quickly leading to the extremely small pores, generally 1–2 μm in diameter. Fig. 1B shows the glass side of the film with the typical larger pores (50–100 μm in diameter). Fig. 1C shows a cross section of the film with the thin skin coupled to the more porous layer. The phase-inversion technique was highly flexible, permitting the use of PLGA or PLLA of a wide range of molecular weights (40–100 kDa) and a reasonably wide range of pore structures, obtained via the addition of glycerol. The membranes exhibited a degree of residual stress which manifested as curling upon removal from the glass slide following drying of the films. This made subsequent manipulation more challenging, particularly cell seeding.

The solid–liquid phase separation technique was based on a modification of Schurgens et al. [15] in which the polymer solution (PLGA in dioxane) was cast on slides and frozen at 0 °C on ice leading to the rejection of the polymer solute from the solid dioxane phase. The dioxane was then sublimated, leaving the PLGA with a distinct pore architecture as a direct artifact of the dioxane crystallization. A wide range of pore architectures may thus be obtained by controlling the dioxane concentration. The scaffolds in Fig. 1D–F were obtained by inducing nucleation of the freezing at the glass surface via contact with a copper coil at −80 °C. From the point of nucleation, the solid phase was observed to grow along the glass slide and then normal to the glass slide.

The SEM micrographs demonstrate the uniform pore structure and high degree of porosity present throughout the scaffolds. Fig. 1D shows the air side of the scaffold, the glass side appears identical. The pores are approximately 100–200 μm in diameter, permitting the efficient seeding of cells into the scaffolds. Fig. 1E shows a closer view into the pores of the scaffold. Fig. 1F shows a cross section of the scaffold demonstrating that the pores are oriented normal to the plane of the scaffold and have walls between them. We hypothesized that the orientation of the pores would provide physical guidance cues to promote the alignment of the RPCs in the scaffold, which we thought might promote the formation of the highly polarized photoreceptor layer in vivo.

The scaffolds in Fig. 1G–I were created using a hybrid solid–liquid phase separation technique coupled with precipitation via a non-solvent. The slides were cooled to 0 °C on ice and, as an alternative to nucleation via the copper coil, water was introduced via atomization from a spray bottle. Fig. 1G shows a cross section with the ladder-like structure typical of the solid–liquid phase separation technique. Fig. 1H shows the air side of the scaffold where the water was introduced which exhibits a fibrous-like quality. Fig. 1I shows the glass slide side of the scaffold which exhibits bundles of fibers. The pores between the bundles of fiber-like structures correlate with the pores in the solid–liquid separation scaffolds. These scaffolds were very friable and not suitable for handling in a tissue engineering application.

### 3.2. Mechanical properties of scaffolds

The elastomeric properties of the scaffolds were important with respect to the significant amount of

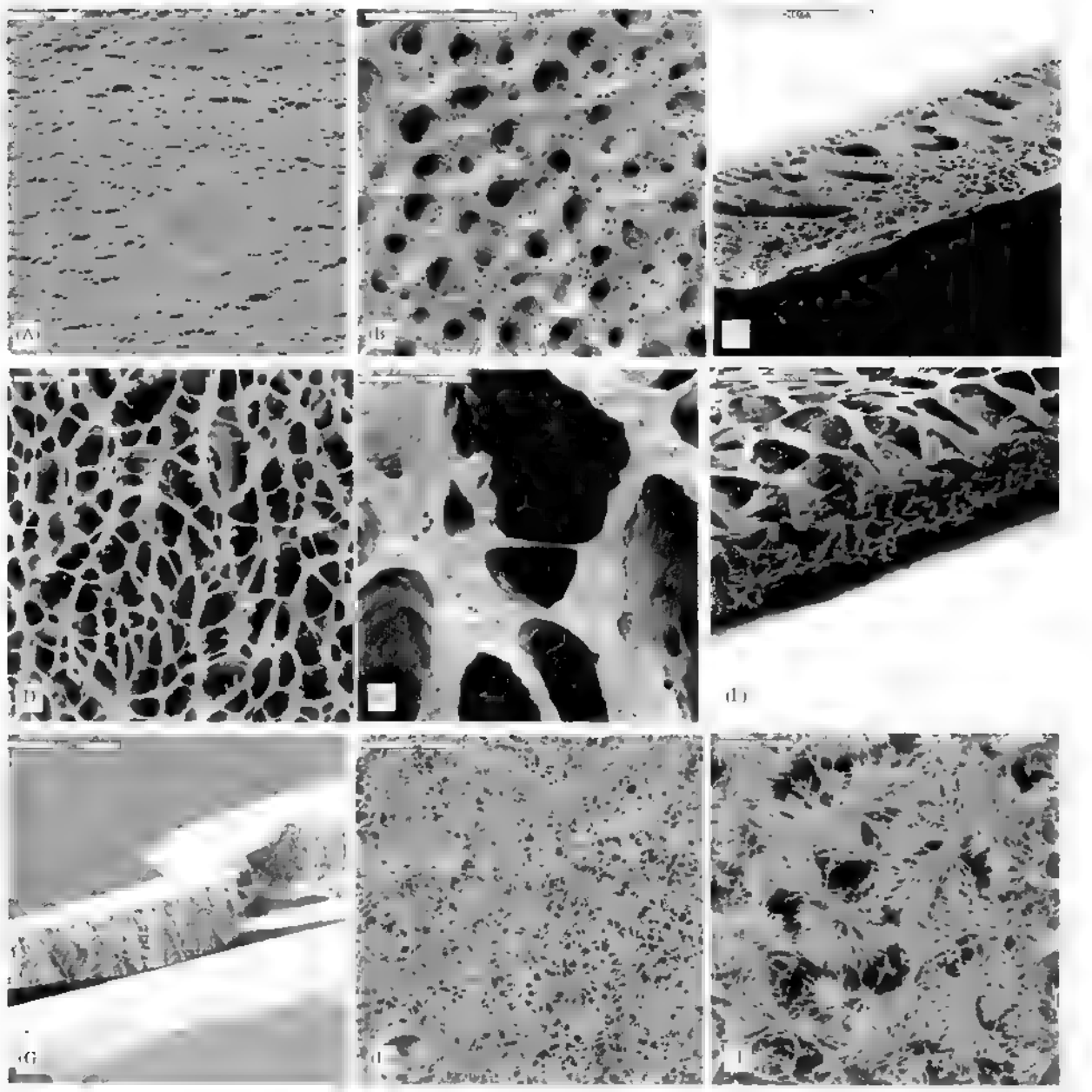

Fig. 1 (A–C) Asymmetric membranes of PLGA (50:50 Mn ~30,000) formed via the phase-inversion process with the addition 20% by volume of glycerol. (A) Water-exposed side. (B) Glass side. (C) Cross section. (D–F) PLGA 755 scaffold prepared using the solid–liquid phase separation technique. (D) Air side which is identical to the glass side. (E) Air side magnified further. (F) Side view of scaffold demonstrating the orientation of the pores. (G–I) PLGA 755 scaffold prepared using the modified solid–liquid phase separation technique. (G) Scaffold side view. (H) Air side of scaffold. (I) Air side at higher magnification.

manipulation required for subretinal transplantation of the scaffolds. In particular, the insertion of the scaffold into the subretinal space, particularly in the small subretinal space of the mouse or rat, required that the scaffold be able to undergo significant deformation without failure. Furthermore, a scaffold with a high modulus might cause damage to surrounding tissue due to the lack of compliance.

Fig. 2 shows the mechanical properties of sets of scaffolds made from different blends of PLLA and PLGA via the solid–liquid phase separation process. PLGA 504 and PLGA 775 could not be tested due to the very poor mechanical properties of the scaffolds made from these individual polymers.

Fig. 2A shows representative curves for each of the four polymers tested. The elastic modulus of each

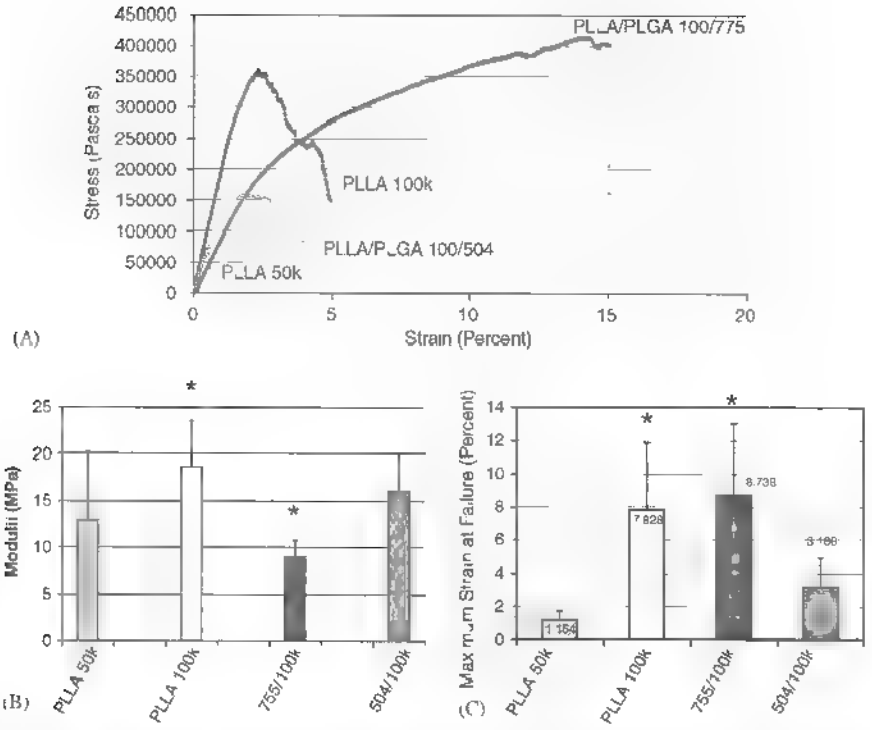


Fig. 2. Mechanical testing results for the solid–liquid phase separation scaffolds. All scaffolds were fabricated from a 5% (w/v) solution of polymer in dioxane. (A) Representative stress–strain curves for the 4 blends of polymers tested. (B) Elastic moduli for the blends of polymers tested. (C) Maximum strain at failure, error bars = SD; *significant difference ($P<0.05$ by ANOVA followed by the Tukey–Kramer multiple comparison test.

of these curves was calculated and the graph in Fig. 2B summarizes the results. The 50:50 blend of PLLA 100k and PLGA 775 led to the lowest elastic modulus of (9.0±1.7 MPa), which was significantly lower than the PLLA 100k (18.6+4.8 MPa) as determined by a one-way analysis of variance (ANOVA) followed by the Tukey–Kramer multiple comparisons test ($P<0.05$). The low modulus leads to scaffolds which are less stiff and more compliant and therefore less likely to injure the tissue surrounding the subretinal space. The maximum strain at which the scaffolds failed is shown in Fig. 2C for all the groups. There was a significant increase in strain to failure for both the PLLA 100k and the 50:50 blend of PLLA 100k and PLGA 775 with respect to the PLLA 50k or the 50:50 blend of PLLA 100k and PLGA 504, as determined by a one-way analysis of variance (ANOVA) followed by the Tukey–Kramer multiple comparisons test ($P<0.05$). Such effects have been seen previously with blends [20,21]. The blending of the polymers overcomes, to a degree, the innate glassy mechanical properties of the family of PLA and PLGA polymers. The higher elongation before failure and lower modulus made the 50:50 blend of PLGA 755 and PLLA 100k the most appropriate choice for the in vitro and in vivo work and was thus used throughout this study.

### 3.3. Culturing of RPCS on the scaffolds

RPCs were seeded on the scaffolds using a number of techniques to identify that technique resulting in the most complete and uniform seeding of RPCs throughout the scaffold. The most successful technique was to seed RPCs as spheres with minimal mechanical dissociation at a concentration of $5\times10^6$ cells/ml drop-wise onto the scaffolds (approximately 1 ml for each 4 mm × 4 mm scaffold) and allowing the cells to attach overnight prior to adding additional medium. Scaffolds seeded using this technique are shown in Fig. 3. Fig. 3A shows a scaffold at 1 day post seeding. The GFP-positive RPCs can be seen throughout the scaffold. By 3 days, the scaffold appears to be filled with RPCs (Fig. 3B). Twenty-micrometer-thick cross sections of the scaffolds viewed using either fluorescence imaging of the GFP cells counterstained with DAPI (Fig. 3C) or H&E (Fig. 3D) demonstrate cells throughout the thickness of the scaffolds.

### 3.4. Immunohistochemistry and RT-PCR on the RPCs on the scaffolds

Fig. 4 shows immunohistochemistry on sister sections of an RPC-seeded scaffold which was fixed 24 h post seeding. The RPCs readily adhered to the polymer in

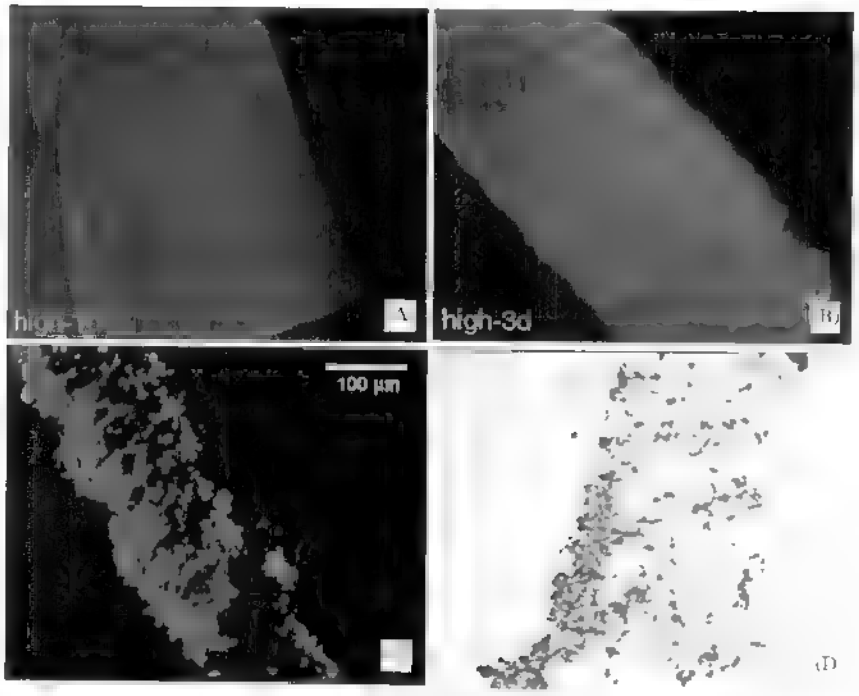


Fig. 3. Seeding of scaffolds. (A) Seeded solid–liquid phase separation scaffold at day 1, 1 day post seeding. The RPCs are green. (B) Same scaffold at day 3. (C) Cross section of similar scaffold at 3 days post seeding. GFP-RPCs (green) counterstained with DAPI (blue). (D) Sister cross section to (C), stained with H&E.

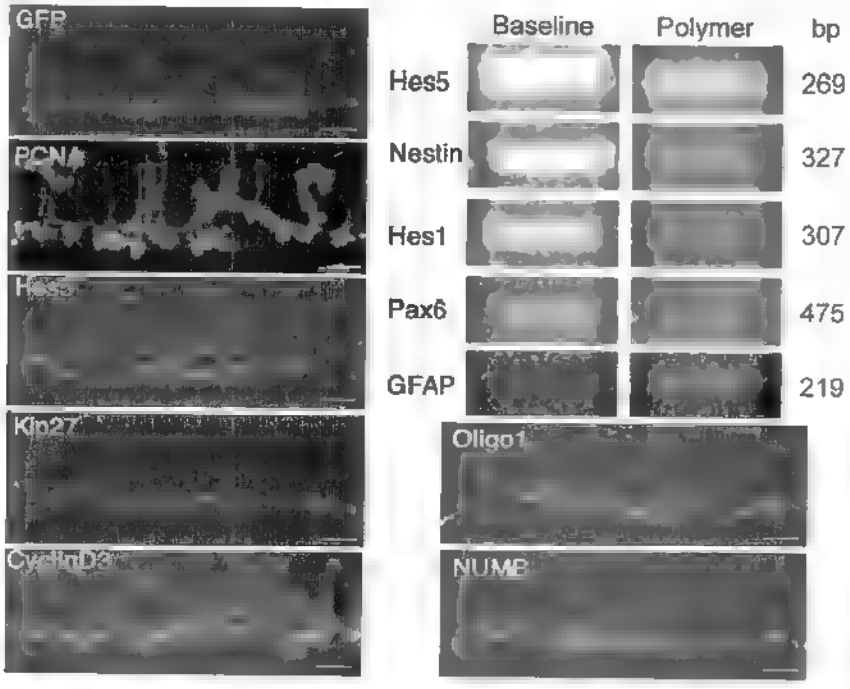


Fig. 4. RT-PCR and immunohistochemistry for RPCs seeded on scaffolds, fixed 24 h post seeding. The cells are down-regulating immature markers and up-regulating markers for differentiation (oligo1 and GFAP). Scale bar = 60 μm.

culture without subsequent surface modification of the scaffolds. This attachment to the polymer scaffold is associated with a change in gene expression by the progenitor cells. The RPCs show co-localization for a number of immature markers including PCNA, NUMB, Cyclin D3 and Hes5, but also some co-localization for

markers of differentiation, specifically Olig01, a marker for differentiation into oligodendrocytes. The accompanying RT-PCR results demonstrate that while the RPCs alone are positive for several immature markers, specifically Hes5, nestin, Hes1 and Pax6, these immature markers are down-regulated in RPCs cultured for 1 week on the polymer scaffold. Furthermore, while the RPCs express little detectable GFAP at baseline, whereas this mature marker is up-regulated in RPCs grown on the scaffolds. These results suggest that attachment to the polymer scaffold may promote differentiation of RPCs.

This observation raises a number of important issues. First of all, the use of a polymer scaffold for cellular grafts cannot be assumed to be without consequences with respect to the cells even in the presence of EGF, the mitogen used to maintain the RPCs in an undifferentiated state. It would appear that the unmodified polymer can influence the gene expression and, in all likelihood, the ontogenetic status of co-grafted progenitor cells. Second, because the vast majority of applications of this technology call for the terminal differentiation of cellular grafts, the pro-differentiation influence of the scaffold may facilitate the desired outcome while simultaneously tending to inhibit any undesirable proliferation. Further investigation is indicated to clarify the nature of the differentiation induced, the mechanism involved, and the extent to which this phenomenon can be generalized to other polymers and undifferentiated cell types. Finally, the possibility of modifying the polymer to bind specific pro- or anti-differentiation factors opens an additional range of phenotypic outcomes potentially available with this system.

### 3.5. Co-culture of RPC-seeded scaffolds with degenerating retinal explants

Following seeding for 7 days, the polymer scaffolds were co-cultured with degenerating retinal explants from rd/rd mice. H&E staining of the co-cultures demonstrates that the majority of the cells in the scaffold were found adjacent to the degenerating retinal explant (Fig. 5A). The polymer scaffolds originally contained cells throughout the construct, so the localization of the cells at the polymer/explant interface suggests either a trophic factor-induced survival effect or an active migration of the cells toward the explant. This last possibility would not be entirely surprising, as stem cells and progenitors have been shown to migrate toward areas of injury [16–18]. The channels of the polymer appeared to induce a longitudinal morphology in the differentiating progenitor cells, with a short neurite-like process directed toward the remaining outer plexiform layer and an elongated cell body directed away from the explant (Fig. 5B). This morphology is consistent with that of a rod photoreceptor and is oriented in manner appropriately for this cell type. While there was no evidence for the expression of photoreceptor-specific markers during the short duration of these studies, this morphological organization has not been previously observed with RPCs in vitro in the absence of a scaffold. The physical guidance of the scaffold via the oriented pore structure appears to promote these morphologies. While more cues may be needed to direct the RPCs, it is encouraging that the cells appear to align longitudinally, a vital prerequisite to functional photoreceptor reconstruction. It is also encouraging that these cells which exhibit the appropriate morphologies also exhibit the cellular polarization required for functional photoreceptors. This suggests that the presence of the appropriate scaffold may influence photoreceptor development.

### 3.6. Implantation of RPC-seeded scaffolds in the rat eye

Fig. 6 shows bright field and UV illuminated images of RPC-seeded scaffolds implanted subretinally in the rat eye at 1 and 14 days. The UV images demonstrate that the RPCs are still present and viable (expressing

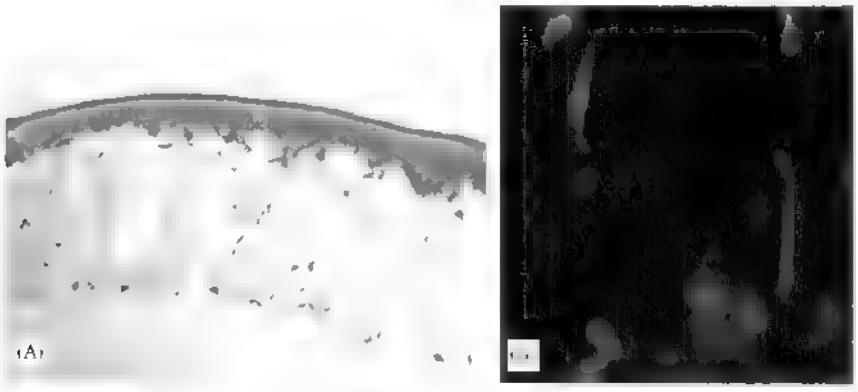


Fig. 5. (A) H&E staining of section of the seeded polymer scaffold co-cultured with a degenerating retinal explant from an rd/rd mouse. (B) GFP-RPCs in sister section from immediately below the explant. The cell morphologies are consistent with those for photoreceptors, but the cells did not express any markers for photoreceptors.

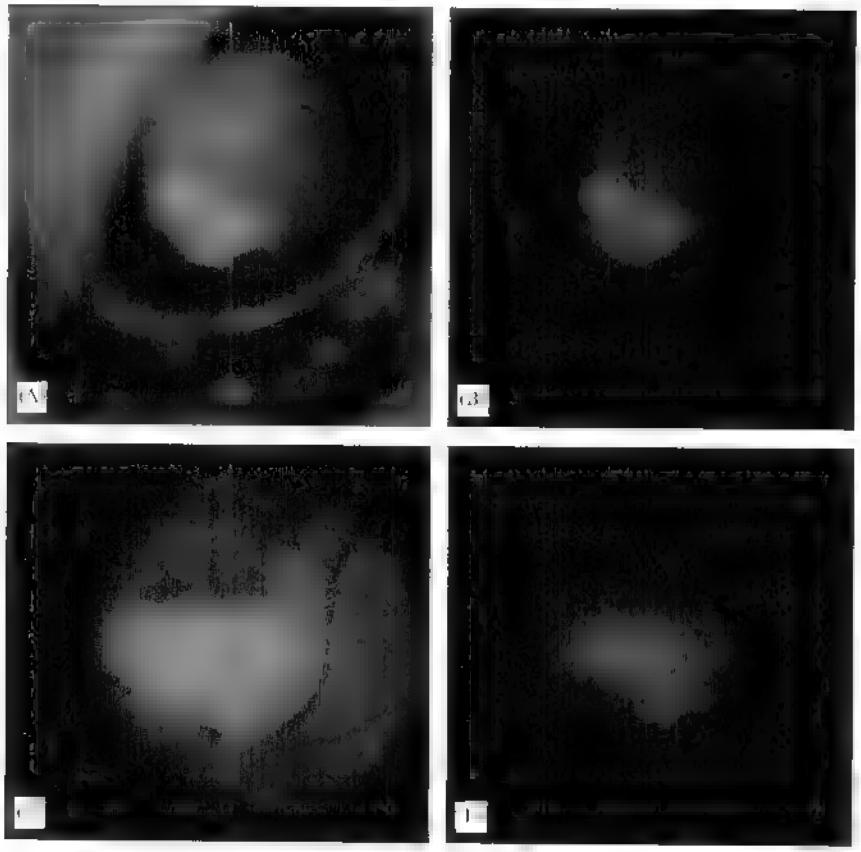

Fig. 6. (A, B) RPC-seeded scaffold implanted subretinally in the rat eye at 1 day post implantation. (C, D) RPC-seeded scaffold in the same rat at 14 days post implantation. Many of the RPCs appear to still be surviving.

GFP) at 14 days throughout the scaffold. Although we did not reconstruct and count individual cells before and after grafting, we estimate that greater than 50% of the cells survived in all animals for 14 days, with the example shown in Fig. 6 suggesting a higher rate of cell survival in xenogeneic hosts without immunosuppression. Grafted cells were found to survive in all 5 recipients at 14 days post grafting. In previous experiments without polymer scaffolds, large numbers of cells were not seen 14 days post grafting [4,19].

Grafting of RPCs on scaffolds in the rat subretinal space has several clear advantages over injection of RPCs as spheres or single cell suspensions. The in vivo fundus image clearly demonstrates the survival of mouse progenitor cells in the rat eye. In particular, the maintenance of a high level of GFP expression indicates that the cells are indeed thriving in this xenogeneic environment, even in the absence of immunosuppression. This result is in stark contrast to previous work with these cells in which murine progenitor cells grafted as small spheres displayed extremely poor survival in the rat eye [4]. The seeded scaffold is inserted subretinally via a slit in the sclera and choroid and, as such, the cells see very limited shearing forces. However, when the RPCs are injected without the polymer, they are exposed to high shear forces as they pass through the needle. In addition, cell preparation prior to grafting does require treatment with enzymes or centrifugation to enrich the cell population. These two factors make the polymer an attractive cell delivery vehicle for CNS grafting, where clinical and animal studies suggest that at least 90% of the cells do not survive the transplantation procedure itself [22,23]. The increase in long-term survival may of course be a direct result of overcoming the cell death at the time of grafting, but we are also investigating the possibility of other factors, including the generation of a local immunoprivileged microenvironment. We have previously shown that neural progenitors are an immune privileged cell type [24], and we have undertaken a detailed study of cell survival with and without polymer substrates in various immunodisparate hosts. This work will provide insight into the mechanism of polymer graft survival, and will also allow us to develop new stem cell transplantation techniques

## 4. Conclusions

We have fabricated biodegradable scaffolds with a wide range of mechanical properties. These scaffolds can

be readily seeded with RPCs which fully cover the scaffold in 3 days. Upon attachment, the RPCs down-regulate immature markers and up-regulate markers of differentiation. This suggests that the polymer scaffold may promote differentiation of RPCs. The cells also show a high degree of alignment within the scaffold and, in conjunction with degenerating retinal explants, take on morphologies suggestive of developing photoreceptors. Coupled with the increasing polarization of the progenitor cells in the polymer scaffold, these data suggest that the scaffold may be a means to assist in the promotion of photoreceptor phenotypes. In addition, implantation of the seeded scaffold into the rat eye leads to better survival of the RPCs as compared to other methods. Taken together, these data suggest that polymer scaffolds provide a useful means for delivering RPCs to the sub-retinal space and may assist in the formation of photoreceptors, although it is clear that more cues are needed to direct the differentiation of RPCs to form functional photoreceptors

## Acknowledgements

We would like to acknowledge Richard D. and Gail Siegal for support (EL, RSL, MJY), Ivan Kirov, Jr. for technical assistance with RT-PCR, funding from the CHOC Foundation, Guilds, and Padrinos (HK); and the NIH (NS044060, HK), the Crown Princess Margaret's Committee for the Blind (KW), the Swedish Association of the Visually Impaired (KW), the Swedish Science Council (Medicine) (KW), 2nd ONCE International Award for New Technologies for the Blind (KW).

## References

[1] Vision problems in the US. prevalence of adult vision impairment and age-related eye disease in America. prevent blindness America and the National Eye Institute, 2002.

[2] Wojciechowski AB, Englund U, Lundberg C, Wictorin K, Warfvinge K. Subretinal transplantation of brain-derived precursor cells to young RCS rats promotes photoreceptor cell survival. Exp Eye Res 2002;75(1):23–37.

[3] Young MJ, Ray J, Whiteley SJO, Klassen H, Gage FH. Neuronal differentiation and morphological integration of hippocampal progenitor cells transplanted to the retina of immature mature dystrophic rats. Mol Cell Neurosci 2000;16(3):197–205.

[4] Mizumoto H, Mizumoto K, Shatos MA, Klassen H, Young MJ. Retinal transplantation of neural progenitor cells derived from the brain of GFP transgenic mice. Vision Res 2003;43(16):1699–708.

[5] Reh TA, Levine EM. Multipotential stem cells and progenitors in the vertebrate retina. J Neurobiol 1998;36(2):206–20.

[6] Tropepe V, Coles BLK, Chiasson BJ, Horsford DJ, Elia AJ, McInnes RR, van der Kooy D. Retinal stem cells in the adult mammalian eye. Science 2000;287(5460):2032–6.

[7] Shatos M, Mizumoto K, Mizumoto H, Kurimoto Y, Klassen H, Young M. Multipotent stem cells from the brain and retina of green mice. Regen Med 2001;2:13–5.

[8] Bhattacharya S, Jackson JD, Das AV, Thoreson WB, Kuszynski C, James J, Joshi S, Ahmad I. Direct identification and enrichment of retinal stem cells/progenitors by Hoechst dye efflux assay. Invest Ophthalmol Visual Sci 2003;44(6):2764–73.

[9] Akagi T, Haruta M, Akita J, Nishida A, Honda Y, Takahashi M. Different characteristics of rat retinal progenitor cells from different culture periods. Neurosci Lett 2003;341(3):213–6.

[10] Marc R, Jones B, Watt C, Strettoi E. Neural remodeling in retinal degeneration. Prog Eye Res 2003;22:607–55.

[11] Klassen H, Sakaguchi DS, Young M. Stem cells and retinal repair. Prog Eye Res 2004;23:149–81.

[12] Ryan SJ. The patho-physiology of proliferative vitreoretinopathy in its management. Am J Ophthalmol 1985;100(1):188–93.

[13] Di Luccio M, Nobrega R, Borges CP. Microporous anisotropic phase inversion membranes from bisphenol A polycarbonate: effect of additives to the polymer solution. J Appl Polym Sci 2002;86(12):3085–96.

[14] Schurgens C, Maquet V, Grandfils Ch, Jerome R, Teyssie Ph. Polylactide macroporous biodegradable implants for cell transplantation. II. Preparation of polylactide foams by liquid–liquid phase separation. J Biomed Mater Research 1996;30:449–61.

[15] Schurgens C, Maquet V, Grandfils C, Jerome R, Teyssie P. Biodegradable and macroporous polylactide implants for cell transplanation. I. Preparation of macroporous polylactide supports by solid–liquid phase separation. Polymer 1996;37:1027–38.

[16] Lu B, Kwan T, Kurimoto Y, Shatos M, Lund RD, Young MJ. Transplantation of EGF responsive neurospheres from GFP transgenic mice into the eyes of rd mice. Brain Res 2002;943(2):292–300.

[17] Ahn TB, Kim JM, Kwon KM, Lee SH, Jeon BS. Survival and migration of transplanted neural stem cell derived dopamine cells in the brain of parkinsonian rat. Int J Neurosci 2004;114(5):575–85.

[18] Boockvar JA, Kapitonov D, Kapoor G, Schouten J, Counelis GJ, Bogler O, Snyder EY, McIntosh TK, O'Rourke DM. Constitutive EGFR signaling confers a motile phenotype to neural stem cells. Mol Cell Neurosci 2003;24(4):1116–30.

[19] Ader M, Meng J, Schachner M, Bartsch U. Formation of myelin after transplantation of neural precursor cells into the retina of young postnatal mice. Glia 2000;30:301–10.

[20] Fromstein JD, Woodhouse KA. Elastomeric biodegradable polyurethane blends for soft tissue applications. J Biomater Sci-Polym Edition 2002;13(4):391–406.

[21] Jones DS, Djokic J, McCoy CP, Gorman SP. Poly(epsilon-caprolactone) and poly(epsilon-capro.actone)-polyvinylpyrrolidone-iodine blends as ureteral biomaterials. characterisation of mechanical and surface properties, degradation and resistance to encrustation in vitro. Biomaterials 2002;23(23):4449–58.

[22] Castilho R, Hansson O, Brundin P. Improving the survival of grafted embryonic dopamine neurons in rodent models of Parkinson's disease. Prog Brain Res 2000;127:203–31.

[23] Hagell P, Brundin P. Cell survival and clinical outcome following intrastriatal transplantation in Parkinson disease. J Neuropathol Exp Neurol 2001;60:741–52.

[24] Takahashi M, Palmer TD, Takahashi J, Gage FH. Widespread integration and survival of adult-derived neural progenitor cells in the developing optic retina. Mol Cell Neurosci 1998;12(6):340–8.

**STEM CELLS, in press**

# Biodegradable polymer composite grafts promote the survival and differentiation of retinal progenitor cells

**Minoru Tomita[1], Erin Lavik[2], Henry Klassen[3], Tasneem Zahir[1], Robert Langer[4], and Michael J. Young[1]**

1) The Schepens Eye Research Institute, Department of Ophthalmology, Harvard Medical School, Boston, MA

2) Yale University, New Haven, CT

3) Children's Hospital of Orange County and U.C. Irvine, Orange, CA

4) Massachusetts Institute of Technology, Cambridge, MA

*Correspondence should be addressed to* **Michael J. Young Ph.D.**

*Address*: The Schepens Eye Research Institute, Department of Ophthalmology, Harvard Medical School, 20 Staniford St. Boston, MA, 02111

Tel: 1-617-912-7419, Fax: 1-617-912-0101

E-mail: mikey@vision.eri.harvard.edu

**Key words**: Retinal transplantation, Retinal progenitor cells, Cell survival, Biodegradable polymer, and Retinal regeneration

## Abstract

Retinal progenitor cells (RPCs) are multipotent central nervous system (CNS) precursors that give rise to all the cell types of the retina during development. Several groups have reported that mammalian RPCs can be isolated and expanded in culture, and can differentiate into retinal neurons upon grafting to the mature, diseased eye. However, cell delivery and survival remain formidable obstacles to application of RPCs in a clinical setting. As biodegradable polymer/progenitor constructs have been shown to be capable of tissue generation in other compartments, we evaluated the survival, migration, and differentiation of RPCs delivered on PLA/PLGA polymer substrates to the mouse subretinal space, and compared these results to conventional injections of RPCs. Polymer composite grafts resulted in a near 10 fold increase in the number of surviving cells after 4 weeks, with a 16-fold increase in cell delivery. Grafted RPCs migrated into the host retina and expressed the mature markers NF200, GFAP, PKC-α, recoverin, and rhodopsin. We conclude that biodegradable polymer/progenitor cell composite grafts provide an effective means of increasing progenitor cell survival and overall yield when transplanting to sites within the CNS such as the retina.

## Introduction

The two major clinical subtypes of retinal degeneration (RD) are retinitis pigmentosa (RP) and age-related macular degeneration (ARMD). A hallmark of these diseases is photoreceptor cell degeneration resulting in visual loss No effective restorative treatment exists for either for RD. Recently, the transplantation of stem and progenitor cells has shown promise as a strategy for photoreceptor replacement [1 4]. Many mammalian tissues, including the retina, contain stem or progenitor cells that can be isolated, propagated, and grafted to animal models of retinal degeneration [3,4]. The goal of these studies is to either replace or preserve the function of photoreceptors in the affected eye. Previously, it has been reported that brain-derived progenitor cells can migrate and differentiate into cells expressing markers of mature neurons and glia when grafted to the retina of mice and rats with RD [3 9] Despite incorporation into the host retina and morphological similarities to various retinal cell types, in each of these studies the transplanted cells failed to express retina-specific markers. In an attempt to overcome this hurdle, retinal progenitor cells (RPCs) have been isolated from two different derivatives of the embryonic eye cup: the ciliary epithelium and the neuroretina. These RPCs have the capacity to differentiate into photoreceptors and other cells of retinal lineage. However, poor survival of grafted cells remains a significant barrier to functional cell replacement. Similar problems have been seen in other cell-based therapies, such as intracerebral grafts in animal models [10] and patients with Parkinson's Disease [11]. Moreover, bolus injection of cells into the subretinal space does not result in a well-organized photoreceptor layer of the type needed for high visual acuity

We have applied tissue engineering techniques to this problem by using biodegradable polymers as a substrate for RPC grafts. Tissue engineering has arisen, in part, to address the shortage of tissues and organs available for transplantation [12]. It has shown promise in the repair of bladder [13], cartilage [14] and skin [15] defects and is being evaluated for a range of additional clinical applications. Moreover, poly (lactic-*co*-glycolic acid) (PLGA)/poly (L-lactic acid) (PLLA) polymers exhibit a high degree of biocompatibility in the brain [16] and spinal cord [17]. Tissue engineering does not yet allow the construction of a functional retina *de novo*, but polymers have the potential to address a number of critical, unsolved problems in retinal transplantation. We hypothesize that an organized graft, containing aligned and polarized cells, is more readily achieved by seeding the cells onto a PLA/PLGA polymer scaffold prior to transplantation. The polymer construct could also increase control over graft size and placement. Importantly, donor cell survival may be improved, as cell death, leakage, and migration from the injection site occurs when RPCs are delivered as a single cell suspension [4].

Biodegradable polymers are attractive in tissue engineering applications for several reasons, including availability and ease of manufacture. The polymers can be easily processed into a variety of structures and degradation can be readily controlled. These constructs have FDA approval for use in a number of applications [18]. Here we develop a biodegradable polymer/retinal progenitor composite graft that provides an effective method for transplantation of progenitor cells to the subretinal space of RD mice by significantly improving survival, control of delivery, and cellular differentiation as compared to injection of dissociated cells.

## Material and methods

### *Scaffold Fabrication*

Polymers were constructed using a 50/50 blend of poly (lactic-*co*-glycolic acid) (PLGA) lactic acid to glycolic acid ratio of 75:25, Mn~ 45,000 g/mol, Boehringer Ingelheim GmbH (Germany) and poly (L-lactic acid) (PLLA) Mn~ 100,000 g/mol, Polysciences (Warrington, PA) dissolved in 5% w/v solution dioxane. We used a modification of the solid-liquid phase separation technique described by Schugens [19] The solution (0.3 to 0.5 mls) was added to a glass slide and allowed to spread uniformly across the slide. The slide was then placed on ice. After 1 minute, a 20-gauge piece of copper wire, which had been sitting in dry ice, was touched to the surface of the slide to initiate nucleation of dioxane crystals The growth front spread along the surface of the slide and then moved normal to the slide, growing towards the solution/air interface. Once the dioxane had completely solidified, the slide was transferred to a freezer at –20°C for at least 1 hour. Slides were then placed on a lyophilizer to sublimate the dioxane, leaving behind the polymer scaffolds whose pore structure was a direct artifact of the freezing process.

The porosity was estimated for the samples by a simple calculation of the ratio of density of a series of six samples via their weight in air divided by their volume to the density of the polymer as reported by the manufacturer. The pore size data was determined by measuring 40-50 pores at the surface of over a series of six scaffolds. Cross sections of the scaffolds in SEM were used to confirm that the pores were generally uniform in diameter from the surface through the thickness of the samples.

***Donor cell line***

Retinal progenitor cells (RPCs) harvested from the retina of P1 (postnatal day 1) EGFP (Enhanced Green Fluorescence Protein) mice (C57BL/6 background; kind gift of Dr Okabe, University of Osaka) were isolated and maintained in culture as previously described [4] Briefly, whole retina homogenates were incubated in 0.1% collagenase and single-cell suspensions obtained. Dissociated cells were then cultured in DMEM/F12 supplemented with N-2 (Gibco) and 20 ng /ml of epidermal growth factor (EGF). The neurospheres that were generated could in turn be dissociated and subcultured to regenerate new spheres.

***Differentiation and characterization of donor cell line***

To examine the differentiation of GFP expressing RPCs *in vitro*, RPC spheres were incubated with trypsin for 1 min to generate a single cell suspension. Cells ($1.0 \times 10^3$) were plated on 8 well laminin-coated chamber slides (BD) in DMEM/F12 media supplemented with 10% fetal bovine serum and were fixed with 4% paraformaldehyde at 1 day, and 2 week after plating. The cells were blocked in 1% BSA (Sigma) + 0.2% Triton-100 (Sigma), then incubated for 2 hours with primary antibody for Ki67 (1:100, cell proliferation marker, Vector), nestin (1:1, immature neuronal marker, DSHB, Iowa), GFAP (1:50, astrocytic marker, Dako), MAP-2 or NF-200 (1:500 and 1: 1000, respectively, neuronal makers, Sigma), PKC-α (1:200, bipolar cell maker, Santa Cruz), 2D4 (1:500, rhodopsin marker, kind gift of Dr. R. Molday, University of BC, Canada), and recoverin (1:1000, photoreceptor marker, Chemicon). After rinsing in PBS, samples were incubated in Cy3-

conjugated species-specific IgG (1:800) for 1 hour. Samples were rinsed again and then coverslipped in poly vinyl alcohol (PVA)-Dabco with DAPI and viewed under fluorescent illumination.

***EGF antibody staining of polymers***

In order to evaluate whether growth or survival factors could be sequestered in the polymer substrate, we stained the polymer for antibodies against EGF. We evaluated grafts containing cells at 1, 2, and 4 weeks after transplantation, and acellular polymers *in vitro* after exposure to EGF-containing media. Polymers were sterilized overnight in 70% ethanol. After rinsing 3 time with HBSS, polymers were incubated with DMEM media with EGF (10 $\mu$g/ml), fixed in 4% PFA, and sectioned at day 7 (n=6). As a control, the polymer treated with 5% PVA (Sigma) for 5 hours were also cultured with EGF. Sections were blocked in 1% BSA (Sigma) + 0.2% Triton-100 (Sigma), then incubated for 2 hours with primary antibody of EGF (1:20, R&D system) for 2 hours, followed by reaction with species- specific IgG conjugated to Cy3 (1:800) for 1 hour. Samples were rinsed again and then coverslipped in PVA-Dabco viewed under fluorescent illumination.

***Graft preparation***

RPCs were seeded onto polymer scaffolds that had been cut into 10 x 10 mm squares, and sterilized overnight in 70% (vol/vol) ethanol. The polymers were incubated with 5 mls laminin solution (0.005 mg/ml) for 60 min at 37 °C and then washed three times in PBS in a 6 well plate After laminin treatment, 4 mls of culture media were added to the 6 well plate. After 60 min in a 37 °C incubator, most of the culture media was removed from the 6 well plate and RPCs (1.0 x$10^6$ cells) were dispersed on the polymer coated with the laminin and

incubated for an additional 60 min. After incubation, 4 mls of culture media was added to the 6 well plates. Three days after initial seeding, most of the culture media was removed and polymers were turned over to seed RPCs onto the obverse side, as described above. Seven days after initial seeding, the polymer/RPCs composites were cut into rectangular pieces of 0.5 x 0.3 mm using a McIlwain tissue chopper (Brinkmann Institutes, Westbury, NY).

***Differentiation and characterization of donor cell line on polymer composite graft***

To examine the differentiation of donor cells before transplantation, some composites were placed into a 24 well culture dish and then fixed with 4% paraformaldehyde for 1 hour. The composites were blocked in 1% BSA (Sigma) + 0 2% Triton-100 (Sigma), then incubated for 2 hours with primary antibodies against Ki67, nestin, Map2, GFAP, PKC-α, recoverin, and rhodopsin (see above) for 2 hours, followed by reaction with species specific IgG conjugated to Cy3 (1:800) for 1 hour. Samples were rinsed again and then coverslipped in PVA-Dabco with DAPI and viewed under fluorescent illumination.

***Recipient animals***

Recipient mice were C57/BL/6 (survival times 1 week, n = 20; 2 weeks, n = 15; 4 weeks, n = 15), and rhodopsin knockout mice (rho -/-) (survival times 1 week, n = 6; 2 weeks, n = 10; 4 weeks, n = 10), grafted at 4 to 8 weeks of age (Jackson Labs, Bar Harbor, ME) All animals were treated in accordance with guidelines defined by the ARVO Statement for Use of Animals in Ophthalmic and Vision Research.

***Transplantation***

Recipient mice were treated with polymer/RPC composite grafts, or single cell injections,

both placed into the subretinal space under general (ketamine/xylazine) and topical (proparacaine) anesthesia as previously described [4]. Transplantation was performed under direct observation using a binocular surgical microscope and viewed through a dilated pupil (topical tropicamide 1%). At the conclusion of all surgeries, fundus examination was performed via surgical microscope to confirm successful graft placement.

***Transplantation of RPC / polymer composite graft***

A conjunctival incision and small sclerotomy were made using an extra-fine disposable scalpel. The polymer composite pieces (each containing ~ 16,000 cells) were inserted through the sclerotomy into the subretinal space using fine #5 Dumont forceps (Fine Science Tools). The polymer could be easily imaged through the pupil using either fluorescent or standard illumination.

***Single cell transplantation***

A small sclerotomy was made and cells were injected into the subretinal space using a glass pipet (internal diameter 150 $\mu$m) attached to a 50-$\mu$l Hamilton syringe via polyethylene tubing. Two $\mu$ls of GFP donor cell suspension, containing 16,000 single cells, were injected into the subretinal space. During transplantation, the intraocular pressure was reduced by making a small puncture through the cornea.

***Tissue preparation***

At 1, 2, and 4 weeks post-transplantation, the grafted eyes were enucleated and immersion fixed with 4% paraformaldehyde, followed by cryoprotection with 20% sucrose Eyes were sectioned at 12 $\mu$m on a cryostat. Sections were stained with antibodies as described above. Some sections were also stained by hematoxylin and eosin stain (H&E).

***Cell counting methods***

One week after culture, composites were cut into 0.3 x 0 5 mm sized pieces with a tissue chopper. Every other piece was fixed in 4% PFA and sectioned to assess the total cell number before transplantation. Alternate pieces were transplanted into the subretinal space. A single cell suspension of RPCs was also transplanted into the subretinal space as a control. Eyes were enucleated, fixed in 4% PFA, and sectioned at day 0, 1, 2, and 4 weeks. Samples were rinsed again and then coverslipped in PVA-Dabco with DAPI and viewed under fluorescent illumination. Both GFP and DAPI+ cells were counted in one out of every four sections. Experimental and control cell numbers were then compared and statistical analysis performed using a Student's t- test.

***Evaluation of TUNEL+ cells with different procedures***

In order to examine the effect of traumatic cell death in the different transplantation methods, we counted the number of TUNEL+ cells under single cell injection and polymer construct conditions. RPC spheres were incubated with trypsin for 1 min to generate a single cell suspension. Cells ($1\ 0 \times 10^3$) were plated on 8 well laminin-coated chamber slides (BD) in DMEM/F12 media supplemented with 10% fetal bovine serum (FBS) using one of two methods: either apulled-glass needle as used in the conventional method of subretinal transplantation (n=6), or a 200 $\mu$l pipet tip (Falcon) as used for seeding polymers (n=6). We also used the same method to seed polymers with RPCs (n=6). Cells were cultured under differentiation conditions with 10% FBS and were fixed with 4% paraformaldehyde at 3 days, with the polymers sectioned as previously described. The cells were blocked in 1% BSA (Sigma) + 0.2% Triton-100 (Sigma) and TUNEL staining was then performed using a

TUNEL staining kit (Roche, Germany). Every sample was rinsed again and then coverslipped in PVA-Dabco with DAPI and viewed under fluorescent illumination. DAPI+ cells and TUNEL+ cells were counted under each condition and statistical analysis was performed using a Student's t- test.

## Results

### *Formulation of polymer scaffolds*

Scaffolds were fabricated using the solid-liquid phase separation technique leading to pores oriented normal to the plane of the scaffold as desired for mimicking the polarized cytoarchitecture of the retina. The pore structure was largely uniform with diameters of approximately 35-50 $\mu$m. The polymer solution (PLGA in dioxane) was cast onto slides and frozen on ice at 0 °C leading to the precipitation of the polymer solute from the solid dioxane phase. The dioxane was then sublimated, leaving the PLGA with a unique pore architecture as a direct artifact of the dioxane crystallization. A wide range of pore architectures can be obtained by controlling the concentration of dioxane, the amount of undercooling, and the thermal gradient. Our goal was to seed the scaffolds with RPCs, thus relatively large, oriented pores were desired. We used very little undercooling (11 °C), coupled with the promotion of nucleation at the glass surface via contact with a copper coil at -80 °C. The solid phase was observed to grow along the glass slide and then normal to the glass slide. Following sublimation of the dioxane, we produced polymers with a large, oriented, and reproducible pore structure (see Fig. 2A-C).

***Characterization of donor cells in vitro***

When grown on conventional substrates in media supplemented with EGF, GFP-transgenic RPCs exhibited high levels of endogenous green fluorescence (Fig. 1A) and maintained an undifferentiated state characterized by ubiquitous Ki67 and nestin immunoreactivity (Fig. 1B and C). Cells could be maintained in this state for up to one year. To examine differentiation *in vitro*, media without EGF was supplemented with 10% fetal bovine serum. After 2 weeks of culture under differentiation conditions, the cells were analyzed immunocytochemically. The number of Ki67+ cells markedly decreased (data not shown) and subpopulations expressed GFAP, Map2, PKC α, recoverin, or rhodopsin. These markers are consistent with differentiation into rod photoreceptors, bipolar cells, and Muller glia, all of which are known to be born late in retinogenesis. Interestingly, these immunopositive cells also showed morphological evidence of differentiation into rod photoreceptor and bipolar cell types (Fig. 1). No immunocytochemical or morphological evidence of early born cell types (e.g., cones or retinal ganglion cells) was observed. These data indicate that RPCs derived from neonatal mice have the intrinsic potential to differentiate into late-born retinal cell types.

***Attachment and incorporation of RPCs onto the polymer substrate.***

The solid liquid phase separation technique using dioxane was able to generate polymers with the appropriate pore structure for the seeding of RPCs. The pore architecture can be seen in SEM images (Fig. 2A-C) before the addition of RPCs. The scaffolds are approximately 95% porous and the pore size is estimated to be 35-50 $\mu$m in diameter. The parameters of the seeding procedure described in this work were developed to ensure the

maximum seeding density without induction of cell death. We used a 2 phase procedure in which one side of the polymer was seeded first and the other 3 days later, followed by an additional 4 days in culture. We determined that this method leads to a composite graft in which RPCs were fully incorporated, yet not overcrowded such that significant cell death could occur. The seeded polymers are shown in SEM images (Fig. 2D-E) and under GFP illumination (Fig. 2F-G).

***Characterization of donor cells on polymer scaffolds prior to grafting***

Polymer/RPC composites were analyzed immunocytochemically to determine whether culturing RPCs on a PLGA substrate induces changes in gene expression indicative of differentiation. Polymer/RPC composites were cultured for 7 days, and then cut into 0.5 x 0.3 mm fragments, as used for transplantation, and examined for the cellular markers listed above. A majority of RPCs expressed Ki67 and nestin (Fig. 2I-N), although at a lower level than that seen when the same cells were grown under identical conditions but without the PLGA substrate. A subpopulation of cells expressed the more mature markers GFAP, Map2, and PKC-α (Fig. 2O-W), however, there was no evidence for expression of the retina-specific markers recoverin or rhodopsin. These data indicate that most of the RPCs cultured on a PLGA scaffold remain relatively undifferentiated prior to grafting, while a subset express early markers of more mature neurons or glia.

***Biodegradable polymers stained for EGF in vivo and in vitro***

Sections were stained with EGF antibody at 1, 2, and 4 weeks after transplantation to subretinal space of B6 mice. We found EGF+ staining throughout the polymer at all time points (Fig. 2H). We also found EGF+ staining of the polymer after 1 week in culture with

EGF (Fig. 2X-I to X III). No EGF+ staining was detected when the polymer was treated with 5% poly-vinyl alcohol (PVA; Fig. 2Y-I to Y-III). These results suggest that the biodegradable polymer used here can adsorb the key cell survival factor EGF, in both an in vitro model and in an in vivo transplantation model. Furthermore, this EGF adsorption is dependent upon the hydrophobic properties of the polymer, as treatment with PVA eliminates this effect The presence of the EGF, and perhaps other factors, on the biodegradable polymer may in part underlie the increased cell survival seen in these experiments

***The fate of RPCs transplanted as a polymer composite graft to the subretinal space***

Survival and integration (defined as morphological incorporation) of grafted RPCs was evaluated by fundus examination as well as immunohistochemical analysis of tissue sections (Fig. 3A-H). Intraocular GFP+ profiles were identified at 1, 2, and 4 weeks post-transplantation using *in vivo* fluorescence microscopy (Fig.3E-H). Survival and integration of grafted RPCs in the retina of non-immunosuppressed host animals were confirmed by histological analysis. In syngeneic C57/Bl6 mice and rhodopsin knockout (rho -/-) mice, surviving RPCs were found in all recipient eyes at all three points (total 76/76; 100%). GFP-expressing RPCs frequently migrated into the host retina where they showed signs of morphological integration. At 1, 2, and 4 weeks post transplantation, integrated RPCs were found in 83%, 100%, and 90% of adult rho . mice, and 85%, 87%, 87% of adult C57/Bl6 mice, respectively (Table 1).

***Polymer degradation***

The breakdown of RPC seeded PLGA scaffolds was examined in cryosections and

compared at 1, 2, and 4 weeks post-transplantation to the subretinal space. Gradual breakdown of the polymer component of the composite grafts was seen over the course of this period (Fig. 3J-L). Pores progressively increased in size and merged, such that at 4 weeks very little of the polymer scaffold remained. Although the average overall thickness of the did not change substantially, degradation was observed as an increase in the pore size, such that large channels were observed in the polymers at 2 and 4 weeks post implantation (Figure 3K-L).

***Migration and differentiation of cells delivered as polymer/RPC composite grafts***

At 1, 2, and 4 weeks post-transplantation, RPCs migrated into retinal laminae adjacent to the graft, and showed morphological evidence of neuronal differentiation (Fig. 3I and 4). GFP+ donor cells co-expressed a number of markers indicative of phenotypic maturation including NF200, GFAP, PKC-α, recoverin, and rhodopsin (Fig. 4 and 5). Expression of these markers increased post-transplantation, with rhodopsin and recoverin becoming more intense and widespread by the 4-week time point. Interestingly, rhodopsin was expressed by RPCs grafted to rho -/ recipients, a finding not seen in previous work using single cell suspension grafts in this model [4].

***Cell survival in polymer/RPC composite grafts vs. single cell suspensions***

RPCs were counted before grafting and at 1, 2, and 4 weeks after transplantation to the subretinal space as a composite graft or single cell suspension. Before transplantation, each polymer graft contained about 16,000 cells (mean±SD =15,800±672; n=7), and this same number of cells was used for the single cell suspension grafts. Since a significant drawback of single cell suspensions is reflux of cells from the injection site, we also counted the

number of cells present immediately after injection. An average of 9,232 cells (57.7% of those grafted) were still present in recipients analyzed at day 0 (n=6), indicating that 43.3% of the grafted cells were either lost due to reflux or did not survive the transplantation procedure. We then assessed the number of surviving cells in the polymer composite grafts at 1, 2, and 4 weeks after transplantation and found 91% (n=6), 96% (n–6), and 78% (n=6) survival at these time points, respectively (Fig. 6A). Results for single cell suspension grafts, calculated relative to the day 0 result (9,232), showed survival of 12.7% (n=6), 9.9% (n=6), and 8 1% (n=6) at 1, 2, and 4 weeks (Fig. 6A). These data show that the percent survival of RPCs delivered as a polymer composite graft is approximately 10 fold higher than cell suspension grafts after 4 weeks ($p<0.01$). Moreover, if one includes in the calculation the number of cells that die or leak out during the grafting procedure, a 16-fold improvement in cell delivery to the subretinal space is obtained using a polymer composite graft.

***TUNEL+ cells are greatly reduced with polymeric delivery methods***

We assessed the number of TUNEL+ cells in cell culture preparations that were analogous to the transplantation methods employed in this study. The preparation that used a conventional glass needle to seed (rather than inject) RPCs resulted in an extremely high rate of cell death (57.8% TUNEL+) at 3 days after seeding onto culture slides (Fig. 6B). In contrast, when we used the pipet method of seeding onto either culture slides, or polymer substrates, the rate of TUNEL+ staining was decreased to 1.56% and 14.9% respectively. These results indicate that traumatic cell death associated with cell injection is greatly reduced by using a large bore pipet rather than a small bore glass needle, and that cell death

is approximately 9.5% higher when seeding onto the biodegradable polymers, compare to standard culture treated slides.

## Discussion

Efficiency of cell delivery, together with the related problem of cell survival, has posed a serious impediment to effective transplantation within the CNS since the earliest attempts at brain repair. This has been documented in studies of neural transplantation for Parkinson's Disease, where populations of cells secreting dopamine or its precursors, are grafted to the striatum as a means of ameliorating the behavioral deficits caused by the loss of dopaminergic neurons in the substantia nigra of the host [20, 21]. The work of Brundin and colleagues has demonstrated that approximately 90% of grafted fetal mesencephalic neurons do not survive the transplantation procedure itself [22]. This fact alone has made clinical application of this technology extremely difficult, as up to 4 donor embryos are needed to provide a sufficient number of grafted cells for each hemisphere of the Parkinsonian patient's brain. This issue has been less extensively studied in the setting of retinal transplantation, but it is clear from the literature that the loss of grafted cells, either by cell death or leakage, remains a significant challenge to widespread cell replacement in this CNS compartment as well. Reflux is a persistent aspect of the problem, particularly when delivering a bolus injection of cells to the subretinal space. The data we present here demonstrates that the use of a biodegradable polymer decreases the number of cells lost to reflux by almost 50%. With respect to leakage of cells from the subretinal space to the choroid or vitreous, this phenomenon is also problematic because of the potential for ectopic cells to initiate additional complications such as tractional retinal detachment,

obstructed trabecular outflow, or intraocular inflammation, all of which would pose serious threats to vision. In terms of donor cell death, this process continues unabated during the first 4 weeks when using a single cell suspension graft, while use of the polymer substrate decreases cell loss by more than 9-fold. Overall, the use of polymer composite grafts results in an increase in cell delivery of nearly 16-fold over cell suspensions.

Recent transplantation studies have demonstrated that neural progenitor cells have the capacity to migrate into the immature, diseased, or injured retina and differentiate into cells that morphologically resemble retinal neurons. However, evidence to date indicates that brain-derived neural progenitor cells, as well as the less mature embryonic stem (ES) cells, fail to differentiate into opsin+ photoreceptors when grafted to the adult mammalian retina [3, 5-9, 23, 24]. In contrast, it has been demonstrated that neural progenitors derived from the retina (i.e., RPCs) can differentiate into cells of retinal lineage, including opsin+ photoreceptors, both *in vitro* and *in vivo*. Following transplantation of RPCs to a mouse model of retinal degeneration, recipients showed improved light sensitivity [4]. Nevertheless, several challenges to the effective application of this treatment strategy remain, including the control of cell delivery, survival of grafted RPCs, and efficiency of differentiation into photoreceptors. The present study demonstrates that each of these parameters can be significantly improved through the use of biodegradable substrates to deliver retinal progenitor cells to the retina.

Our experiments *in vitro* and *in vivo* shed light upon the mechanisms underlying increased cell survival through polymeric delivery. Our *in vitro* modeling of the transplantation procedure demonstrates that significant cell death occurs when delivering progenitor cells

through the small bore glass needle typically used for subretinal transplantation. The use of a large bore pipet tip (as used in the polymer seeding) greatly reduces this cell death.

The mechanism underlying the increased survival of grafted cells at extended time points is more difficult to determine. The evidence we present showing that the scaffold is capable of growth factors adsorption such as EGF is one possible explanation. As this binding takes place in both the *in vitro* model, as well as the *in vivo* experimental paradigm under study here, the continued availability of the survival factor EGF (and likely other proteins) suggests a further role for the polymer in promoting the survival of grafted progenitor cells. Interestingly, the concentration of EGF appears to be at survival (<10 $\mu$g/ml), rather than mitogenic levels, as proliferation of the progenitor cells was not detected after transplantation (data not shown). These results point to the use of modified polymer substrates in the development of cell delivery systems.

The use of a polymer composite graft also appears to promote the differentiation of RPCs towards rod photoreceptors. Whereas we were previously unable to demonstrate the expression of rod photoreceptor markers following bolus injection of RPCs to the rho -/- subretinal space, in the present study RPCs delivered to these same hosts as polymer composite grafts matured into cells expressing both recoverin and the rod-specific marker rhodopsin. This finding is consistent with our other work showing an increased tendency towards differentiation of RPCs co-cultured on a PLGA/PLLA substrate [25].

It is widely appreciated that biodegradable polymers provide an excellent substrate for cell transplantation and tissue engineering [12, 26-30]. For instance, biodegradable polymers cultured with bone marrow-derived cells have been used to promote regeneration of the

diseased skeletal system [29, 30]. In another report, biodegradable polymers were seeded with neural stem cells and the composite grafts transplanted to the injured spinal cord, resulting in regeneration of host axons with concomitant behavioral recovery [27]. To our knowledge however, there has been no prior report comparing the survival of cells delivered as a single cell suspension versus as a polymer composite graft.

In addition to the benefits enumerated above, the use of polymer composite grafts confers additional advantages in the setting of retinal repair. For instance, placement of a graft in the subretinal space requires the formation of a focal, transient detachment of the retina. The position of this detachment can shift during the time the retina is elevated, potentially resulting in sub-optimal graft placement. Because of their physical properties, polymer composite grafts provide stable graft placement relative to single cell suspensions, hence ensuring delivery of cells to the desired retinal location. This will be particularly important when attempting to either target, or avoid, placement under the macula, as might be envisioned in the setting of retinal degenerative diseases such as ARMD and retinitis pigmentosa, respectively. In addition, the inclusion of a polymer in the composite affords the opportunity of providing polymer based extended drug delivery to the graft site [12].

Looking ahead, our data strongly suggest that polymer composite grafts will ultimately provide an improved method of RPC transplantation, as compared to single cell suspensions, although this technology is not yet mature. As it evolves, polymer scaffolds may allow the delivery of larger, more flexible grafts that can be "scrolled up", drawn into a cannula, and extruded into the subretinal space through a small retinotomy, such as has previously been proposed for photoreceptor and retinal pigment epithelial grafts [31,32].

The PLGA/PLLA polymer used in the present study, while providing an excellent substrate for cell attachment, does not possess the flexibility required for this delivery method. It may, however, be possible to develop a hybrid hydrogel, or other polymer, with the necessary properties. Similarly, the polymer we have used has a minimum thickness of approximately 150 $\mu$m, which is substantially thicker than the photoreceptor layer of the mouse retina This physical constraint presents a substantial barrier to functional photoreceptor replacement in mouse models. We have therefore begun studies in the pig, an animal model with an eye similar in size, structure, and function to that of humans. Demonstration of functional efficacy in such a model represents an important prerequisite to clinical application of polymer composite graft technology. We suggest that the use of a biodegradable polymer/progenitor cell composite graft offers the opportunity of achieving this goal and, potentially, a therapeutic option for degenerative diseases of the retina.

**Acknowledgements**

This study was supported by grants from the Siegal Foundation (MJY, EL, RL), the Minda de Gunzburg Center for Retinal Transplantation (MJY), the NEI (09595, MJY), and Department of Defense (MJY).

**Figure legend**

***Fig. 1: Differentiation and characterization of donor cells in vitro.***

RPCs formed GFP+ neurospheres when grown in serum-free media supplemented with EGF: viewed under FITC illumination (A). RPCs were plated on 8 well slides coated with laminin and were cultured in the absence of EGF and the presence of 10% FBS for 1 (B and C) or 14 days (D, E, F, G, and H). The cells were stained for Ki67 (B), nestin (C), GFAP (D), Map2 (E), PKC $\alpha$ (F), recoverin (G), and rhodopsin (H). At day 1, cells expressed Ki67 (B), and nestin (C). At day 14, some cells differentiated morphologically into specific cell types expressing GFAP (D), Map2 (E), PKC-$\alpha$ (F), recoverin (G), and rhodopsin (H).

***Fig. 2. Polymer structure, differentiation and characterization of donor cell line on polymer composite graft.***

SEM of the polymer substrate before (A, B, and C) and after seeding with RPCs (D and E). The polymer /RPC composite grafts were cut into rectangular pieces of 0.5 x 0.3 mm, and viewed under FITC illumination under low (F) and high magnification (G). The polymer composite grafts were cut into smaller pieces for transplantation and some of these pieces were then analyzed immunocytochemically using an epi-fluorecent microscope: constitutive GFP expression (I, L, O, R and U), antibody/ Cy3 immunoreactivity, Ki67 (J), nestin (M), GFAP (P), Map2 (S), and PKC-$\alpha$ (V) and merged images (K, N, Q, T and W). Arrows indicate cells co-expressing these labels. GFP+ RPCs co expressed Ki67 on the

composite graft (I-K). GFP+ RPCs co-expressed nestin on the polymer composite graft (L N). Some cells co-expressed GFAP (O-Q), Map2 (R-T), PKC- $\alpha$ (U-W) on the composite graft. Most of the RPCs on the composite grafts continued to express Ki67 and nestin, although some cells now expressed neuronal and astrocytic markers prior to transplantation. Polymer composite grafts were EGF+ at 1 week after transplantation to subretinal space *in vivo* (H). Polymer incubated with media containing EGF were EGF+ (X-I to X-III), while polymers pretreated with 5% PVA prior to EGF incubation were EGF- (Y-I to Y-III) after 1 week *in vitro*.

***Figure 3***

***Fundus examination after composite graft transplantation***

Fundus pictures of the same C57/Bl6 mouse at 2 weeks (A) and 4 weeks (B) Fundus pictures of the same rho -/- mouse at 2 weeks (C) and 4 weeks (D). The arrowheads show the optic nerve head and arrows show the same retinal vessel. In each eye, surviving RPCs were confirmed to be GFP+ by fundus examination via fluorescent microscopy (E-H). A large number of RPCs migrated into the host retina (I). H&E staining after operation at 1 (J), 2 (K), and 4 weeks (L). These polymers in the subretinal space were gradually degraded at 1, 2 and 4 weeks, with pores increasing in size over this period (arrows) (J-L).

***Figure 4***

***Migration and differentiation of RPCs from polymer composite grafts into C57/Bl6 mice retina.***

Epi-fluorecent (A-F) and confocal (G-O) images of the expression of neural and photoreceptor markers by RPCs following polymer composite grafting to the eye of normal adult C57/Bl6 mice, seen at 2 and 4 weeks post grafting; constitutive GFP expression (A, D, G, J, and M), antibody/ Cy3 immunoreactivity for NF200 (B), GFAP (E), PKC- $\alpha$ (H), recoverin (K and N), and merged images (C, F, I, L, and O). NF200 co-expressing RPCs extended neural fibers (A-C). GFAP co expressing RPCs migrated from the composite graft into the host retina and some RPCs in the polymer also expressed GFAP (D-F). PKC- $\alpha$ co-expressing RPCs were found in the host inner nuclear layer (G-I). Recoverin co-expressing RPCs were found in the composite graft (J-L) and the host retina (M-O) of C57/Bl6 mice at 2 weeks and 4 weeks after transplantation.

***Figure 5***

***Migration and differentiation of RPCs from polymer composite grafts into the rho -/- retina.***

Confocal (A-F, and J-L) and epi-fluorecent (G-I) images of the expression of neural and photoreceptor markers by RPCs following polymer composite grafting to the eye of adult rho -/- mice at 2 and 4 weeks post-grafting. Constitutive GFP expression (A, D, G, and J), antibody/ Cy3 immunoreactivity for recoverin (B and E), rhodopsin (H and K), and merged images (C, F, I, and L). Recoverin co-expressing RPCs were found in the retina of rho -/- mice at 2 weeks (A-C) and 4 weeks (D-F) after transplantation. Rhodopsin co expressing RPCs were found in rho -/- mice at 2 weeks (G-I) and 4 weeks (J-L).

***Figure 6***

***Integration and cell survival of RPCs: comparison of polymer composite grafts and single cell suspensions.***

A· Cell numbers were compared with composites before transplantation and in eyes after composite transplantation. At 1, 2, and 4 weeks after transplantation, 91% (n=6), 96% (n=6), and 78% (n=6) of the cells survived in the eye. To examine the number of cells transplanted, cell numbers at 1, 2, and 4 weeks were compared with cell numbers at day 0. At 1, 2, and 4 weeks after single cell suspension transplantation, 12.7% (n=6), 9.9% (n=6), and 8.1% (n=6) survived in the retina. This data shows polymer composite grafts can deliver 10-fold more cells, compared to single cell suspension transplantation. $*p < 0.01$, *Student's t*-test.

B: The number of TUNEL+ cells in the group injected using the conventional method with a glass needle (glass needle-slide), a plastic pipet tip (pipet tip-slide), or using the pipet to seed the polymer composite graft (pipet tip-polymer), were 57.8%, 1.56%, and 14 9% at 3 days. $*p < 0.01$, *Student's t*-test.

Table 1

Survival and integration of grafted RPCs in the eye of non-immunosuppressed host animals at 1, 2, and 4 weeks post-transplantation.

## References


1. Ahmad I, Dooley CM, Thoreson WB, Rogers JA, Afiat S. In vitro analysis of a mammalian retinal progenitor that gives rise to neurons and glia. Brain Res 1999;831:1-10.
2. Tropepe V, Coles BL, Chiasson BJ et al. Retinal stem cells in the adult mammalian eye. Science 2000;287:2032-2036.
3. Klassen H, Sakaguchi DS, Young MJ. Stem cells and retinal repair. Prog Retin Eye Res 2004;23:149-181.
4. Klassen HJ, Ng TF, Kurimoto Y et al. Multipotent retinal progenitors express developmental markers, differentiate into retinal neurons, and preserve light-mediated behavior. Invest Ophthalmol Vis Sci 2004;45:4167-4173.
5. Mizumoto H, Mizumoto K, Shatos MA, Klassen H, Young MJ. Retinal transplantation of neural progenitor cells derived from the brain of GFP transgenic mice. Vision Res 2003;43:1699-1708.
6. Lu B, Kwan T, Kurimoto Y, Shatos M, Lund RD, Young MJ. Transplantation of EGF-responsive neurospheres from GFP transgenic mice into the eyes of rd mice. Brain Res 2002,943:292 300.
7. Young MJ, Ray J, Whiteley SJ, Klassen H, Gage FH. Neuronal differentiation and morphological integration of hippocampal progenitor cells transplanted to the retina

of immature and mature dystrophic rats. Mol Cell Neurosci 2000;16:197-205.

**8.** Nishida A, Takahashi M, Tanihara H et al. Incorporation and differentiation of hippocampus-derived neural stem cells transplanted in injured adult rat retina. Invest Ophthalmol Vis Sci 2000;41:4268-4274.

**9.** Takahashi M, Palmer TD, Takahashi J, Gage FH. Widespread integration and survival of adult-derived neural progenitor cells in the developing optic retina. Mol Cell Neurosci 1998;12:340-348.

**10.** Schierle GS, Hansson O, Leist M, Nicotera P, Widner H, Brundin P. Caspase inhibition reduces apoptosis and increases survival of nigral transplants. Nat Med 1999;5:97-100.

**11.** Brundin P, Dunnett S, Bjorklund A, Nikkhah G. Transplanted dopaminergic neurons: more or less? Nat Med 2001;7:512-513.

**12.** Langer R, Vacanti JP. Tissue engineering. Science 1993;260:920-926.

**13.** Atala A. Tissue engineering for bladder substitution. World J Urol 2000;18:364-370.

**14.** Temenoff JS, Mikos AG. Review: tissue engineering for regeneration of articular cartilage. Biomaterials 2000;21:431-440.

**15.** Pomahac B, Svensjo T, Yao F, Brown H, Eriksson E. Tissue engineering of skin. Crit Rev Oral Biol Med 1998;9:333-344.

**16.** Kou JH, Emmentt C, Shen P et al. Bioerosion and biocompatibility of poly (d, l-lactin-co-glycolic acid) implants in brain. J. contral release 1997;43:123-130.

**17.** Gautier SE, Oudega M, Fragoso M et al. Poly(alpha-hydroxyacids) for application

in the spinal cord: resorbability and biocompatibility with adult rat Schwann cells and spinal cord. J Biomed Mater Res 1998;42(4):642-654.

18. Lavik E, Teng YD, Snyder E, Langer R. Seeding neural stem cells on scaffolds of PGA, PLA, and their copolymers. Methods Mol Biol 2002;198:89-97.

19. Schugens C, Maquet V, Grandfils C, Jerome R, Teyssie P. Polylactide macroporous biodegradable implants for cell transplantation. II. Preparation of polylactide foams by liquid-liquid phase separation. J Biomed Mater Res 1996;30:449-461.

20. Bjorklund LM, Isacson O. Regulation of dopamine cell type and transmitter function in fetal and stem cell transplantation for Parkinson's disease. Prog Brain Res 2002;138:411-420.

21. Hagell P, Piccini P, Bjorklund A et al. Dyskinesias following neural transplantation in Parkinson's disease. Nat Neurosci 2002;5:627-628.

22. Brundin P, Petersen A, Hansson O. Graft survival. J Neurosurg 1999,90:804-806.

23. Meyer JS, Katz ML, Maruniak JA, Kirk MD. Neural differentiation of mouse embryonic stem cells in vitro and after transplantation into eyes of mutant mice with rapid retinal degeneration. Brain Res 2004;1014:131-144.

24. Hara A, Niwa M, Kunisada T et al. Embryonic stem cells are capable of generating a neuronal network in the adult mouse retina. Brain Res 2004;999:216-221.

25. Lavik EB, Klassen H, Warfvinge K, Langer R, Young MJ. Fabrication of degradable polymer scaffolds to direct the integration and differentiation of retinal progenitors. Biomaterials 2005;26:3187-3196.

26. Lavik E, Langer R. Tissue engineering: current state and perspectives. Appl

Microbiol Biotechnol. Jul 2004;65(1):1-8.

**27.** Teng YD, Lavik EB, Qu X et al. Functional recovery following traumatic spinal cord injury mediated by a unique polymer scaffold seeded with neural stem cells. Proc Natl Acad Sci U S A 2002;99:3024-3029.

**28.** Levenberg S, Huang NF, Lavik E, Rogers AB, Itskovitz-Eldor J, Langer R. Differentiation of human embryonic stem cells on three-dimensional polymer scaffolds. Proc Natl Acad Sci U S A 2003;100:12741-12746.

**29.** Ochi K, Chen G, Ushida T et al. Use of isolated mature osteoblasts in abundance acts as desired-shaped bone regeneration in combination with a modified poly-DL-lactic-co-glycolic acid (PLGA)-collagen sponge. J Cell Physiol 2003;194:45-53.

**30.** Tsuchiya K, Mori T, Chen G et al. Custom-shaping system for bone regeneration by seeding marrow stromal cells onto a web-like biodegradable hybrid sheet. Cell Tissue Res 2004;316:141-153.

**31.** Kaplan HJ, Tezel TH, Berger AS, Wolf ML, Del Priore LV. Human photoreceptor transplantation in retinitis pigmentosa. A safety study. Arch Ophthalmol 1997;115:1168-1172.

**32.** Del Priore LV, Kaplan HJ, Tezel TH, Hayashi N, Berger AS, Green WR. Retinal pigment epithelial cell transplantation after subfoveal membranectomy in age-related macular degeneration: clinicopathologic correlation. Am J Ophthalmol 2001;131:472-480.

Figure 1

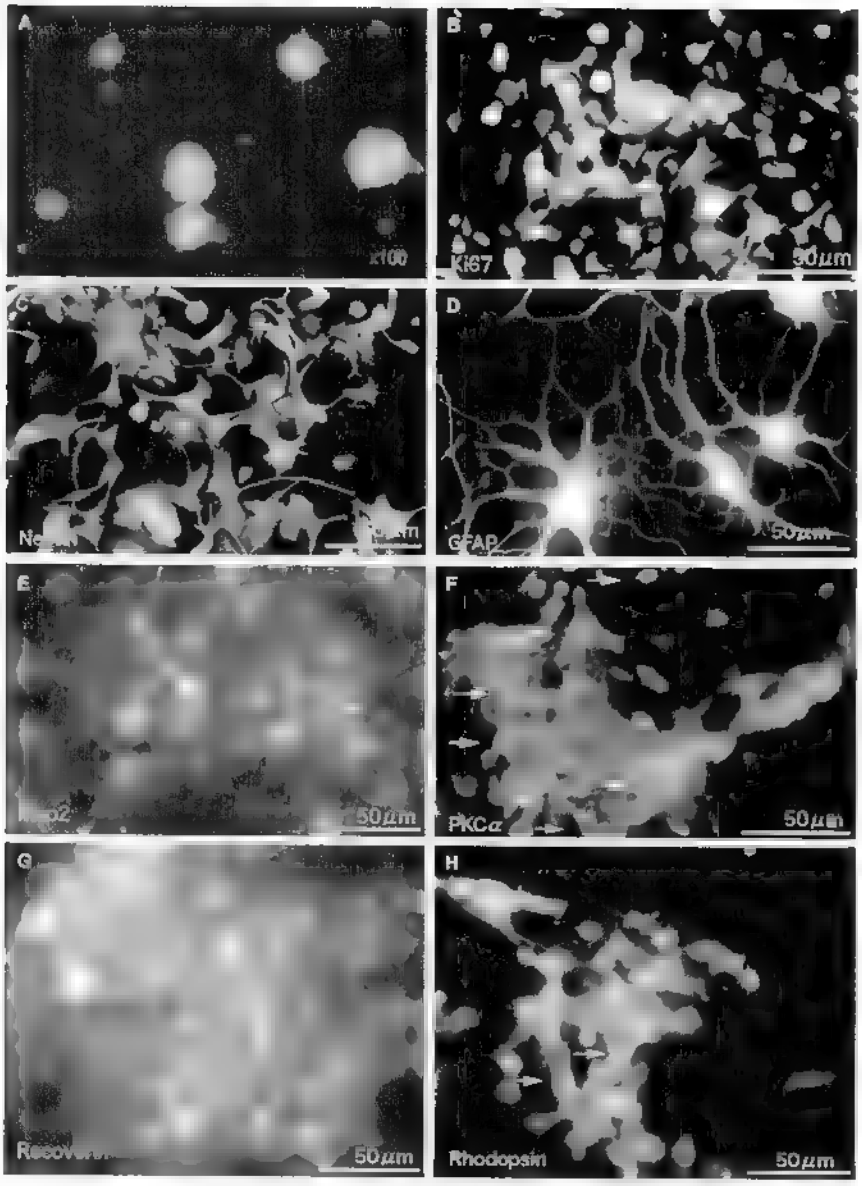
A
B
Ki67
50μm
C
D
GFAP
50μm
E
50μm
F
PKCα
50μm
G
50μm
H
Rhodopsin
50μm

Figure 2

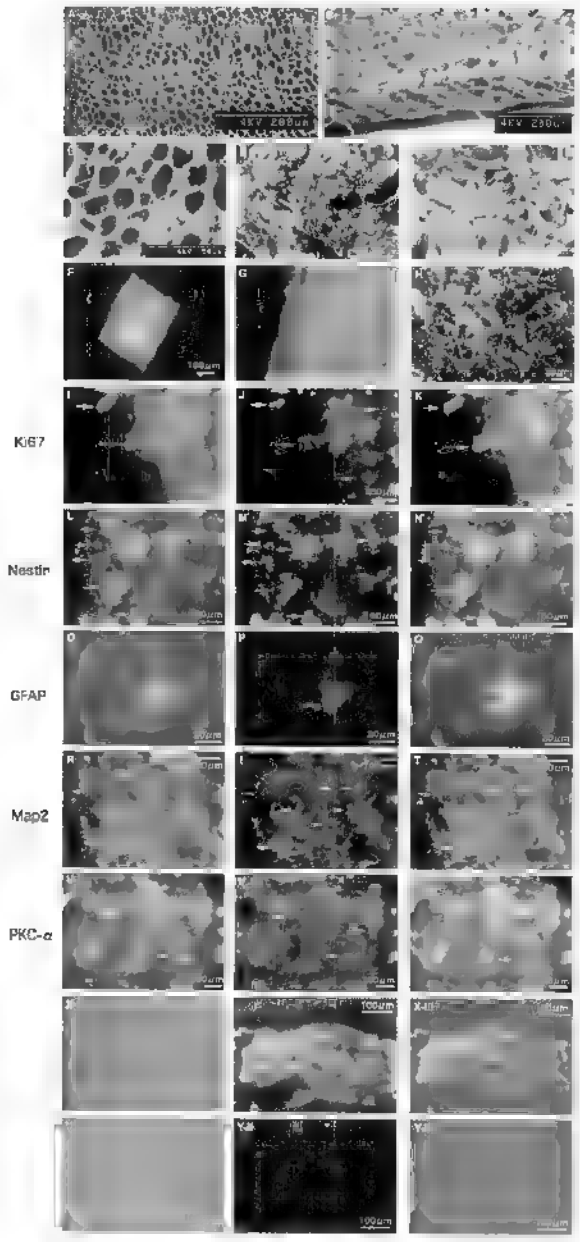

Figure 3

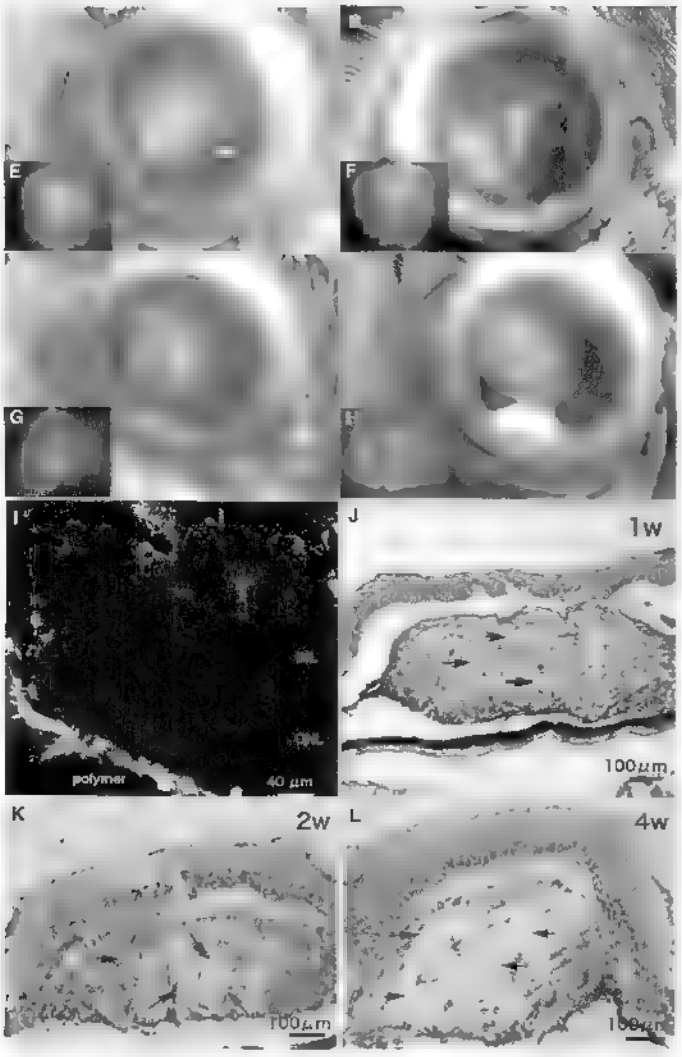

Figure 4

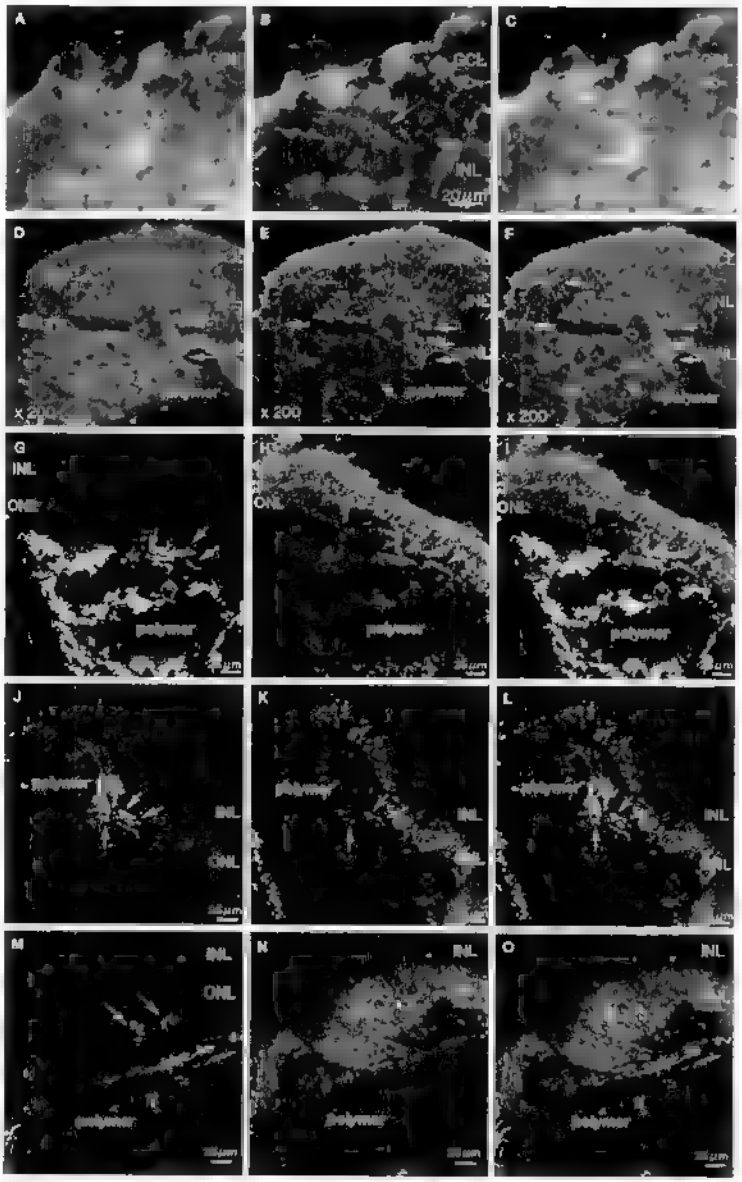
NF200
(C57/Bl6)
2w
GFAP
(C57/Bl6)
2w
PKC-α
(C57/Bl6)
4w
Recoverin
(C57/Bl6)
2w
Recoverin
(C57/Bl6)
4w
A
B
C
D
E
F
G
I
J
K
L
M
N
O
GCL
INL
ONL
x 200

Figure 5

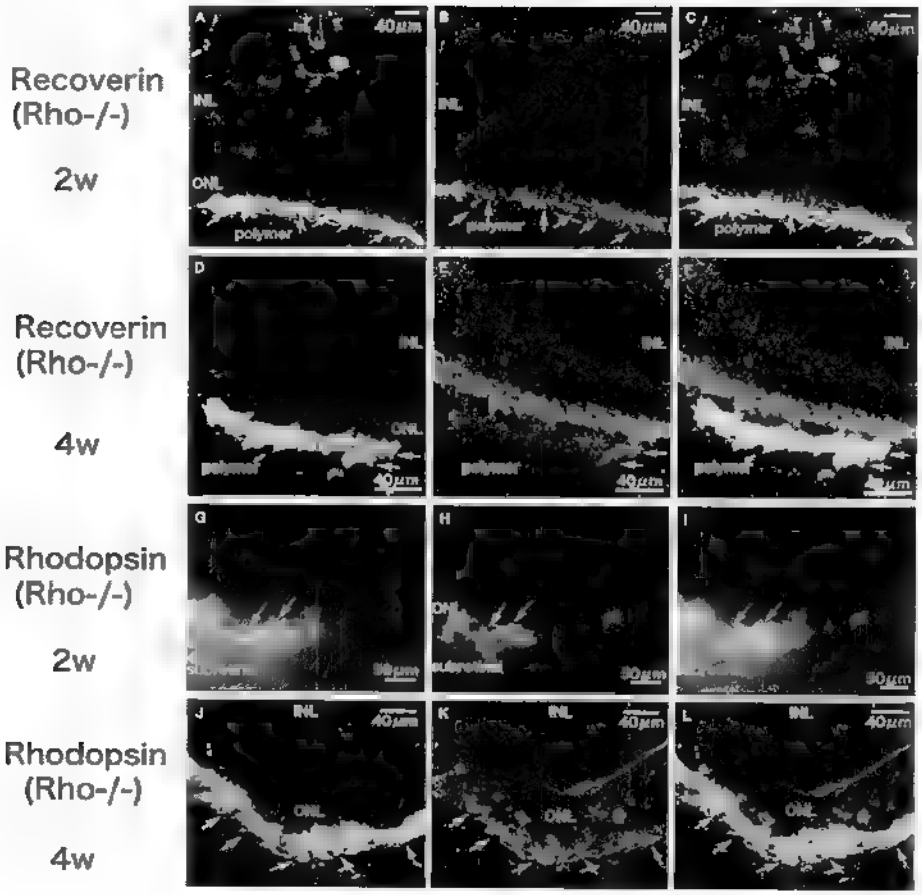
Recoverin
(Rho-/-)
2w
Recoverin
(Rho-/-)
4w
Rhodopsin
(Rho-/-)
2w
Rhodopsin
(Rho-/-)
4w
A
B
C
D
E
F
G
H
I
J
K
L
INL
ONL
polymer
40μm
50μm

Figure 6

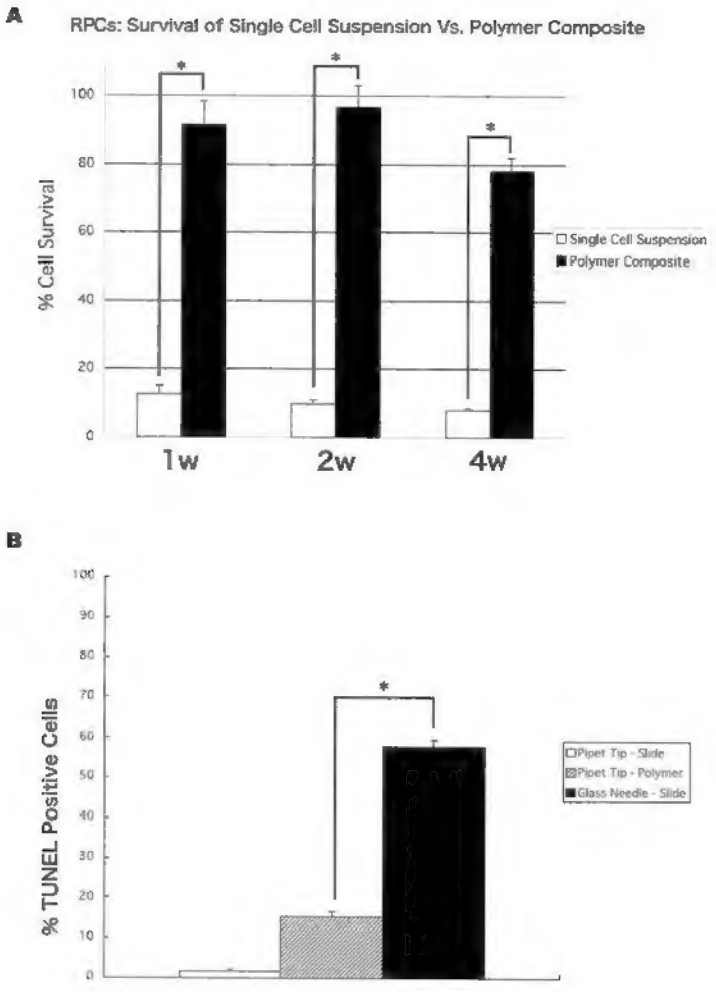
A
RPCs: Survival of Single Cell Suspension Vs. Polymer Composite
% Cell Survival
100
80
60
40
20
0
1w
2w
4w
Single Cell Suspension
Polymer Composite
B
% TUNEL Positive Cells
100
90
80
70
60
50
40
30
20
10
0
Pipet Tip - Slide
Pipet Tip - Polymer
Glass Needle - Slide

Table 1

| | Recipient Age | Number | 1w | 2w | 4w |
|---|---|---|---|---|---|
| C57/BL6 | 6w - 8w | N = 50 | N = 20 | N = 15 | N = 15 |
| | | survival / integration | N=20/17 | N=15/13 | N=15/13 |
| Rho -/- mice | 4w - 6w | N = 26 | N = 6 | N = 10 | N = 10 |
| | | survival / integration | N=6/5 | N=10/10 | N=10/9 |

## Appendix 4, Abstracts, #1

**Program#/Poster#:** 587/B561
**Abstract Title: Proteomic Comparison Between Retinal Progenitor Cells and Brain Progenitor Cells Derived From Early Neonatal Mice**
**Presentation Start/End Time:**
Sunday, May 01, 2005, 8:30 AM -10:15 AM
**Location:**Hall B/C
**Reviewing Code:** 261 retina: cell biology - RC
**Author Block:**
*H.Greenlee[1A], T.E. Dunn[1B], D.S. Sakaguchi[1C], M.J. Young[2].* [A]Biomedical Sciences, Bioinformatics and Computational Biology, and Interdepartmental Neuroscience, [B]Biomedical Sciences and Bioinformatics and Computational Biology, [C]Department of Genetics, Development & Cell Biology and Interdepartmental Neuroscience, [1]Iowa State University, Ames, IA; [2]Schepens Eye Research Institute, Department of Ophthalmology, Harvard Medical School, Boston, MA.
**Keywords:** 674 retinal development, 639 proteomics
**Purpose:**To perform a proteomic analysis comparing retinal progenitor cells with brain progenitor cells. Different populations of stem cells and progenitor cells are likely to possess unique molecular fingerprints that may be correlated with their ability to survive, differentiate and integrate after transplantation. By characterizing the molecular fingerprint of cells that give the most promising results, we may be able to begin to identify the fundamental protein expression requirements for a given transplant application. We are using two-dimensional gel electrophoresis to characterize the proteome of two populations of progenitor cells (brain progenitor cells; BPCs, and retinal progenitor cells RPCs) isolated from mice of the same age and genetic background.
**Methods:** RPCs and BPCs used in this study were isolated and expanded in vitro from neonatal mice as reported previously (Shatos et al., J. Reg. Med.(2), 2001). The cells were maintained as neurospheres in supplemented neurobasal medium with 20 ng/mL EGF. Cells were sonicated in hypotonic buffer with protease inhibitors and centrifuged to remove nuclei. 35 $\mu$g of protein was focused using pH 3-10 7.7cm IEF strips and separated in the second dimension on 4-12% Bis-Tris gels. Gels were stained with Sypro Ruby and analyzed for significant changes in the intensity of protein spots using Phoretix Expression 2D software.
**Results:** Our analysis has thus far identified 323 distinct protein spots on the RPC gels and 233 distinct spots on the BPC gels. Of the proteins present in samples from both RPCs and BPCs, expression was greater (at least 2-fold) at 14 spots and lesser (at least 2-fold) at 32 spots in BPCs compared to RPCs.
**Conclusions:** In our analysis comparing progenitor cells from the retina and brain demonstrates significant differences in 136 distinct protein spots. These results demonstrate the utility of proteomics for characterization of different progenitor cell populations in an effort to gain a better understanding of their fundamental, molecular similarities and differences. Ultimately, these molecular differences may be used to target different populations of cells for the most appropriate therapeutic applications.
**Support:** Department of Defense, Siegal Foundation, the Minda de Gunzburg Center for Retinal Transplantation (MJY), NEI (EY09595, MJY)

## Appendix 4, Abstracts, #2

**Program#/Poster#:**3227/B780
**Abstract Title:**
**Enhanced Survival and Differentiation Into Photoreceptor in Retinal Progenitor Cells Transplantation Using Polymer Composite Graft**
**Presentation Start/End Time:**
Tuesday, May 03, 2005, 11:15 AM - 1:00 PM
**Location:**Hall B/C
**Reviewing Code:**283 stem cells: retinal and vascular precursors - RC
**Author Block:**
*M.Tomita1, E.Lavik2, H.Klassen3, T.Zahir1, R.Langer4, M.J. Young1.* 1Department of Ophthalmology, The Schepens Eye Research Institute, Harvard Medical School, Boston, MA; 2Yale University, New Haven, CT; 3Children's Hospital of Orange County and U.C. Irvine, Orange, CA; 4Massachusetts Institute of Technology, Cambridge, MA.
**Keywords:**715 transplantation, 663 regeneration, 664 retina
**Purpose:** Mammalian retinal progenitor cells (RPCs) can be isolated and expanded in culture, and differentiate into retinal neurons upon grafting to the eye. However, cell delivery and survival remain formidable obstacles to clinical application of RPCs. In order to overcome this hurdle, we studied whether the use of polymer composite grafts result in increased cell survival and differentiation into photoreceptor cells when placed in the subretinal space, compared to conventional injections.
**Methods:** The biodegradable polymer (PLA/PLGA) coated with laminin was cultured with RPCs isolated from EGFP mice. One week after culture, composites were cut into 0.3 x 0.5 mm pieces. Every other piece was sectioned to assess total cell number before transplantation. Alternate pieces were transplanted into the subretinal space of C57BL/6 and rho-/- mice (n=57). A single cell suspension, containing the same number of RPCs, was also transplanted as a control. Eyes were enucleated and sectioned at day 0, 1 week, 2 weeks, and 4 weeks. Samples were stained with DAPI, and cell survival was assessed. The sections were also stained for markers of mature retinal neurons and astrocytes.
**Results:** Composite grafts result in at least a 10-fold increase in surviving cells at 4 weeks, with a 16-fold increase in cell delivery, compared to conventional transplantation. Grafted RPCs migrated into host retina, and expressed NF200, GFAP, PKC-alpha, recoverin, and rhodopsin. Only cells grafted on the polymer substrate expressed rhodopsin in rho -/- mice.
**Conclusions:** Biodegradable polymer/progenitor cell composite grafts provide an effective means of increasing progenitor cell survival and differentiation into photoreceptor when transplanted to the subretinal space.
**Commercial Relationship:**
**M. Tomita**, None; **E. Lavik**, None; **H. Klassen**, SERI P; **T. Zahir**, None; **R. Langer**, None; **M.J. Young**, SERI P.
**Support:** Department of Defense, Siegal Foundation, the Minda de Gunzburg Center for Retinal Transplantation (MJY), NEI (EY09595,MJY)